Behaviour of oxygen transfer in a simulated multiphase hydrocarbon-based bioprocess in a bubble column reactor

By:

Ayman A. Abufalgha

Thesis presented in partial fulfilment
of the requirements for the Degree

of

MASTER OF ENGINEERING
(PROCESS ENGINEERING)

in the Faculty of Engineering
at Stellenbosch University

Supervisor:
Prof. K.G. Clarke
Co- supervisor
Dr. R. W. M. Pott

March 2018

DECLARATION

By submitting this thesis electronically, I declare that the entirety of the work contained therein is my own, original work, that I am the sole author thereof (save to the extent explicitly otherwise stated), that reproduction and publication thereof by Stellenbosch University will not infringe any third party rights and that I have not previously in its entirety or in part submitted it for obtaining any qualification.

Date: March 2018

ABSTRACT

Linear alkane hydrocarbons can be converted into higher value products and product-precursors through the addition of an oxygen moiety. One method of upgrading these hydrocarbons is through biologically-mediated oxidation, whereby an oxygen group is added to the alkane backbone by a microorganism to produce a more reactive, and more valuable molecule. To achieve this, operating conditions conducive to this biological process need to be reached; one key is liquid-phase oxygen concentration, which is governed by the oxygen transfer rate into the reaction fluid.

This study focuses on the behaviour of the overall volumetric oxygen transfer coefficient *(K_La)* and, the interfacial area (a), in a model four-phase (air-water-hydrocarbon-deactivated yeast) hydrocarbon-based bioprocess in a bubble column reactor (BCR). It sought to give an understanding on the impact of the alkane concentration, superficial gas velocity and yeast loading on the K_La and the interfacial area of the system. The experiments were conducted at different alkane concentrations of (2.5 to 20% v/v n-C_{14-20}), superficial gas velocities of (1 to 3 cm/sec), and yeast loading of (0.5 to 6 g/l *Saccharomyces cerevisiae*). The yeast cells were deactivated by heating, to suppress oxygen utilisation, while maintaining cell integrity.

The K_La was measured using the gassing-out method (GOP) using a dissolved oxygen (DO) probe which recorded the rate of DO in the system every 5 seconds until oxygen saturation was achieved. The probe constant *(K_p)* was evaluated at all experimental conditions to ensure the accuracy of the K_La determination. The interfacial area was calculated from the gas hold-up (ε_G), and Sauter mean diameter (D_{32}) data. D_{32} was evaluated by high-speed photography and image analysis on the acquired images, performed using MATLAB software, while the ε_G was calculated as the difference in the liquid level before and after sparging the reactor.

For three phase systems (air-water-hydrocarbons), it was found that at low superficial gas velocity the system was non-homogeneous, with an increased hydrocarbon concentration at the top of the reactor. The spatial homogeneity of the system has not been previously investigated in the literature, particularly in the the bubble column reactor when the process contains hydrocarbons. The K_La measurements were thus affected by the spatial variations in concentrations and therefore could not be reliable. To overcome this, the system was analysed for spatial liquid-phase homogeneity using a physical sampling methodology, which

established the optimal superficial gas velocity (2 cm/sec) to achieve homogenous flow in the three phase system. For the four-phase system, the addition of yeast to the BCR resulted in a change in the flow regime and therefore increased the homogeneity in the system at low superficial gas velocity (1 cm/sec). This result suggets that the addition of yeast cells to the reactor likely changed the fluid properties such as viscosity and the surface tension.

Investigations on the impact of yeast loading, alkane concentration and superfical gas velocity on K_La and interfacial area in a multiphase hydrocarbon-based bioprocess in a BCR were undertaken for this project. It was found that an increase in the yeast loading resulted in a decrease in K_La at constant superficial gas velocity in the three phase (air-water-deactivated yeast) system. This decrease might be attributed to the existence of diffusion blocking effects as well as the increasing fluid viscosity in the system. A similar effect was found in a four phase (air-water-hydrocarbon-deactivated yeast) system, when the values of K_La were depressed with increasing yeast concentration at high superficial gas velocities and constant alkane concentration (2.5% v/v). However, increasing the constant alkane concentration at the same conditions caused a decrease in K_La for all superficial gas velocities. At low yeast loading (0.5 g/l), the interfacial area increased to an average of 190 m^2/m^3 when the superficial gas velocity increased from 1 to 3 cm/sec. However, increasing yeast loading from 0.5 g/l to 6 g/l saw a decrease in the interfacial area to approximately 70 m^2/m^3 at the maximum levels of superficial gas velocities. The observed decrease in the interfacial area at high yeast loadings was a result of the increasing D_{32}, likely due to the effect the yeast has on fluid properties.

Increasing the hydrocarbon concentration from 2.5 to 10% v/v decreased K_La, possibly due to the increase in fluid viscosity and the surface tension, dampening turbulence in the system. However, further increases in alkane concentration above 10% v/v caused a significant increase in K_La for the lowest superficial gas velocities and constant yeast loading. An increase in the superficial gas velocity also decreased the values of K_La with an average of 0.3 s^{-1} at highest alkane concentration (20% v/v) for all constant yeast loading. The interfacial area had marginal increases of about 20 m^2/m^3 when the alkane concentration was increased from 2.5 to 20% v/v. This increase in interfacial area with increasing superficial gas velocity was due to the increase in the gas hold up, since D_{32} was not influenced by the alkane concentration.

It can be concluded that these trends of K_La values were not entirely as expected, since the strongest effect came from alkane concentration, rather than superficial gas velocity, which is

usually identified as the strongest factor in oxygen transfer studies. Further, the interfacial area was significantly influenced by the variations in superficial gas velocity (1 to 3 cm/sec). The oppositional effects between the interfacial area and K_La values suggest that the interaction between the yeast cells and the hydrocarbons may have changed the system hydrodynamics such that the oxygen transfer coefficient K_L was effected, since interfacial area is seen to be fairly constant over the variable ranges.

This work significantly furthers our understanding of the fluid mixing properties and K_La in a bubble column reactor, as well as the behaviour of the overall volumetric oxygen transfer coefficient in simulated hydrocarbon-based processes in this reactor configuration, which has the potential to impact and inform the operation of an industrially relevant hydrocarbon based bioprocess.

ABSTRACT (AFRIKAANS)

Dit is moontlik om lineêre alkaan koolwaterstowwe te omskep in hoër waarde produkte asook voorloperprodukte deur die toevoeging van ‘n suurstofgedeelte. Sulke koolwaterstowwe kan opgegradeer word deur biologies-bemiddelde oksidasie: ‘n suurstofgroep kan by die alkaan basis bygevoeg word deur ‘n mikro-organisme om ‘n meer reaktiewe en meer waardevolle molekule te produseer. Om dit te bewerkstellig is dit belangrik om operasionele toestande bevorderlik vir hierdie biologiese proses te behaal. Een noodsaaklike item is vloeibare fase suurstofkonsentrasie, wat geaffekteer word deur die suurstof oordragstempo in die reaksievloeistof in.

Dié studie fokus op die gedrag van die algehele volumetriese suurstofoordragskoëffisiënt (K_La) en die gas-vloeistof oppervlakarea (a) in ‘n vierfase model (water, koolwaterstof, lug en mikrobiese vastestowwe) koolwaterstofbioproses wanneer dit deur ‘n borrel-kolom reaktor (BCR) gestuur word. Dit mik om die impak van die alkaan konsentrasie, oppervlakkige lugsnelheid en gisbelading op die K_La en die gas-vloeistof oppervlakarea van die stelsel te verduidelik. Die eksperimente is uitgevoer teen verskillende alkaan konsentrasies (van 2.5 – 20 vol% n-C_{14-20}), diskrete oppervlakkige gas snelhede (van 1 – 3 cm/sek), en gisbelading (van 0.5–6 g/l *Saccharomyces cerevisiae*). Om suurstofbenutting te onderdruk sonder om handhawing van sel integriteit te verloor was die gisselle gedeaktiveer deur dit vir 60 minute teen 70°C te verhit.

Die K_La is gemeet met ‘n opgeloste-suurstof (DO) meter en die gas uitlatings metode (GOP). Die stelsel se DO was elke 5 sekondes gemeet tot suurstof-versadiging bereik is. Die instrument se reaksie sloering (K_P) was tydens alle eksperimentele toestande geëvalueer om die akkuraatheid van die K_La bepaling te verseker. Die gas-vloeistof oppervlakarea is gedefinieer as ‘n funksie van die gas ophou (ε_G), en gemiddelde Sauter deursnit (D_{32}). D_{32} is geëvalueer deur ‘n foto-analise algoritme. Die beeldontleding is uitgevoer met behulp van MATLAB sagteware, terwyl die $\varepsilon_G$bereken is deur veranderinge in die werkende vloeibare vlakke in die reaktor te meet.

Vir driefase-stelsels (gas-water-koolwaterstowwe) is dit gevind dat die stelsel nie-homogeen was by lae oppervlakkige lug snelheid met ‘n toeneming in koolwaterstof konsentrasie by die bopunt van die reaktor. Dus is die K_La en gas-vloeistof oppervlakarea metings deur die

ruimtelike verskille in konsentrasies geaffekteer en kan dit nie as betroubaar beskou word nie. Om ‘n betroubare meting te vind is die stelsel geanaliseer vir ruimtelike vloeibare fase-homogeniteit deur ‘n fisiese steekproefneming metodologie te gebruik. Dit is dus bevestig dat (u_G) teen 1.8 cm/sek optimale homogene vloei in ‘n driefase stelsel bereik word. In die vierfase-stelsel het die byvoeging van gis tot die BCR gelei tot ‘n verandering in die vloeisisteem en dus ‘n verhoging in die homogeniteit van die stelsel teen lae vloei (1 cm/s). Hierdie resultaat bevestig dat die toevoeging van gisselle in die reaktor die vloeistof eienskappe soos viskositeit, borrel samesmelting, sowel as die oppervlakspanning verander.

Die impak van gisbelading op K_La en gas-vloeistof oppervlakarea tydens meervoudige fase koolwaterstof-gebasseerde bioprosesse in ‘n BCR is eerste ondersoek. Dit is gevind dat ‘n toename in die gisbelading gelei het tot ‘n afname in K_La in die driefase (lug-water-gis) stelsel teen ‘n konstante. Hierdie afname kan toegeskryf word aan die bestaan van diffusie blokkerende effekte asook ‘n toenemende vloeistofsviskositeit. ‘n Soortgelyke effek is in ‘n vierfase (lug-water-koolwaterstof-gis) stelsel aangetref; verlaagde K_La waardes en toenemende gislading is opgemerk by hoë oppervlakkige gas snelheid met ‘n konstante alkaan konsentrasie (onder 10% v/v). Daar is egter ‘n afname in K_La waardes opgemerk by alle oppervlakkige gas snelheid wanneer die alkaan konsentrasie op dieselfde toestande verhoog is. By lae gislading (0,5 g/l) het die gas-vloeistof oppervlakarea toegeneem tot ‘n gemiddelde van 190 m^2/m^3 wanneer die oppervlakkige gas snelheid verhoog is (van 1 – 3 cm/sek). Wanneer gislading van 0,5 g/l tot 6 g/l verhoog is is ‘n afname in die gas-vloeistof oppervlakarea na ongeveer 70 m^2/m^3 bevestig teen maksimum vlakke van oppervlakkige gas snelhede. Die afname in die gas-vloeistof oppervlakarea by hoë gisbeladings was die gevolg van hierdie toename, waarskynlik as gevolg van die effek van die gis op vloeibare eienskappe.

‘n Verhoging van 2,5 tot 10% v/v koolwaterstof konsentrasie het gelei tot ‘n afname in K_La met enige verhogings in vloeistof viskositeit en oppervlakspanning sowel as ‘n demping van die onstuimigheid in die stelsel. Verdere toename in alkaan konsentrasie (bo 10% v/v) het wel tot ‘n beduidende toename in K_La gelei vir die laagste oppervlakkige gas snelhede en konstante gislading. ‘n Verhoging in die oppervlakkige gassnelheid het verder die K_La waardes met ‘n gemiddeld van 0.3 s^{-1} verlaag by hoogste alkaan konsentrasie (20% v/v) vir alle konstante gisladings. Die gas-vloeistof oppervlakarea het minimale verhogings van ongeveer 20 m^2/m^3 getoon wanneer die alkaan konsentrasie van 2,5 tot 20% v/v verhoog is. Hierdie toename in

die gas-vloeistof oppervlakarea met toenemende oppervlakkige gassnelheid was te danke aan die klein toename in D_{32} aangesien dit nie deur die alkaan konsentrasie beïnvloed is nie.

Daar kan afgelei word dat die K_La waardes se neigings nie heeltemal na verwagting was nie aangesien die sterkste verandering van alkaan konsentrasie af gekom het eerder as oppervlakkige gas snelheid, wat gewoonlik die sterkste faktor in suurstofoordrag is. Verder was die gas-vloeistof oppervlakarea aansienlik beïnvloed deur die variasies in oppervlakkige gassnelheid (1 tot 3 cm/sek). Die teenoorgestelde effekte tussen die gas-vloeistof oppervlakarea en K_La dui dat die interaksie tussen die gisselle en die koolwaterstowwe die stelsel hidrodinamika verander het wat gelei het tot ‘n veranderde suurstof oorplasing koëffisiënt K_L.

Hierdie werk bevorder ons begrip van vloeistofmengsel eienskappe en K_La in ‘n borrel-kolom reaktor wat die potensiaal het om die ‘n industrieel relevante koolwaterstof gebaseerde bioproses beter te verstaan en moontlik te bevorder.

ACKNOWLEDGEMENTS

I would like to acknowledge several people and institutions involved in this work:

- **Prof K. Clarke** for her advice, time and her knowledge on this research as well as her guidance to make this work a success.
- **Dr R. Pott** for his encouragement and confidence in my research, especially for teaching me skills, ideas, and organizing my thoughts scientifically. Without Dr Pott, I would never have come up with this piece of work.
- My Family for their love, trust and support, especially **My Parents** for contacting and encouraging me all the time.
- **Dr M. Molteno** for his assistance to develop the MATLAB code for the image analysis.
- **Dr V. Rangarajan** for the yeast deactivation process.
- **Wilhelm Burger** for designing the bubble column.
- My **friends** and my **colleagues** for the good times and exchange of ideas and knowledge.
- The workshop team of the Department of Process Engineering.
- **Libyan Embassy** in South Africa and the **Ministry of High Education** (Libya), for the excellent service and for the financial support on this journey of education.
- Centre of Excellence in Catalysis (**C*change**) and **Department of Process Engineering** for providing the equipment, space and the network to me as one of its postgraduate student.

Table of contents

Table of figures

List of tables

NOMENCLATURE

Letter	Definition	Unit
$\boldsymbol{a}$	Gas-Liquid interfacial area per unit volume	m^2/m^3
$\boldsymbol{A_P}$	Projected bubble area	m^2
C	Measured oxygen concentration	mol/m^3
$\boldsymbol{C_A}$	Molar concentration of component A	mol/m^3
C*	Oxygen concentration at saturated condition	mol/m^3
$\boldsymbol{C_P}$	Dissolved oxygen concentration giving by the probe	mol/m^3
$\boldsymbol{D_F}$	Feret diameter	m
$\boldsymbol{D_{32}}$	Sauter mean diameter	m
$\boldsymbol{D_p}$	Particle diameter	m
H	Liquid height during the aeration	m
H_0	Liquid height before the aeration	m
$\boldsymbol{K_La}$	The overall volumetric oxygen transfer coefficient	s^{-1}
$\boldsymbol{K_L}$	Oxygen transfer coefficient	s^{-1}
$\boldsymbol{K_P}$	The probe response lag constant	s^{-1}
$\mathbf{\varepsilon_G}$	Gas hold-up	m
T	time	s
$\boldsymbol{u_G}$	Superficial gas velocity	m/s
$\boldsymbol{\tau_P}$	Probe response lag time	s
P	Solids density	kg/m^3
BCR	Bubble column reactor	-
STR	Stirred tank reactor	-
DO	Dissolved oxygen	-
GOP	Gassing out procedure	-
PSP	Pressure step procedure	-
OTR	Oxygen transfer rate	-
CCD	Central composite design	-

1. INTRODUCTION

Advancement in gas to liquid (GTL) technologies has increased the production of global alkane hydrocarbon products. SASOL (South Africa) is one such an industry leader in GTL fuels conversion. A wide range of different isomers of alkanes can be produced from GTL, from linear (*n*-alkanes) to cyclic (*cyclo*-alkanes) as well as branched (*iso*-alkanes). By employing bioprocess systems, high-value pre-curser molecules or products like amino acids, organic acids, vitamins, carbohydrates, enzymes, antibiotics, lipids and citric acid, can be directly produced from the hydrocarbon molecular structure (Fukui and Tanaka, 1980).

Whereas chemical processes require conditions of high temperatures and pressure and expensive catalysts, bioprocesses using aerobic bacteria and fungi can be employed at moderate conditions to convert these feedstock hydrocarbons to high-value products (Shennan and Levi, 1973). However, the bioprocess route for the hydrocarbon conversion still presents various challenges including microbial growth inhibition, immiscibility of the alkane with the aqueous phase, fire risks that may cause explosions, volatility, concerns regarding the environmental impact of hydrocarbon use, and limitations of mass transfer between phases. Significantly, there is a substantial difficulty in the provision of adequate oxygen transfer to the conversion organisms in these bioprocesses (Schmid *et al.*, 1998).

The hydrocarbon conversion process is accomplished by the addition of oxygen to the hydrocarbon molecule to create a functional group (Correia and Clarke, 2009). This process is often limited by the oxygen transfer to the cells. The oxygen transfer rate can be enhanced through several operational modifications, like increasing agitation (linked to aeration rates in bubble column reactors (BCRs)) or increasing the partial pressure of O_2 in the sparged gas. It is critical that the oxygen transfer rate (OTR) is maintained at sufficient levels to meet the oxygen demand of the cells for process optimisation (Clarke *et al.*, 2006).

The supply of oxygen into the reaction medium versus oxygen utilisation by growing and metabolising cells causes an oxygen concentration gradient. A higher concentration of oxygen is found in air bubbles than in the liquid medium containing the cells, and due to this concentration gradient, oxygen is transferred from the bubble to the medium (Doran, 1995). By introducing hydrocarbons at higher concentrations in hydrocarbon processes, there is an increase in system viscosity and therefore increased resistance to oxygen transfer and

depression of the K_La (Clarke and Correia, 2008). This depression in K_La restricts the transfer of oxygen, and therefore the metabolism of the organisms, in bioprocess systems.

Alkane bioprocessing is an example of a multiphase system where mass transfer limitations require a deep understanding of the oxygen transfer coefficient and gas-liquid interfacial area, in order to optimise the system for product formation. While the behaviour of K_La and the gas-liquid interfacial area in bioprocess systems has been investigated in previous works by Clarke and Correia, (2008 and 2009), Clarke and Manyuchi, (2012), and Hollis and Clarke, (2016) in stirred tank reactors, there is still significant work to be done in characterising and articulating the characteristics in BCRs where they significantly influence the fluid properties and system hydrodynamics.

The oxygen transfer rate is defined by the K_La, an important parameter which is known to be affected by a range of operation variables, including system geometry, the substrate composition, gas composition and flow rate. In addition, the measurement of K_La is not trivial, and the results obtained can be dependent on the measuring and determination methodology employed (Montes *et al.*, 1999; Correia and Clarke, 2009; Clarke and Manyuchi, 2012). These factors underline the need for this study to further understand the behaviour of K_La in multiphase systems (air, water, hydrocarbon, deactivated yeast), particularly in a BCR.

In this study, K_La was measured according to the gassing out procedure (GOP) by measurement of the dissolved oxygen (DO) response, accounting for the probe constant (K_P), to record DO after a step change in the sparge gas from nitrogen to oxygen (Doran, 1995; Garcia-Ochoa and Gomez, 2009; Correia and Clarke, 2009).

The interfacial area in multiphase systems can be difficult to measure directly. However, there are parameters which can be more easily measured from which interfacial area can be inferred. In this study, the interfacial area was calculated as a function of the Sauter mean bubble diameter and the gas hold up (Mouza *et al.*, 2005a). The Sauter mean diameter was measured by high-speed digital photography and image analysis while the gas hold-up was measured using the height difference method (Schugerl, 1980; Dhanasekaran and Karunanithi, 2012). Image analysis methodologies are evolving and becoming more accurate and faster due to the advent of more powerful image capturing and analysis tools, such as MATLAB® software (Galindo *et al.*, 2005). The measurement of these two factors (the interfacial area and the

oxygen transfer coefficient (K_L)) significantly influences the reported value and certainty of K_La. These factors are in turn dependent on the fluid properties and the system hydrodynamics (Cascaval *et al.*, 2006; Chisti and Moo-Young, 1988).

By employing BCRs instead of stirred tank reactors (STRs), higher oxygen transfer rates can be achieved without subjecting the system to shear forces caused by mechanical impellers in STRs (Clarke and Correia, 2008). BCRs offer approximately 30% higher interfacial areas and therefore higher K_La values than STRs for the same levels of power consumption in aqueous systems (Bouaifi *et al.*, 2001).

To further the understanding of oxygen transfer, this study investigates the behaviour of K_La and interfacial area in a four phase system (air, water, hydrocarbons and yeast) in a BCR. It seeks to complement previous studies by other researchers, e.g. Hollis and Clarke, (2016), who investigated oxygen transfer in STRs, using the same hydrocarbon cut, n-$C_{14\text{-}20}$ (2.5 – 20% v/v alkane), and deactivated yeast, as the non-viable microbe (0.5 – 6 g/l), as used in this study in the in BCR. This study provides a fundamental undestanding of the behaviour of the voulmetric oxygen transfer coefficient K_La and the interfacial area in multipahse haydrocarbon based-bioprocess systems in a BCR.

2. LITERATURE REVIEW

2.1 The application of hydrocarbon bioprocesses

Gas to liquid technology is increasingly producing alkanes as by-products, most of which end up being used as low-value fuels. These hydrocarbons, however, could be converted into a range of industrially useful intermediates and products through bioconversion processes (Fukui and Tanaka, 1980). The conversion processes require the introduction of oxygen into the hydrocarbon backbone because the hydrocarbon molecule (unlike carbohydrate molecules) do not contain oxygen and are therefore unreactive and difficult to functionalise (Clarke and Correia, 2008). The oxidation method has been reported to be a difficult process to achieve using normal chemical synthesis owing to the inert nature of the alkane carbon backbone and the difficulty in forming stable long-chain products (Correia and Clarke, 2009).

These challenges, however, can be avoided if the chemical process route is dropped in favour of a bioconversion process, where microorganisms (both prokaryotic and eukaryotic), are employed to use alkanes as a carbon and energy source through the use of specialised enzyme systems and metabolic pathways (Wentzel *et al.*, 2007). There is a wide range of bacteria and fungi capable of performing the conversion process into an equally significant intermediate product profile (Clarke and Correia, 2008). The products from bioprocesses are often also preferentially soluble in alkanes, making alkanes even more advantageous for use as substrate in the conversion processes. Based on that, this might significantly simplify the product purification steps and eliminate products inhibitory to microbial growth (Clarke and Correia, 2008).

Some of the microorganisms applicable for this alkane metabolism include yeast species such as *Candida, Pichia, Kloekera, Torulopsis, Rhodotorula* and *Saccharomycopsis* (Walker, 1998). *Psuedomonas*, *Mycobacteria* and certain moulds, as well as genetically modified *Esherichia coli* and other bacteria are also suitable candidates (Fukui and Tanaka, 1980). These microorganisms require adequate oxygen supply for the establishment aerobic conditions at the site of cellular respiration. Reports by Shuler and Kargi, (2009) confirmed that a sufficient supply of oxygen is critical to ensure that mass transfer ceases to be the limiting factor. Oxygen deficient systems produce lower yields, thus oxygen transfer is essential in the scale-up of any aerobic bioprocess (Bandyopadhyay *et al.*, 1967; Montes *et al.*, 1999).

The oxygen solubility in the aqueous phase is reduced by increasing the hydrocarbon chain length in the mixture (Makranczy *et al.*, 1976; Cascaval *et al.*, 2006; Galaction *et al.*, 2005; Hesse *et al.*, 1996; da Silva *et al.*, 2006; Ngo and Schumpe 2012; Rols *et al.*, 1990). However, despite the decrease of oxygen solubility with increasing alkane chain length, the solubility of oxygen in hydrocarbons reportedly remains as high as 20 times that of pure water. The most easily metabolised hydrocarbon chain lengths are those in the range $C_{10} - C_{20}$ (Shennan and Levi, 1974), even better those in the lower C_{10} - C_{14} range. Lower alkane chains than C_{10} cannot be assimilated by yeasts, although oxidation was reported to take place when n-nonane and shorter alkanes were used as substrates (Shennan and Levi, 1974). Hydrocarbon based bioprocesses have the potential to produce valuable products, but are constrained by oxygen transfer, which is a complicated function of the hydrocarbons and the system, and therefore further study in this arena is warranted.

2.2 Bubble column reactors (BCRs)

A bubble column reactor is defined as a rector which employs a gas sparger through a liquid or a liquid-solid suspension for mixing and species transfer. The high energy efficiency, low capital cost and their ability to maintain monoseptic conditions, as well as the lack of moving parts, have seen the BCR increasing in popularity industrially (Christl *et al.*, 1989; Doran, 1995). For instance, BCRs have been utilised in ethanol fermentation and the production of acetic acid using *Acetobacter aceti*. Kantarci *et al.*, (2005) and Maceiras *et al.*, (2010) investigated the optimisation of aqueous phase systems in BCRs and reported that the systems' oxygen transfer and flow regimes are influenced by factors such as fluid properties, column geometry and sparger design.

2.2.1 Advantages of BCRs

Studies show BCRs to be advantageous over STRs in a number of areas, owing to their simple construction, with only a sparger at their base, and no mechanical agitators, keeping their maintenance and operating costs to a minimum (Maceiras *et al.*, 2010; Prakash *et al.*, 2001; Kohler, 1986; Christl *et al.*, 1989; Doran, 1995). Other advantages of BCRs include a superior gas dispersion efficiency, improved reactor performance and capacity (Kohler, 1986) as well as an improved oxygen transfer rate due to a greater interfacial area (Bouaifi *et al.*, 2001). It is against this background that BCRs are attractive in bioprocessing operations.

Pino *et al.*, (1992) and Kantarci *et al.*, (2005) reported that BCRs could be operated either in batch or continuous modes. In the batch operation process, the liquid suspension is inoculated first, and then air is sparged into the system continuously throughout the course of the reaction, while the liquid and gas are concurrently fed from the column base in a continuous mode. However, some disadvantages, like a higher superficial gas velocity, is required for adequate mixing during the operation (Kantarci *et al.*, 2005) which may consume too much energy to achieve good mixing and then this operational mode becomes uneconomical. In addition, some other difficulties in operations such as sterilisation and cleaning, especially for large columns, can complicate the use of BCRs.

2.2.2 Design of BCRs

Three BCR design parameters affect the rate of oxygen transfer (separately to reactor contents): the sparger design, the aspect ratio (height to diameter ratio) and column diameter (Lubbert *et al.*, 1996). Typical aspect ratios for industrial-scale BCRs used for bioprocess applications vary between 2 and 5. Large diameters are reported to be essential for operations at large gas throughputs. Taller columns however allow enough time for oxygen transfer, therefore improving the conversion of reactants to products.

According to Kantarci *et al.*, (2005), wall effects become apparent in small diameter (less than 15 cm) research purpose reactors, resulting in operating conditions significantly deviating from large column conditions and therefore producing results which are difficult to compare to larger reactor geometries.

In this study, a BCR designed by Wilhelm Burger, (2012), with a diameter of 15 cm and operating with a liquid height of 60 cm was used, giving an aspect ratio of 4, which falls within the specifications of the geometry of bioprocess application BCRs. A 14 cm porous sparger was selected to provide a large gas-liquid interfacial area for oxygen transfer in the system. The sparger covered almost the entire cross section area of the BCR. Porous spargers have an added advantage of producing high numbers of small sized bubbles (Kantarci *et al.*, 2005).

2.2.3 Flow regimes in BCRs

Some of the contributing factors when considering the performances of BCRs, besides the column geometry and the sparger design, include mixing as well as heat and mass transfer (Lubbert *et al.,* 1996). Depending on the superficial gas velocity and column diameter, three characteristic flow regimes are distinguishable; homogenous, heterogeneous and slug flow regimes (Camarasa *et al.,* 1999; Kantarci *et al.,* 2005). Classification of flow regimes in a BCR was reported by Ruzicka and collegues, (2001) based on the different behaviour of the interaction between the gas hold-up and the superficial gas velocity under different flow conditions. Other authors like Maceiras *et al.,* (2010) reported findings that support with this classification of regimes, by showing distinct flow regimes in diethanolamine (DEA) aqueous dispersions in a BCR.

Figure 2-1 shows the map of the three regimes within aqueous systems for prediction of the flow regime behaviour during BCR operation (Kantarci *et al.,* 2005; Deckwer *et al.,* 1980). The diagram shows that for aqueous systems in a 15 cm diameter BCR, the operation stays in the transition flow regime for most superficial gas velocities. The BCR flow regime maps as shown on Figure 2-1 are descriptive of aqueous phase systems, they therefore cannot be used to describe regime characteristics in systems containing hydrocarbons and yeast since the hydrodynamics and fluid properties are likely to be affected. The flow regimes which are displayed on the map are described in the succeeding sections.

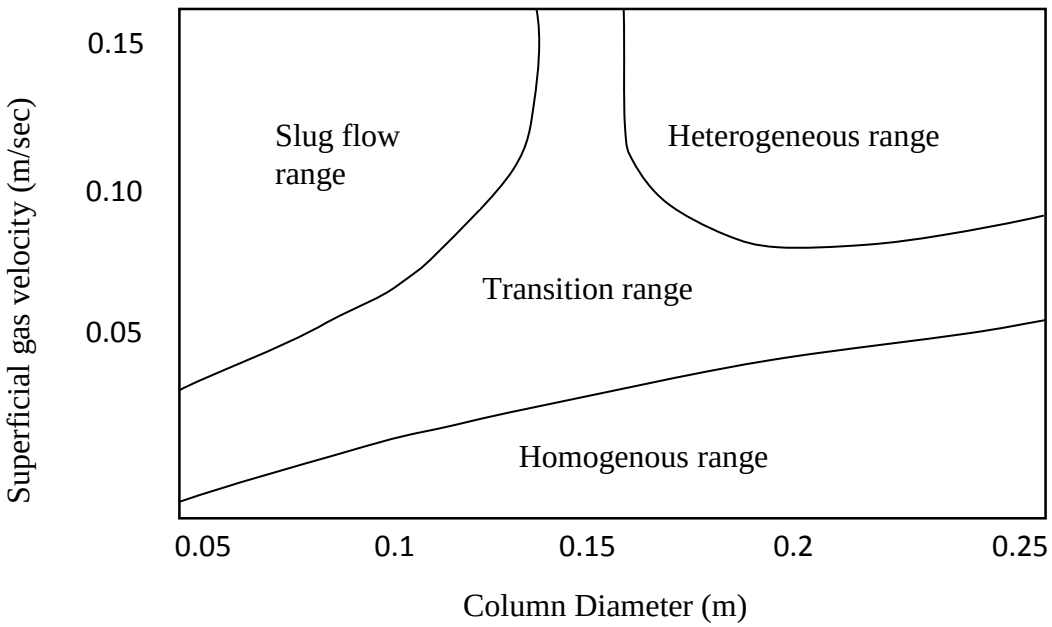

Figure 2-1: Flow regime map for bubble columns using aqueous media, Redrawn from Kantarci *et al.* (2005) and Deckwer *et al.* (1980).

2.2.3.1 The homogenous flow regime

The homogeneous (or bubbly) flow regime as shown in Figure 2-2 is characteristic of low superficial gas velocity in batch operations. The superficial gas velocity is said to be low when it is less than 0.05 m/sec (Kantarci *et al.*, 2005). The bubbles in this flow regime are evenly distributed across the BCR cross section and maintain their sizes as formed by the sparger (Kantarci *et al.*, 2005; Camarasa *et al.*, 1999). Since low the superficial gas velocity produces low mixing, the homogenous regime bubbles are almost uniform in size and have low interaction rates.

According to an investigation carried out by Maceiras collegues, (2010) on the influence on the bubble size distribution of height above the sparger in a BCR under a homogeneous regime, the bubble size distribution, although significantly varying at the beginning of the operation, ultimately reaches equilibrium and maintains a uniform bubble size as height increases above the sparger.

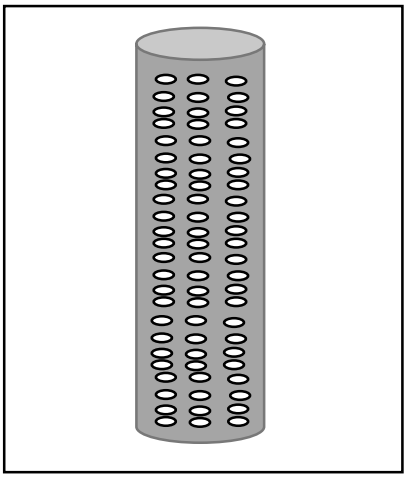

Figure 2-2: Schematic diagram of a BCR operating under homogenous flow regime. Redrawn from Camarasa *et al.* (1999) and Kantarci *et al.* (2005).

2.2.3.2 The heterogeneous flow regime

By increasing the superficial gas velocity, liquid recirculation starts to manifest, with system turbulence ultimately leading to the formation of large and small bubbles as bubbles begin to interact and coalesce. An in-between regime phase, called the transition regime is formed which changes to the heterogeneous (or churn-turbulent) flow regime when the superficial gas velocity is increased further (Camarasa *et al.*, 1999).

In the heterogeneous regime, depicted in Figure 2-3, the increase in the superficial gas velocity increases bubble interaction which in turn leads to bubble coalescence and the formation of larger bubbles. There is also simultaneous bursting of bubble films due to the increased system turbulence, and therefore formation of smaller bubbles. Thus the bubble size distribution is expanded, with significant differences from the sizes formed by the sparger. Increased gas hold up also becomes apparent in this flow regime. Since the heterogeneous regime consists of a range of bubbles sizes, modelling and calculation of the interfacial area must include different correlations for both small and large bubble sizes (Camarasa *et al.*, 1999).

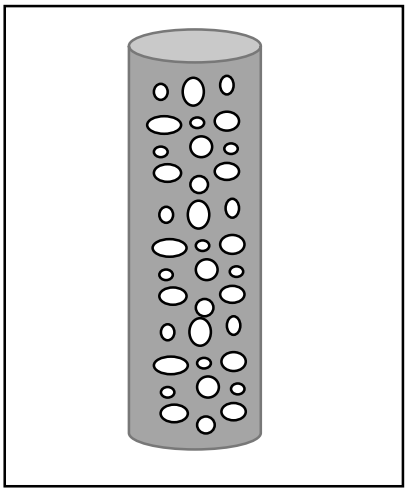

Figure 2-3: Schematic diagram of a BCR operating under heterogeneous flow regime. Redrawn from Camarasa *et al.* (1999) and Kantarci *et al.* (2005).

2.2.3.3 The slug flow regime

The slug flow regime is a result of the wall effects in small diameter (less than 15 cm) BCRs at high the superficial gas velocity. However, in the large diameter (greater than 20 cm) the slug flow does not occur (Kantarci *et al.,* 2005). The regime is unsteady and large bubbles (bubble slugs) are formed as large bubbles stabilise against the column walls (Hyndman, Larachi and Guy, 1997). The slug flow regime is diagrammatically represented on Figure 2-4.

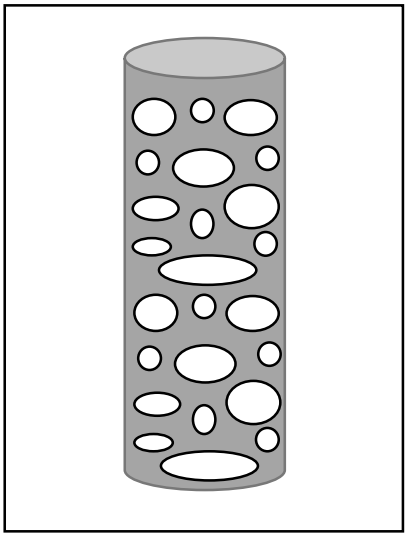

Figure 2-4: Schematic diagram of a BCR operating under the slug flow regime. Redrawn from Camarasa *et al.* (1999) and Kantarci *et al.* (2005).

According to Ruzicka collegues, (2001) an increase in superficial gas velocity initially increases the gas hold up in the homogenous flow regime. However, a further increase in the superficial gas velocity changes the flow regime from homogenous to heterogeneous, and the gas hold up drops. This influence on gas holdup of the superficial gas velocity affects the measurement of the interfacial area, and ultimately K_La. The superficial gas velocity is therefore a key parameter in the gas-liquid and liquid-liquid homogeneity of the system. However, it effects more than just spatial differences in the reactor, but also oxygen transfer, which will be discussed in detail in the following section.

2.3 Mechanism of oxygen transfer

The mechanism of oxygen transfer from the bubble to the oxygen reaction site within a cell involves several steps. These pathways of oxygen transfer will be described for the gas-aqueous-microbe systems as well as the hydrocarbons-aqueous-microbe systems.

2.3.1 Oxygen transfer in gas-aqueous-microbe systems

As oxygen moves from the air bubbles to the cells, it needs to overcome a series of resistances (boundary layers, the gas liquid interface and the bulk liquid phase). There are a total of eight steps which explain the mechanism of oxygen transfer from the gas bubble through the liquid, and ultimately to the site of oxidative phosphorylation in the cells (Doran, 1995), as shown in Figure 2-5.

Step 1: Oxygen diffusion from the gas interior to the gas-liquid interface
Step 2: Transfer across the gas-liquid interface
Step 3: Transfer through the stagnant liquid film around the gas bubble
Step 4: Diffusion through bulk liquid
Step 5: Transfer across stationary film around the cell clump
Step 6: Diffusion through solids-liquid interface of the cell
Step 7: Transport to an individual cell in a floc or cell clump
Step 8: Intracellular movement across cytoplasm to the reaction site of the cell.

Several system properties significantly influence the overall oxygen transfer rate. The factors include the composition of the components, the degree of mixing, bubble sizes and interfacial area (Doran, 1995).

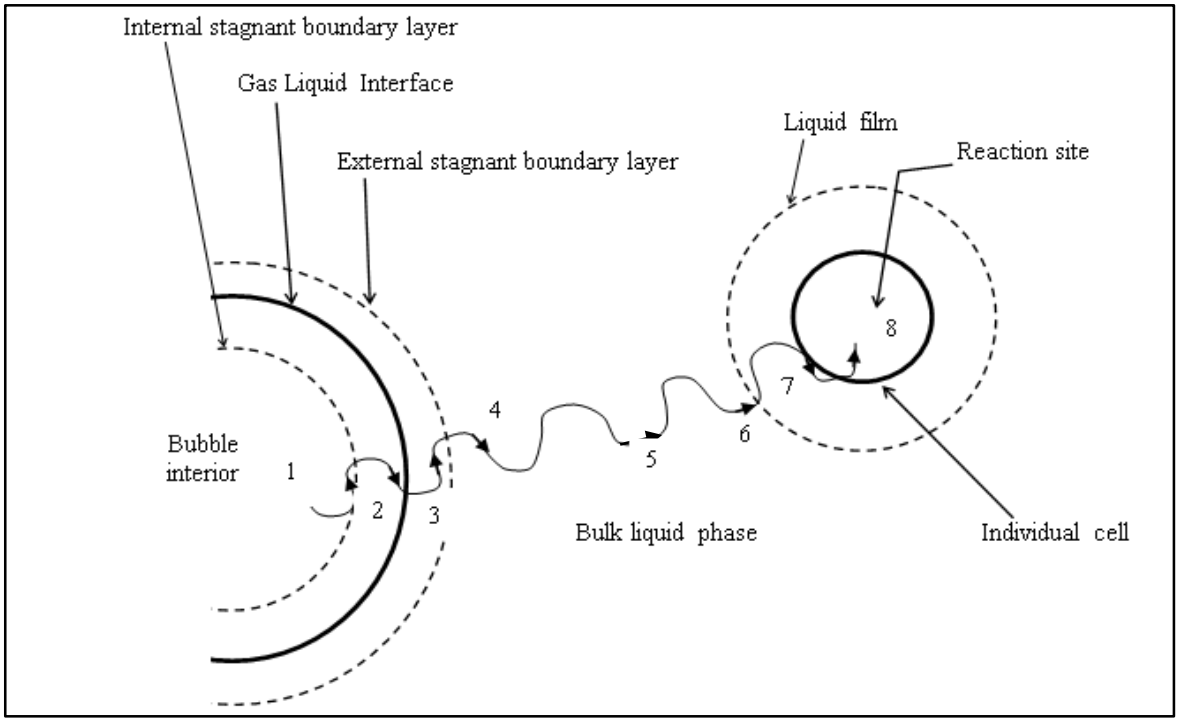

Figure 2-5: Steps necessary for oxygen transfer from gas bubble to cell. Redrawn from Doran, (1995).

2.3.2 Oxygen transfer in hydrocarbon- aqueous-microbe systems

The introduction of an immiscible hydrocarbon phase into the system has two contrasting effects on the system. Since oxygen is more soluble in the hydrocarbons than in water, adding alkanes has the potential to increase the oxygen transfer. However, there is need to offset the adverse effect of an increased viscosity as a result of the same added alkanes (Rols *et al.*, 1990). Based on that, the resultant effect, either an increase or decrease in oxygen transfer, will then be a function of the system hydrodynamics. The presence of the hydrocarbons introduces another parameter that influences the mechanism of the oxygen transfer from the gas bubble to the cells. Figure 2-6 shows the various possible paths for oxygen transfer in hydrocarbon, aqueous, and microbes system (Rols *et al.*, 1990). Five pathways of the oxygen diffusion in hydrocarbon, aqueous, and microbes system are described as following.

1) **Pathway one (Air bubble-water-cell).**

This pathway involves the transfer of oxygen from the air bubble, through the bulk liquid phase (water) to the cell. It is similar to the oxygen transfer in air, aqueous and microbe systems as described in Section 2.3.1.

2) **Pathway two (Air bubble-cell).**

In this pathway, the cell is attached to the air bubble surface, therefore oxygen diffuses directly from the gas bubble to the cell. According to Rols and colleagues (Rols *et al.*, 1990), microbial cells tend to adhere to the air bubble, thus resulting in a direct movement of oxygen to the cell.

3) **Pathway three (Air bubble-water-hydrocarbon-water-cell).**

This oxygen transfer pathway is mostly common in systems where the hydrocarbons form droplets in the water phase (Dumont and Delmas, 2003). The oxygen moves from the air bubble into the water phase and then transfers to the alkane droplet. It then leaves the droplet back into the water phase and then ultimately into the cells.

4) **Pathway number four (Air bubble-hydrocarbon-water-cell).**

When an alkane droplet is attached to the air bubble surface, oxygen diffuses from the bubble to the alkane phase directly and then through the bulk liquid to the cells. This pathway is also common for systems in which the hydrocarbons spread into a film around the air phase (Rols and Goma, 1989).

5) **Pathway number five (air bubble-hydrocarbon-cell).**

In this mechanism, the hydrocarbon phase lies in-between, and in contact with both the cell and the gas phase where the oxygen has to move directly from the air bubble to the hydrocarbon and finally to the cell.

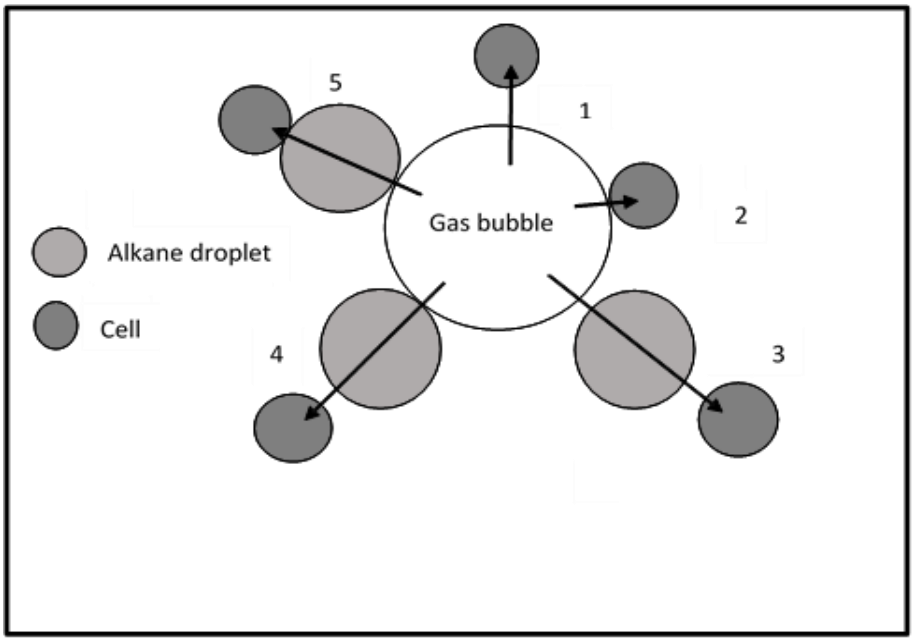

Figure 2-6: Pathways for the oxygen transfer from the bubble gas to the cells. Redrawn from Rols *et al.* (1990).

There is possible sixth pathway of oxygen transfer mechanism which is, however, not documented in literature in which the cell adheres to the hydrocarbon phase and remains detached from the air bubble. In such an instance, the oxygen moves from the gas bubble to the bulk liquid to the alkane phase and ultimately to the cells as shown in Figure 2-7.

The process conditions such as the oxygen solubility, the hydrocarbon interaction and the surface tension of the gas-hydrocarbon and gas-water interfaces determine the occurrence of oxygen transfer in one specific pathway.

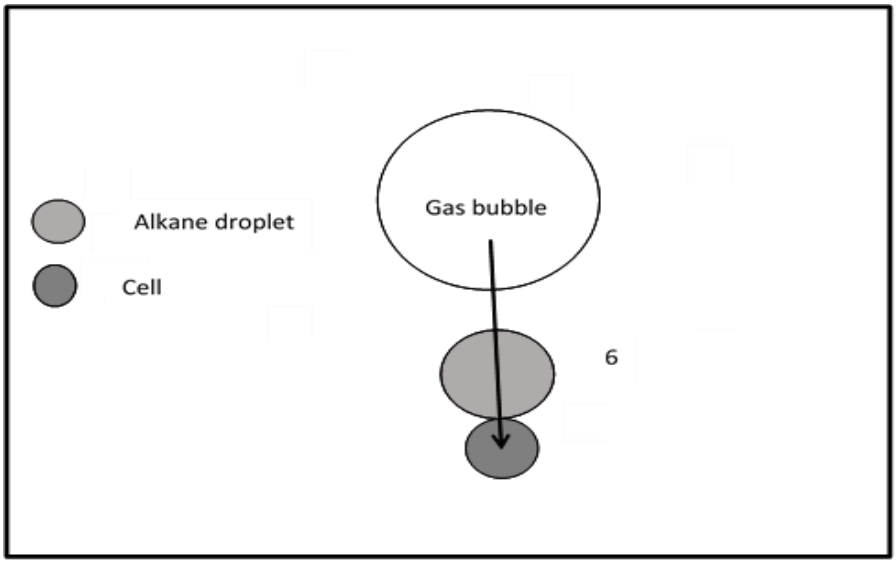

Figure 2-7: Sixth pathway for the oxygen transfer from the bubble gas through the bulk liquid to alkane phase and then to the cells. Redrawn from Rols *et al.* (1990).

2.4 The overall volumetric oxygen transfer coefficient (K_La)

The overall volumetric oxygen transfer coefficient (K_La) is an important parameter that controls the oxygen transfer rate and is quantified in terms of the gas-liquid interfacial area (a) and the oxygen transfer coefficient (K_L). K_La in bioprocesses is commonly measured through one of two physical methods: the gassing out procedure (GOP) and the pressure step procedure (PSP) (Garcia-Ochoa and Gomez, 2009), although other methods for K_La determination do exist. A significant advantage in employing these physical methods is that they do not affect the fluid properties and the behaviour of the oxygen transfer since they do not utilise any chemical reagents (Garcia-Ochoa and Gomez, 2009).The measurement of K_La with the GOP has been carried out successfully at high agitation rates, corresponding well to the BCR under consideration here (Correia and Clarke, 2009). The GOP method involves the measurement of the dissolved oxygen (DO) response to a step change in the sparged gas composition (from pure nitrogen to air) (Correia and Clarke, 2009). This study utilises the GOP method, since it is simple enough to be performed in the test reactor, and is sufficiently sensitive to illuminate the effects of the system parameters.

The determination of K_La using the GOP with first order model, as well as with the effect of the probe constant (K_P) derived in the second order model will be further explained.

2.4.1 Measurement of K_La using the GOP method fitted to a 1st order model

The GOP is the most commonly accepted method for K_La measurement (Doran, 1995).The procedure starts with eliminating the system oxygen by sparging nitrogen into the reactor. Then the step change in gas composition is introduced by sparging air, whilst maintaining the aeration rate. The probe response to the DO is recorded whilst sparging air until a point of system oxygen saturation (Correia and Clarke, 2009; Garcia-Ochoa and Gomez, 2009). The K_La is then determined from DO data by the linearization of the first order model as seen in Equation 2-1 (Doran, 1995).

The first order model follows the form:

$$\frac{dC}{dt} = K_L a(C^* - C) \qquad \text{Equation 2-1}$$

Where C is the actual DO concentration and C* is the saturation oxygen solubility in the system.

While the use of the first order model is common in the literature, Correia and colleagues (Correia and Clarke, 2009) reported that the method could underestimate K_La measurement by up to 49% in aqueous-hydrocarbon dispersions. There is therefore a need to utilise a more accurate model to extract the value of K_La from the experimental data. One such method, taking into account the response lag of the DO probe, has been proposed and extensively used in the literature (Correia and Clarke, 2009; Clarke and Manyuchi, 2012).

2.4.2 Measurement of K_La using the GOP method with incorporation of K_P

Measurement of DO is done with polarographic probes which make use of a membrane-covered solid electrode system (Benedek and Heideger, 1970). A reduction at the cathode causes a current which the probes detect for DO measurement as described in Appendix 9.6. During transient GOP phases, a time lag (τ_P) occurs with the DO reading as a result of a resistance caused by the membrane around the electrode. K_P, the inverse of τ_P, is defined as the probe response constant. Liquid properties have been found to significantly affect τ_P by changing the system parameters. Based on these observations, Clarke and Manyuchi, (2012) reported that the alkane concentration and long alkane chain length significantly affect K_P, and so K_P must be taken into account when calculating K_La in aqueous-hydrocarbon systems.

The depression in K_P can be ascribed to an increase in fluid viscosity which obstructs oxygen transfer to the probe (Dang, Karrer and Dunn, 1977).

In order to take this effect into account, the measurement of τ_P is conducted by transferring the DO probe from a 0% DO system to an oxygen saturated system at 100%. The 0% DO system is obtained either by using a nitrogen sparged vessel or a saturated solution of sulphide (Na_2SO_3) (Clarke and Manyuchi, 2012; Nakanoh and Yoshida, 1980; Benedek and Heideger, 1970). The probe constant is modelled as a first order response, given in Equation 2-2, where C_p is the DO concentration recorded by the probe.

$$\frac{dC_p}{dt} = K_p\left(C - C_p\right) \qquad \text{Equation 2-2}$$

Ultimately, incorporating Equation 2-2 into Equation 2-1 produces the second order model (Equation 2.3) as is given below.

$$\%DO_{2nd} = C_P/C_P^* = 1 - \frac{1}{K_P - K_L a}\left(K_P e^{-K_L a t} - K_L a e^{-K_P t}\right) \qquad \text{Equation 2-3}$$

In this methodology, K_P has to be measured for each experimental condition to ensure the accuracy of the K_La measurement (Clarke and Manyuchi, 2012). The integrating process of the second order model is detailed in Appendix 9.4.

2.5 The interfacial area

The interfacial area (a) is determined from the fractional gas hold-up (ε_G) and the Sauter mean bubble diameter (D_{32}). Once the interfacial area is determined, the volumetric overall oxygen transfer coefficient (K_La) (calculated from the data as described in Section 2.4.2) is then used to estimate the oxygen transfer coefficient (K_L). Measurements of interfacial area in multiphase systems in recent times have been done through the use of high speed digital photography. Mena *et al.* (2005), measured the interfacial area in a BCR containing water, air and calcium alginate beads and reported that the high speed cameras presented challenges in removing the optical distortion from the curved reactor as well as needing sufficient light for capturing clear images and accurately analysing the resultant images. To address these challenges, Galindo and colleagues (Galindo *et al.*, 2005), designed a water filled square Perspex box that removes the optical distortion from the curved reactor. They also developed a computerised program for

image analysis that enhances the quality of the images to calculate the correct bubble sizes. In a related study by Galindo *et al.* (2005), employed a stereoscope microscope and connected it to a video camera, creating a versatile, reproducible and a wide ranging method for interfacial area measurement in multiphase systems.

Correia *et al.* (2007), developed a MATLAB® code, recently modified by Hollis and Clarke, (2016) to enhance the image analysis of the bubbles. The images were captured by a high speed camera and enabled the calculation of the projected area (A_P) of the bubbles. The A_P extracted by the code provides the bubble Feret diameter (D_F), which is also referred to as the equivalent bubble diameter, and was computed according to Equation 2-4 (Mena *et al.*, 2005).

$$D_F = 2\sqrt{\frac{A_P}{\pi}} \qquad \text{Equation 2-4}$$

The Sauter mean diameter (D_{32}) which is a statistical average of bubble diameters in the system, is calculated from Equation 2-5 (Junker, 2006; Das *et al.*, 1985; Bouaifi *et al.*, 2001).

$$D_{32} = \frac{\sum_{i=1}^{N} n_i D_{F,i}^3}{\sum_{i=1}^{N} n_i D_{F,i}^2} \qquad \text{Equation 2-5}$$

The gas hold up (ε_G), which is the volume fraction of the gas phase in the bioreactor at any point, is calculated according to Equation 2-6 (Schugerl, 1980; Dhanasekaran and Karunanithi, 2012).

$$\varepsilon_G = \frac{H - H_0}{H} \qquad \text{Equation 2-6}$$

Where H_o is the height of reactor liquid at steady state without aeration and H is the liquid height when the reactor is sparged with air.

The interfacial area is then calculated from the values of D_{32} and ε_G according to Equation 2-7. The equation is only valid when an assumption that all the bubbles detected were spherical (Fukuma *et al.*, 1987; Kawase *et al.*, 1987; Wilkinson *et al.*, 1994; Tobajas *et al.*, 1999; Mouza *et al.*, 2005; Correia *et al.*, 2007).

$$a = \frac{6\varepsilon_G}{D_{32}} \qquad \text{Equation 2-7}$$

2.6 Effects of different variables on K_La and interfacial area

Several studies have reported that K_La and the interfacial area in aqueous-hydrocarbon-microbe systems are significantly affected by three operating factors, namely: the alkane concentration, the agitation rate and the solids loading (Clarke and Correia, 2008; Hollis and Clarke, 2016; Hassan and Robinson, 1977). However, since BCRs do not have mechanical impellers, mixing is totally dependent on the aeration rate (characterised by the superficial gas velocity). These critical parameters, which influence K_La and the interfacial area, will be discussed in the subsequent sections.

2.6.1 Influence of the alkane concentration on K_La and the interfacial area

The literature reports that K_La is affected by the alkane concentration in the system. K_La can be separated into its constituent parameters, K_L and the interfacial area (a), both of which are related to the fluid properties (such as surface tension and viscosity). For instance, an increase in alkane concentration decreases K_L. In the review by Clarke and Correia, (2008), a decrease in K_L of 44%, 50% and 62.5% was reported upon the addition of n-hexanol, n-heptanol and n-octanol.

Alkane concentration has been seen to effect surface tension in aqueous-hydrocarbon systems (Clarke and Correia, 2008; Clarke and Manyuchi, 2012). It is therefore apparent that low surface tension allows the escape of bubbles at smaller sizes (Kazakis, Mouza and Paras, 2008). The smaller bubbles, which form as a result of a lower surface tension, have slower rise velocities and hence longer residence times. For a constant sparging rate, the decrease in bubble size results in more bubbles which increase the gas hold up due to their longer residence time (Asgharpour, Mehrnia and Mostoufi, 2010), and therefore increase the interfacial area (Garcia-Ochoa and Gomez, 2009). Increasing hydrocarbon concentration in water reduces the water-hydrocarbon system surface tension since the added hydrocarbon acts like a surface active agent (Rols *et al.*, 1990). Researchers have shown that addition of alkanes to a system increases the interfacial area available for oxygen transfer (Rols *et al.*, 1990). Queimada *et al.* (2004) found a linear relationship between the natural logarithm of surface tension and the reciprocal of viscosity for pure n-alkanes.

The work by Correia *et al.* (2010) augmented previous studies by reporting a decrease in the bubble size on increasing alkane concentration up to 5% (v/v), which increased the interfacial area. However, a further increase in alkane concentration beyond 5% (v/v) reportedly decreased the interfacial area as a result of a decline in the gas hold up, as fluid properties such as viscosity and surface tension were affected.

A recent study by Hollis and Clarke, (2016) in a four phase system (air, water, hydrocarbons and yeast loading) in an STR reported the effect of alkane concentration on K_La and interfacial area. K_La increased with an increase in alkane concentration until 11% (v/v) and declined with further increases in alkane concentration at a constant yeast loading of 5 g/l. On the other hand, an inverse relationship was found between alkane concentration and interfacial area at similar yeast loading rates.

2.6.2 Influence of yeast loading on K_La and the interfacial area

To simulate the influence of solids loading on oxygen transfer in bioprocess systems, solids such as non-viable yeast, calcium alginate beads and cornflour have been added to elucidate their effect. The purpose of using non-viable cells instead of living cells is to eliminate the oxygen utilisation rate, so that the oxygen transfer rate can be accurately measured. Solids alter the system properties, which in turn affect K_La. The behaviour of solids in a bioprocess system is a result of a range of factors, including: solids type, solids density (ρ), solids loading (wt%), activity, and particle size distribution (D_P). Mena *et al.* (2005) reported the presence of a depressive effect on K_La by changing both the K_L and the interfacial area when the solids (calcium alginate beads) with size of 1.2 mm and 2.1 mm were added (0 to 10 vol%) in a BCR. These findings were supported by Clarke and Manyuchi, (2012) who found a decrease in K_La from 0.05 s^{-1} to 0.025 s^{-1} when solids particles were increased from size of 3 µm ($CaCO_3$) to 14 µm (corn flour) in a system containing 2.5% (v/v) $C_{14\text{-}20}$ at a solid loading of 1 g/l.

Solids loading also causes an increase in system viscosity, thereby inflicting a depressive effect on the K_La (Galaction *et al.*, 2004; Cascaval *et al.*, 2006). By increasing the viscosity of the bioprocess system, the solids affects the oxygen transfer by increasing bubble coalescence as well as reducing the bulk liquid turbulence.

Investigations by researchers such as Galaction *et al.* (2005) and Cascaval *et al.* (2006) to establish the effect of nonviable microbial cells on oxygen transfer on hydrocarbon bioprocess systems were done in stirred tank reactors (STRs). The yeast in both investigations was applied after deactivating by 0.2% pyrogallic acid and 0.4% potassium hydroxide. However, the findings of these surveys on the oxygen transfer may be different to BCRs since the two types of reactors have different mixing mechanisms.

An attempt by Jhawar and Prakash, (2011) to investigate the effect of non-viable yeast cells (0.1 -0.4 wt%) on the oxygen transfer on an aqueous-hydrocarbon system in a BCR faced the challenge of excessive foaming. The existence of foam could suggest the presence of proteins in the medium, potentially from the lysis of cells during deactivation. In this case, the results are of limited use, since proteins act as surface active compounds, changing K_La, and lysed cells will affect the system differently to whole cells.

According to a recent study by Hollis and Clarke, (2016) on the influence of yeast loading on K_La and the interfacial area in a multiphase system (air, water, hydrocarbons and yeast loading) in an STR, an increase in yeast loading resulted in a decrease in K_La at a constant alkane concentration of 11% v/v. The same study also found yeast loading to be inversely related to the interfacial area at the same alkane concentration of 11% v/v. This is in agreement to several findings by different researchers such as Prakash *et al.* (2001), Hyndman *et al.* (1997) and De Swart *et al.* (1996) who observed an increase in D_{32} with increasing solid concentrations due to increased bubble coalescence in the system.

It can be concluded that the presence of solids particles in the hydrocarbon system can affect the oxygen transfer. In this study, non-viable microbes (*Saccharomyces cerevisiae*) of approximately 5 µm size and concentration range of 0.5 g/l to 6 g/l were used to investigate the influence of solids loading on the oxygen transfer in a BCR.

2.6.3 Influence of superficial gas velocity on K_La and the interfacial area

The aeration rate (and by implication the superficial gas velocity) is a critical parameter which influences the mixing mechanisms in a BCR since BCRs do not use mechanical agitation like STRs. Based on that, an increase in the aeration rate results in an increase in fluid mixing, and hence an increase the K_La in BCRs (Vandu, Koop and Krishna, 2004). Nguyen-tien *et al.*

(1985) confirmed the same findings and concluded that increasing aeration rate increases the penetration of the liquid-side diffusion film, ultimately enhancing $K_L a$.

Ruzicka *et al.* (2001) defined the effect of the superficial gas velocity on the oxygen transfer in a BCR by constructing a diagram illustrating the relationship between the superficial gas velocity and gas holdup (Figure 2-8). The diagram shows that an increase in the superficial gas velocity causes an increase in gas hold up, which translates to an increase in interfacial area when in the homogenous flow regime. However, a further increase in the superficial gas velocity changes the flow regime and the curve attains a maximum in the transition regime after which the gas hold up decreases with continued increase in the superficial gas velocity. Further increase in the superficial gas velocity changes the flow regime from transition to heterogonous flow. Maceiras *et al.* (2010) suggested that the increase in interfacial area in the homogenous flow regime was a result of increasing of gas hold-up and decreasing bubble size as bubbles break up with increasing the superficial gas velocity.

From the results above, it is apparent that the superficial gas velocity is an important parameter in BCR operation since mixing depends on aeration rate. In this study mixing is an important parameter for another reason: the aqueous and hydrocarbon phases tend to separate and so in order to operate within a spatially homogenous regime, the mixing (and therefore aeration rate) must be sufficient to achieve this homogeneity. Therefore in this study comparatively high aeration rates will be required to achieve sufficient mixing for spatial homogeneity to be achieved. The generalised flow regimes for aqueous phase systems in BCRs as influenced by gas hold up and superficial velocity as shown in (Figure 2-8) cannot however fully describe either three or four phase systems since it is based only on aqueous-gas systems. There is therefore significant work still required to understand the flow regimes and mixing patterns in three and four phase systems, particularly within a BCR.

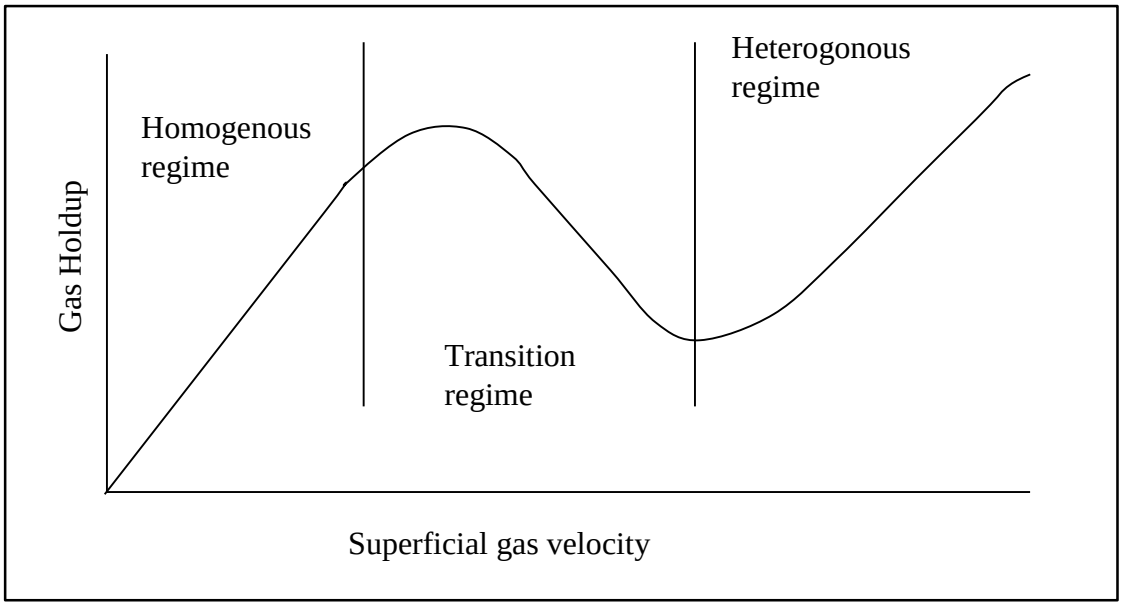

Figure 2-8: Generalised flow regime map. Redrawn from Ruzicka *et al.* (2001).

2.7 Literature Summary

Some fundamental conclusions can be made from the literature about the conversion of low value hydrocarbon substrates into high value products, through biologically-mediated oxidation. The availability of linear alkanes and their potential for use as feedstock in the production of valuable products presents significant motivation to study conversion bioprocesses. However, the work is not without challenges. The major challenge in the application of the available technologies is the limitation of oxygen transfer in the process.

Understanding of the oxygen transfer rate is the key to enhancing the bioconversion process. Operation parameters like solids loading, alkane concentration and superficial gas velocity, when properly modelled, can shed light on the behaviour of oxygen transfer in a multiphase hydrocarbon bioprocess system. Previous work by researchers like Clarke and Correia, (2008), Correia and Clarke, (2009), Correia *et al.* (2010), Clarke and Manyuchi, (2012), and Hollis and Clarke, (2016) on oxygen transfer in hydrocarbon bioprocesses in stirred tank reactors can be used as a foundation to understand the oxygen transfer in the bubble column reactors.

Several theories exist for the mechanisms of oxygen transfer in hydrocarbon-based systems, however oxygen transfer is likely to occur in various ways, making its determination a challenging process. This has seen the measurement of oxygen transfer evolving by the development of the second order model combining the overall volumetric transfer coefficient (K_La) and the probe constant (K_P). This improves accuracy in the determination of the oxygen transfer and therefore contributes to the overall understanding of the compound nature of the multiphase systems.

This study is the first to use four phases (air, water, hydrocarbons and yeast loading) in a bubble column reactor. Previous studies Hollis and Clarke, (2016) with similar conditions were done in stirred tank reactors therefore work will be done in migrating some of their findings to provide a basis for the study of multiphase systems in bubble column reactors, although their hydrodynamics are different. This investigation will provide an understanding of the behaviour of K_La and the interfacial area in a multiphase hydrocarbon based bioprocess system in a bubble column reactor.

3. RESEARCH HYPOTHESES AND OBJECTIVES

3.1 Hypotheses

Hypotheses were crafted based on the outcomes of the literature review and focus mainly on the impact of the operational parameters (alkane concentration, yeast loading and the superficial gas velocity) on both the interfacial area and K_La in a BCR. Any impact of each parameter on the interfacial area would eventually influence K_La as well.

Hypothesis 1: Superficial gas velocity is the only parameter that enhances the mixing in the BCR, since the BCR does not have impellers like the stirred tank reactor. Mixing will require an optimal superficial gas velocity to achieve homogeneity, especially when the process contains immiscible liquid.

Hypothesis 2: An increase in the superficial gas velocity results in an increase in the interfacial area as well as in K_La. It was found in literature that the increase in the turbulence results in bubble break up which will reduce the average bubble size and therefore increase the gas hold up. This increase in the gas hold up, as well as the decrease in the bubble size, will then increase the interfacial area in the system and therefore enhance the value of K_La.

Hypothesis 3: An increase in alkane concentration would initially enhance the interfacial area and K_La values, followed by a decrease in both the interfacial area and K_La, when alkane concentration further increases. This is due to the change in the fluid properties such as viscosity and surface tension, which effect the bubble coalescence and therefore the bubble size and the gas hold up.

Hypothesis 4: An increase in the yeast loading decreases the interfacial area and K_La. This was reported in literature to be as a result of an increase in D_{32} which ultimately reduces the interfacial area in the system and therefore the value of K_La.

3.2 Research Aims and Objectives

The main objectives of this work are to determine the effect of alkane concentration, solids loading as well as superficial gas velocity on the interfacial area and ultimately the behaviour of K_La in a four phase system (air-water-hydrocarbons-deactivated yeast) in a bubble column reactor. As a pathway to investigating the four phase system in a bubble column reactor, the K_La in two-phase (air-water) and three-phase (air-water-deactivated yeast and air-water-hydrocarbon) systems were investigated first. In order to achieve this overarching aim, the following objectives were defined:

1. To measure the effect of the probe constant (K_P) for each set of experimental conditions so that K_La can be accurately determined.
2. To calculate the K_La of each system with the incorporation of K_P.
3. To evaluate the K_La under different conditions of alkane concentration, yeast loading and superficial gas velocity.
4. To assess the spatial liquid-liquid homogeneity of the system under each condition.
5. To determine the Sauter mean diameter (D_{32}) of the gas phase under each condition using high speed photography and image analysis.
6. To calculate gas hold-up ε_G by measuring the changes in the liquid level in the reactor.
7. To calculate the interfacial area using D_{32} and gas hold-up ε_G.
8. To evaluate the effects of alkane concentration, solids loading and superficial gas velocity on the interfacial area.

4. MATERIALS AND METHODOLOGY

4.1 Materials

The study was developed in a model hydrocarbon-based bioprocess system comprising four phases, namely: deionised water, compressed air (from the laboratory reticulation), an alkane mixture and deactivated yeast cells in a bubble column reactor. The hydrocarbon composition as well as deactivated yeast biomass are explained in Sections 4.1.1 and 4.1.2 respectively.

4.1.1 Hydrocarbon mixture

The hydrocarbon mixture used in this study was supplied by Sasol Wax (via Organic Synthesis), South Africa. A straight chain hydrocarbon n-$C_{14\text{-}20}$ cut was employed for the experimental study. The cut was analysed using gas chromatographic analysis (Hollis and Clarke, 2016), and the composition is shown in Table 4-1.

Table 4-1: Composition of the hydrocarbon cut, n-$C_{13\text{-}21}$.

Name	Chain length	Composition %
n-Tridecane	n-C_{13}	0.81
n-Tetradecane	n-C_{14}	28.06
n-Pentadecane	n-C_{15}	26.62
n-Hexadecane	n-C_{16}	22.67
n-Heptadecane	n-C_{17}	15.51
n-Octadecane	n-C_{18}	5.37
n-Nonadecane	n-C_{19}	0.82
n-Eicosane	n-C_{20}	0.10
n-Heneicosane	n-C_{21}	0.03
Impurities		6.00

4.1.2 Deactivated yeast

Fresh wet viable yeast (*Saccharomyces cerevisiae*) was supplied by Anchor Yeast, Cape Town, and kept refrigerated at 4°C until use. Three samples of the wet yeast were dried at 60°C overnight to quantify the moisture content, as shown in Table 4-2, so that a dry biomass equivalent could be used for experimentation.

Table 4-2: Moisture content in yeast.

Sample number	Wet weight	Dry weight (g)	Weight of water (g)	% moisture
1	10	5.98	4.03	40
2	15	7.75	7.25	48
3	20	11.00	9.00	45
			Average	44

The yeast cells were deactivated to prevent oxygen utilisation through cell respiration, which would introduce uncontrolled variations in the oxygen transfer rate and ultimately influence results. Deactivation was carried out through a modified version of the thermal shock method developed by Hollis and Clarke, (2016), described as follows.

A pre-weighed quantity of wet yeast biomass was measured into a 500ml glass beaker containing 200ml of saline solution (0.9% (w/v) sodium chloride). The beaker was then placed on a hot plate/magnetic stirrer (VELP) and heated to 75°C while stirring. After 60 minutes of heating and stirring, the mixture was then cooled until it reached 25°C. The cooled mixture was then transferred to 50 ml Eppendorf centrifuge tubes and centrifuged (Eppendorf 5702 R) at 14000 RPM for 5 minutes to form yeast pellets. The saline solution was then removed from the Eppendorf using a Pasteur pipette, leaving only the yeast pellets in the tubes. The Eppendorf tubes were filled again with deionised water and vortexed to resuspend the yeast. After suspension, the mixture was centrifuged at the same conditions as before. This washing procedure was repeated two further times in order to ensure that all lysed cell proteins were removed, in order to prevent foaming in the BCR.

To verify that the yeast was successfully deactivated, two samples of the yeast suspension were taken before and after the deactivation process. The samples were plated onto potato dextrose agar and incubated (Labcon Orbital Shaker Incubator) at 30°C for a 72 hour incubation period

and compared for growth. There was no growth on the deactivated sample, confirming that the deactivation method was successful, as compared to the active sample which showed significant growth (Figure 4-1).

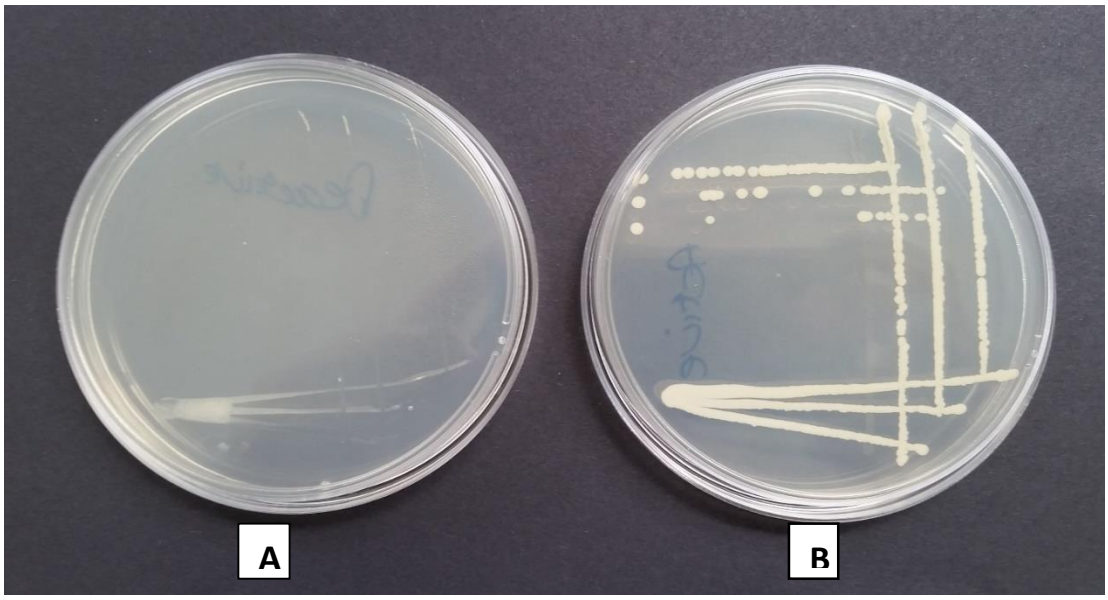

Figure 4-1: Yeast cells before (B) and after (A) deactivation process.

The yeast samples were also examined using light microscopy (Zeiss AxioStar Plus binocular) at 400X magnification to confirm that the cells remained whole, and were not disintegrated by the deactivation process. Figure 4-2 shows that the cells were not disintegrated after the deactivation process.

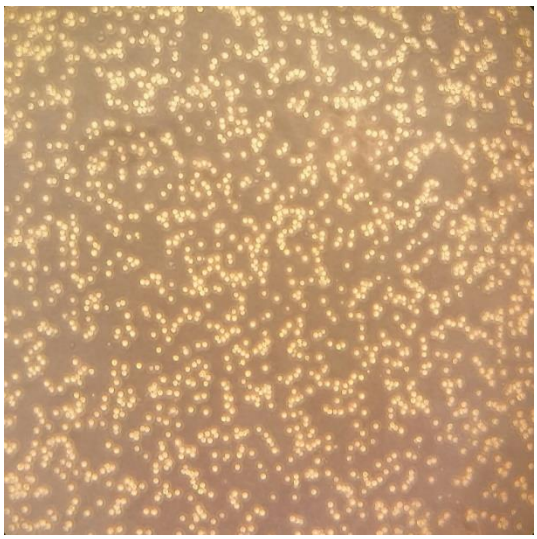

Figure 4-2: Cells of the deactivated yeast sample as viewed under a microscope (400X).

4.2 Methodology

4.2.1 Experimental setup

The BCR is schematically illustrated in Figure 4-3 was used to conduct the experiments. The BCR (3) was designed by Wilhelm Burger, (2012), with an inner diameter of 15 cm and liquid working height of approximately 65 cm. The column was made up of two identical glass cylinders of 45cm each, connected at the central part with stainless steel rings to give a total height of 90 cm. A sparger (4) with a diameter of approximately 14 cm was fitted to the column bottom, through which compressed air was sparged into the system.

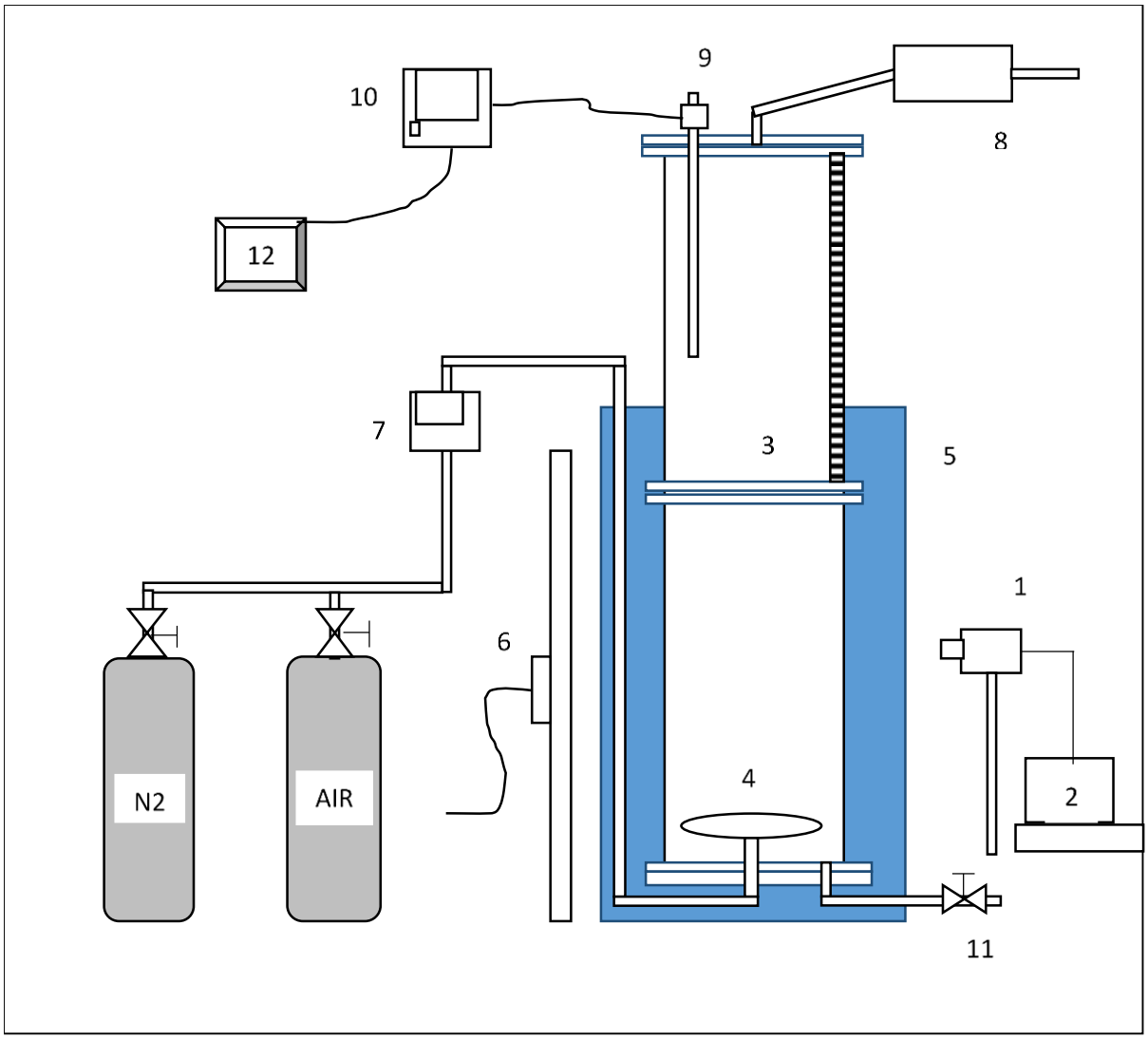

Figure 4-3: Schematic diagram illustrating the Bubble Column Reactor set-up.

A flow meter (7) (Cole-Parmer 150mm) was used to measure the compressed air flowrate. Its calibration curve is provided in Appendix 9.8. At the top of the column, an air outlet made provision for the escape of undissolved air. The air outlet was then connected to a condenser (8) which condensed and trapped the alkanes to prevent them from exiting into the laboratory environment, as well as to keep the system composition constant. An outlet (11) was provided at the reactor bottom for discharge of the slurry after the experiment.

The BCR was positioned inside a Perspex box (5), which was filled with water to remove the optical distortions of the curved cylindrical surface of the BCR. The Perspex box was also used to keep the temperature of this system constant at 22 ± 0.5^{o}C. To control the temperature in the Perspex box, a centrifugal pump was used to circulate hot water from an external water bath (temperature controlled) through a coil to heat water in the perspex box.

A panel of white light-emitting diodes (6) (LEDs) of voltage 12V and a power supply of 12V×120W were used to provide enough light for the image processing. LED strip-lights were secured to an aluminium sheet and then placed at the back of the reactor, outside the Perspex water bath. To avoid interference from the room light, a dark environment was created by designing a wooden frame in which the set-up was placed as shown in Figure 4-4. This controlled light environment served to enhance image outline of the gas bubbles.

A high-speed camera (1), model mvBlueFOX-124G, placed 30 cm in front of the column was used to capture the system images. It was set up on a set up on a tripod 30 cm above the sparger. The camera was further connected to a computer (2) which kept and processed the images using the mvImpact Acquire software. The camera specifications are described in Appendix 9.5.

To measure *Kp* and $K_L a$, a Metter-Toledo InPro 6800 polarographic oxygen sensor (9) fitted with a Teflon membrane was inserted through the reactor lid into the system. The sensor was in turn directly connected to a Mettler-Toledo M300 analytical transmitter (10) as described in Appendix 9.7. The data logger device (IFC 200/202 USB, supplied by MadgeTech) was connected from the transmitter to the computer to store data from the transmitter every 5 seconds.

Figure 4-4: Photo of the experimental set up inside the light control box.

4.2.2 Experimental procedure

The BCR was rinsed with deionised water to remove any residual solids and alkane from previous experiments before beginning new experiments. The Perspex box was then filled with water and the temperature in the water bath set at 22^{o}C. Yeast deactivation was conducted as described in section 4.1.2. The reactor was then filled with the required amount of water, deactivated yeast and hydrocarbons as per experimental run, and the liquid height was measured. The reactor lid was then secured, and gas outlet was connected to the condenser. After measuring the liquid height, the gas inlet was opened and adjusted according to the desired superficial gas velocity for each experimental condition. Sparging was continued for ten minutes before measurements of the gas hold up.

The liquid heights, both before and after sparging, were measured in order to determine gas hold up. After which DO measurements were collected, in triplicate to ensure repeatability of the experiments, in order to calculate both K_P and K_La.

For image analysis, the experimental set up was covered with a wooden box to enhance image capture. The high-speed camera was then positioned in front of the reactor and connected to the computer. For each experimental run, 45 images were captured. At the conclusion of each run the column was drained, cleaned and filled with 1 litter of a dilute bleach solution (sodium hypochlorite 5% v/v) to protect the sparger from microbial growth.

4.3 Measurement of the liquid-liquid spatial homogeneity

Liquid-liquid homogeneity was mesured using a physical sampling methodology. Firstly, the hydrocarbons were coloured with a dye (0.125 g/l) (Red Oil O), supplyed by Sigma-Aldrich before they were added to the reactor. After addition to the reactor and the system sparged for 10 minutes to reach steady state, a total of 5 x 50 ml volume samples of reactor fluid were withdrawn using a syringe. The syringe was connected to a stainless steel tube which was fitted to the reactor lid, 10 cm above the sparger. The samples were then allowed to settle in a measuring cylinder, allowing the two phases (water – with or without solids – and coloured oil) to separate and the volume of each phase was measured. For this study a measure of homogeneity was defined as the measured percentage of hydrocarbon in a sample, over the total BCR hydrocarbon concentration, according to Equation 4-1. Homogeneity was considered to be attained if the percentages of oil in the reactor and the measuring cylinder were equal. This was achieved by increasing the superficial gas velocity, thereby increasing oil dispersion in the reactor until it became homogenous. The superficial gas velocity at which homogeneity occurred was recorded as the minimum superficial gas velocity required for sufficient mixing.

$$\text{Homogeneity\%} = \frac{\left(\frac{Vh_c}{Vw_c+Vh_c}*100\right)}{H\%_r} * 100 \qquad \text{Equation 4-1}$$

Vh_c Volume of the hydrocarbon in the measuring cylinder

Vw_c Volume of the water in the measuring cylinder

$H\%_r$ Hydrocarbon concentration in the reactor

4.4 Measurement of the overall volumetric oxygen transfer coefficient (K_La)

The measurement of K_La using the GOP and the first order response model is described in Section (2.4.1), the measurement of the probe response lag time and its inclusion to formulate the second order for accurate measurement of K_La is described in Section (2.4.2). These measurements will be further discussed in the following sections.

4.4.1 Measurement of the probe response lag time

The probe response lag time (τ_P), the inverse of the probe constant (K_P), was measured using DO data under each experimental condition. The K_P was determined by first placing the probe within a vessel sparged with nitrogen, to give a 0% DO concentration (i.e. where C=0). The probe was then quickly transferred into the air-sparged BCR containing the experimental conditions at oxygen saturation (i.e. where C=C*). To facilitate a quick transfer, and to reduce the effect of transfer time, the nitrogen sparged vessel was positioned as close to the BCR as possible. The time taken to move the DO probe from the nitrogen vessel to the BCR (dead time) was approximately 2 seconds. DO data was then recorded via Data-logger until it reached the saturation concentration and then stored in the computer.

The probe constant was then calculated by integrating Equation 2-2 with C = C* to produce Equation 4-2. The rate of response of the DO was recorded every 5 seconds until the probe reached the oxygen saturation point (100% DO) in the system. K_P was determined as the gradient by plotting a graph of $\ln\left(1-\frac{Cp}{C^*}\right)$ against time as illustrated in Figure 4-5.

$$ln\left(1-\frac{Cp}{C^*}\right) = -Kp.t \qquad \text{Equation 4-2}$$

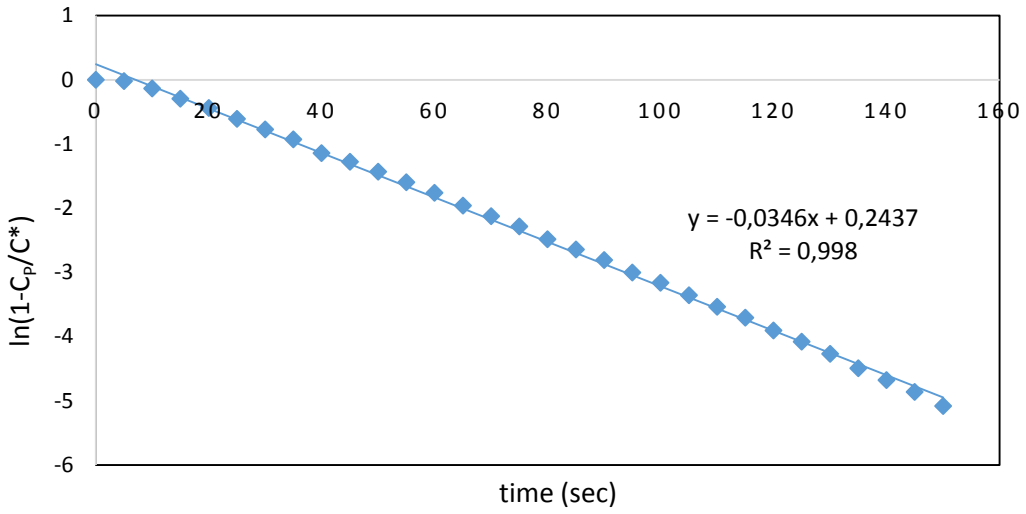

Figure 4-5: Graph illustrating the method for determining *Kp* from DO data using linear regression of a first order probe response model, at alkane concentration of 7.88% v/v, yeast loading of 1.62 g/l and u_G of 1.62 cm/sec.

4.4.2 Measurement of K_La using the gassing out procedure and the first order response model

As first, and potentially inaccurate, method for determining K_La from DO data, a first order model which assumes a negligible response lag time was used. This first estimate was then improved using a second order model which does not make this assumption but incorporates the effect of K_P, as discussed in Section 4.4.3.

To generate the required DO data, the BCR, containing the appropriate concentration of water and alkanes and deactivated yeast, was initially sparged with nitrogen, until DO reached 0%. A step change from pure nitrogen to air was then performed. The response in DO was measured after every 5 seconds until saturation was reached.

Linearization of the first order model (Equation 2-3) of the oxygen transfer rate (OTR) produces Equation 4-3, which allows determination of K_La from the slope of the graph. Figure 4-6 is an example of a linearized curve, for one experimental condition. The K_La determined using this method may be significantly inaccurate especially in hydrocarbon-based systems as shown by Correia and Clarke, (2009) and Clarke and Manyuchi, (2012).

However, it can be used as an initialisation point for the iterative method needed to determine K_La from the second order model.

$$ln\left(1-\frac{c}{c^*}\right) = -K_L a.t \qquad \text{Equation 4-3}$$

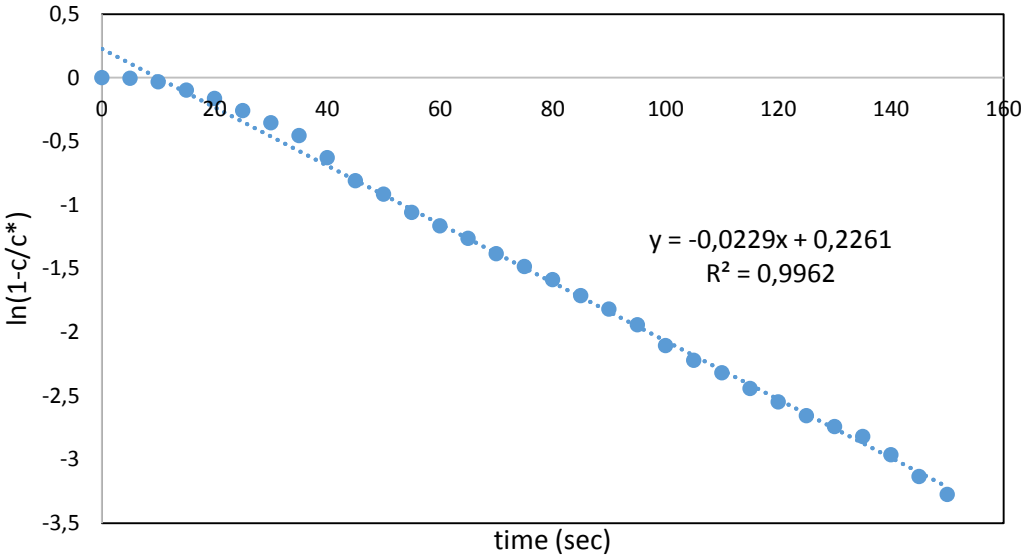

Figure 4-6: Graph illustrating the method for determining K_La from DO data using linear regression of the first order model at an alkane concentration of 7.88% v/v, yeast loading of 1.62 g/l and u_G of 1.62 cm/sec.

4.4.3 Measurement of K_La using the gassing out procedure and the second order response model

The DO probe response lag time is not taken into account in the determination of K_La using the first order model, however a second order model (Section 2.4.2) (Equation 2-3) can be derived which does include this factor, in the form of K_p (Aiba and Huang, 1969). In order to solve for K_La in this model an iterative method to minimize the total sum of positive errors between the data and the second order model was utilised. The K_La determined using the first order model was used as an initial guess, and Excel's solver function was used to converge on a least squares solution (Clarke and Manyuchi, 2012).

The sum of errors between the DO 2nd order model and the experimental data was calculated using Equation 4-4 for each interval. Figure 4-7 shows the minimised errors between experimental data and the 2nd order model (Equation 2-3) after using the solver algorithm.

$$\sum(Errors)^2 = \sum(\%DO_{2nd}) - \sum(\%DO_{ex}) \qquad \text{Equation 4-4}$$

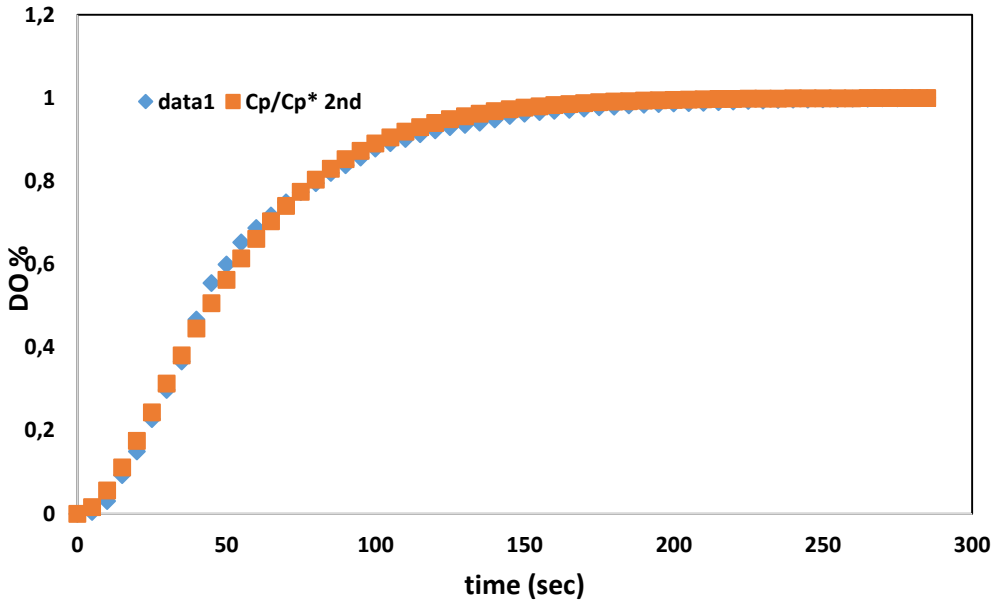

Figure 4-7: The use of the solver algorithm to minimise the SUM of the errors between the experimental data and DO 2nd order model.

4.5 Measurement of the interfacial area

Gas liquid interfacial area is calculated from two parameters: the bubble diameter (estimated from the Sauter mean diameter) and the gas hold up. Measurements of both the gas hold up, and the Sauter mean diameter will be discussed in ensuing sections.

4.5.1 Measurement of gas hold up

The gas hold up of the system is defined as the fraction of gas in the medium. To measure the gas hold up, the height of the liquid in the column before aeration (H_o) and during steady state aeration (H) were measured by using a ruler attached to the reactor as shown in Figure 4-8 (Schugerl, 1980; Dhanasekaran and Karunanithi, 2012). The gas hold up was then calculated using Equation 2-6 (Section 2.5). Due to turbulent conditions (high superficial gas velocity) in the bubble column reactor, the reading was taken three times to improve accuracy of the measurement.

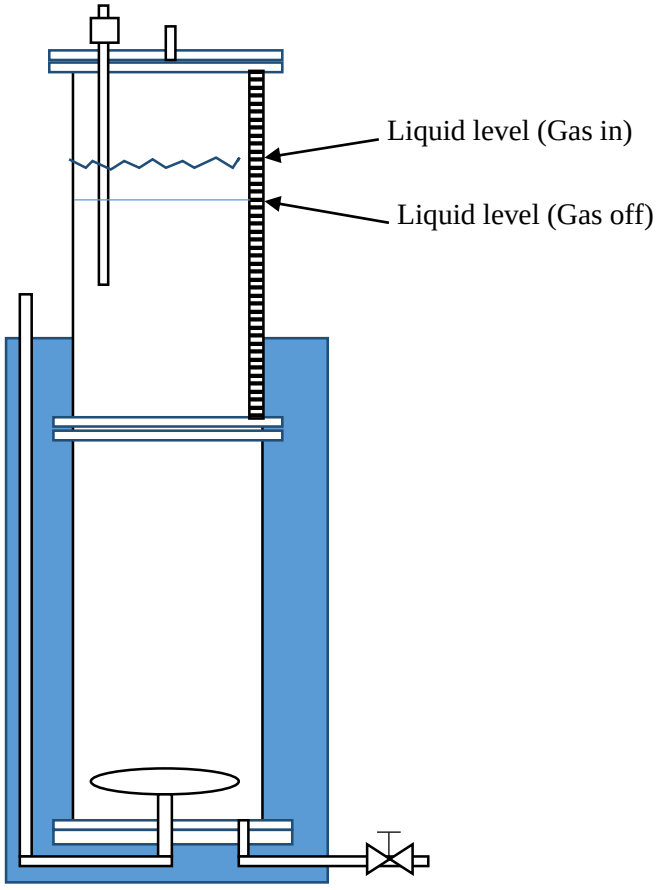

Figure 4-8: Schematic diagram illustrating the measurement of gas hold up.

4.5.2 Measurement of the bubble diameter with image analysis

4.5.2.1 Image capturing

Images were captured using a Matrix Vision mvBlueFOX 124G high speed camera, installed with mvImpact software. The camera has a 1.9 megapixels resolution which enables acquisition of high-quality images. The images were then stored individually as bitmap files (.bmp) and then converted to JPEG (.jpg), which occupies less storage space.

The camera, situated 30 cm from the BCR and 30 cm above the sparger height on a tripod, was used to capture images of the air bubbles from the side of the bioreactor at the same point to ensure consistency. The camera stand position and the reactor position were marked to ensure consistency after being moved for cleaning. A line of 10 mm in length was drawn on the reactor surface, to calibrate the image sizes for conversion from pixels to millimetres.

To provide enough data for statistically significant conclusions, the literature employed an average sample size which ranged from 30 to 10000 bubbles in BCRs systems. Maceiras *et al.* (2010) reported the use 30 bubbles per sample for the analysis whilst Bailey *et al.* (2005) used 10000 bubbles. Colella *et al.* (1999) used 500 bubbles and reported that 500 bubbles provided a sample large enough to understand the behaviour of the interfacial area in BCR. Based on Colella *et al.* (1999)'s findings, a sample size of at least 500 bubbles (captured within several images) was used under each condition.

4.5.2.2 Image processing

Measurement of bubble diameter was done using a MATLAB photography imaging procedure as developed by (Clarke and Correia, 2008; Hollis and Clarke, 2016). The MATLAB® code was modified in this study by Matt Molteno (personal communication), in order to enhance its accuracy and reduce the processing time by integrating it into an automated data processing structure, which could iteratively load, analyse images and save the analysis output. The procedure can be used for image enhancement and determination of contrast gradients to determine the Sauter mean diameter.

Moreover, the image quality was further improved by adding an ellipse-based estimation method, as described in Appendix 9.3. After capturing the images, the following steps were employed using a series of MATLAB functions;

Step 1: The appropriate image was read using `imread`. Determination of the scales of the images was done for enhanced accuracy before the analysis could take place. To achieve this, a line of 10 mm was drawn on the outside of the reactor surface and was used as a scale to convert the pixel dimensions of the bubbles to metric units and therefore determine the actual sizes of the detected bubbles as shown in Figure 4-9.

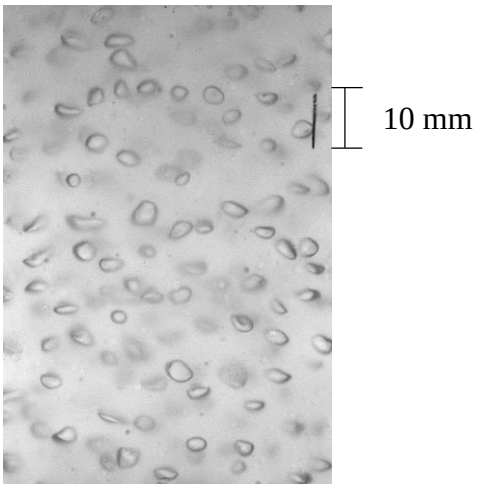

Figure 4-9: Image using scaling line at alkane concentration of 2.5% v/v, yeast loading of 3.25 g/l and superficial gas velocity of 2 cm/sec.

Step 2: The image then went through a series of enhancing processes. Median filter using `medfilt3` was the first enhancement step. The median filter eliminated noise by setting each pixel to the median of the neighbouring ($3 \times 3 \times 3$) matrix pixels. The use of a median value instead of a mean value to determine the pixel value in the new image enabled the removal of outlier pixels whilst maintaining the sharpness of the image (Clarke and Correia, 2008). After the filtering, linear interpolation, using the function '`interp2`' was used to reproduce more filtered images, producing images such as that shown in Figure 4-10.

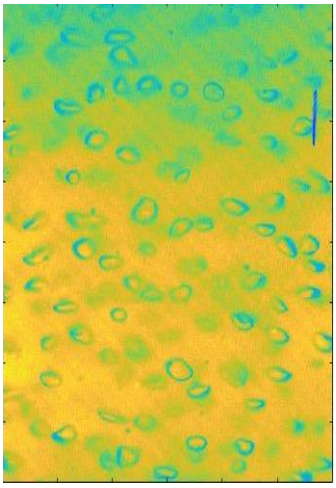

Figure 4-10: Image using median filter at alkane concentration of 2.5% v/v, yeast loading of 3.25 g/l and superficial gas velocity of 2 cm/sec.

Step 3: This involved by converting grey scale images into binary images. The threshold value of 0.5 was used because it is the middle point between black and white images, without taking image class into consideration, as shown in Figure 4-11.

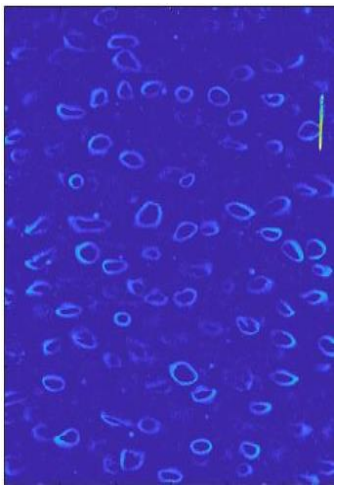

Figure 4-11: Image after converting grey scale images into binary images with threshold value of `0.5`, at alkane concentration of 2.5% v/v, yeast loading of 3.25 g/l and superficial gas velocity of 2 cm/sec.

Step 4: After the threshold function, the function `medfilt2`, was employed to filter the images. It produced a median value of a (2×2) matrix pixel of neighbouring images around a corresponding pixel in the input image. The resultant image is shown in Figure 4-12.

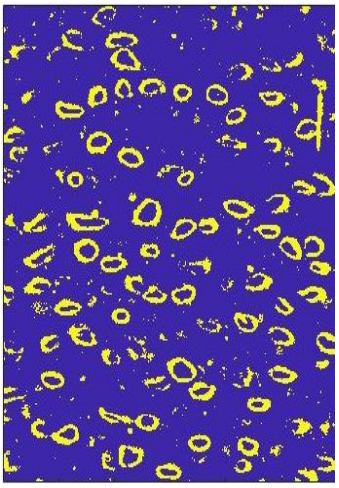

Figure 4-12: Image after the use of `medfilt2` function at alkane concentration of 2.5% v/v, yeast loading of 3.25 g/l and superficial gas velocity of 2 cm/sec.

Step 5: This step involves using two functions, `imdilate` (image dilate) and `imerode` `which` were then used to join the pixels together. The `imdilate` function produced dilated images from the grayscale, binary, or packed binary image, then the `imerode` function produced eroded images from the grayscale, binary, or packed binary images, as shown in Figure 4-13.

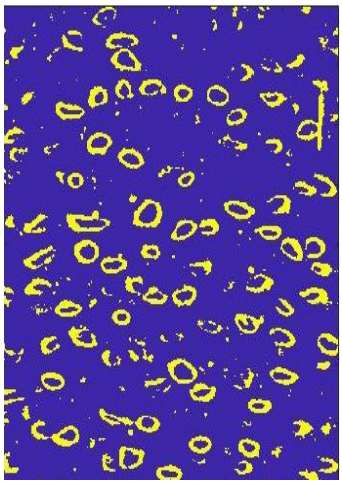

Figure 4-13: Image after `imdilate` and `imerode` at alkane concentration of 2.5% v/v, yeast loading of 3.25 g/l and superficial gas velocity of 2 cm/sec.

Step 6: Two functions, `imdilate` as described in step 5 and `bwmorph` were employed in this step. The `bwmorph` function applied specific morphological operations to the binary images. The option "`skel`" was used in this function to remove pixels (noise) on the boundaries of objects without allowing objects to break apart, as shown in Figure 4-14.

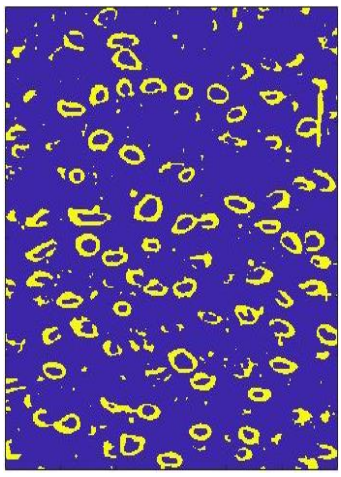

Figure 4-14: Image after removing the noise at alkane concentration of 2.5% v/v, yeast loading of 3.25 g/l and superficial gas velocity of 2 cm/sec.

Step 7: The function `medfilt2` was employed as described in step 4 to remove the small pixels (noise). The resulting image is shown in Figure 4-15.

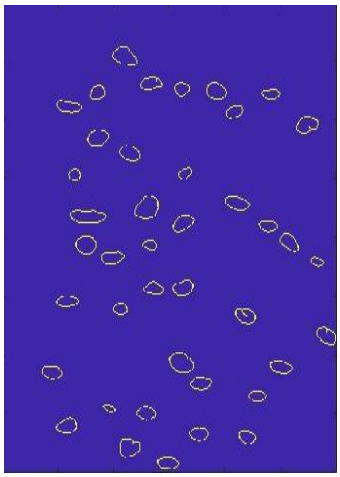

Figure 4-15: Image after removing the noise at alkane concentration of 2.5% v/v, yeast loading of 3.25 g/l and superficial gas velocity of 2 cm/sec.

Step 8: After fully processing the image, the exterior image boundaries were then defined by setting the circularity option to 0.2, which filled up the holes in bubbles and provided a projected area of each one of them as shown in Figure 4-16.

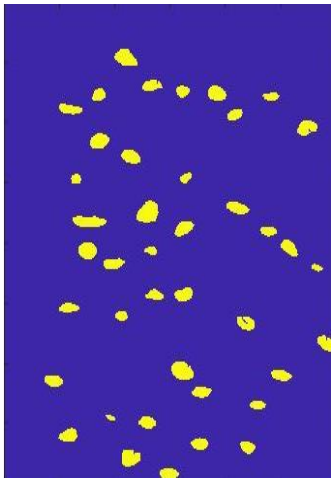

Figure 4-16: Image obtained after processing and filling up the holes at alkane concentration of 2.5% v/v, yeast loading of 3.25 g/l and superficial gas velocity of 2 cm/sec.

Step 9: This step uses two independent methods to measure the area of the bubbles. The first method (the projected area method) read the background of the bubble and then measured the projected area. The second method (the ellipse) used two parameters (X and Y) drawn as a cross inside a bubble, and fitted with an ellipse, which was then measured as the bubble area. Bubbles close to the border (green bubbles) were ignored whilst the blue bubbles were picked, to produce images as shown in Figure 4-17. The results were then exported to an excel sheet for calculation of the interfacial area. These two methods were used to improve confidence in the measured values, since both have different limitations.

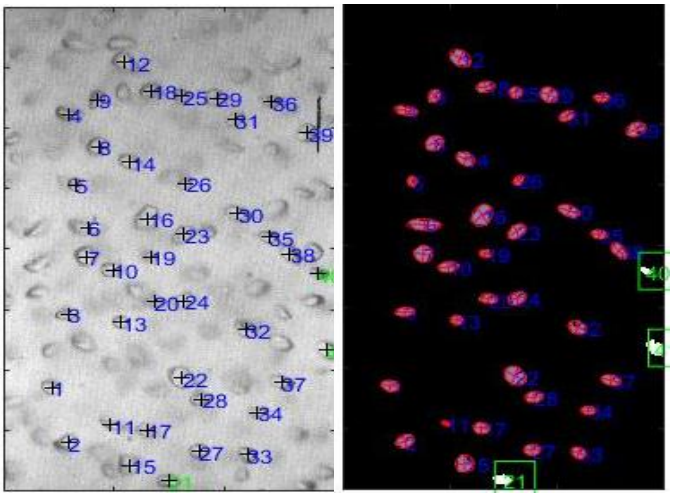

Figure 4-17: The output of the image after the enhancement process, at alkane concentration of 2.5% v/v, yeast loading of 3.25 g/l and superficial gas velocity of 2 cm/sec.

4.6 Experimental and statistical design

A response surface methodology, central composite design (CCD), was used to model the influence of three factors, alkane concentration, solids loading and superficical gas velocity on oxygen transfer in a simulated hydrocarbon bioprocess system. The model comprised a full factorial set of experiments, central and axial data points. Five levels ($-\alpha$, -1, 0, $+1$, $+\alpha$) were applied for each treatment in a circumscribed central composite design (CCD), with replications at the centre. The levels (± 1.414) were star points, (± 1) were the high and low levels whilst (0) represented the centre points. The range of the factor levels was based on the findings of Hollis and Clarke, (2016) who studied the effect of yeast loading, hydrocarbons and agitation rates on oxygen transfer in a STR. In this study, the yeast loading range was 0.5-6 g/l, hydrocarbon concentration was 2.5-20% (v/v), and superficial gas velocity was 1-3 cm/sec. The factor names, coded names and levels are shown in Table 4-3. The order of experimental runs is further presented in Table 4-4.

Table 4-3: CCD factor levels

Variables	**Units**	**Exlow**	**Low**	**Mid**	**High**	**ExHigh**
Factor level		-1.414	-1	0	+1	+1.414
Superficial gas velocity	cm/sec	1	1.62	2	2.38	3
Alkane concentration	(% v/v)	2.5	7.88	11.25	14.62	20
Yeast loading	g/l	0.5	1.62	3.25	4.88	6

Table 4-4: Run orders

Run	Alkane concentration (% v/v)	Yeast loading (g/l)	Superficial gas velocity (cm/sec)
1	-1	-1	-1
2	-1	-1	+1
3	-1	+1	-1
4	-1	+1	+1
5	+1	-1	-1
6	+1	-1	+1
7	+1	+1	-1
8	+1	+1	+1
9	-1.414	0	0
10	+1.414	0	0
11	0	-1.414	0
12	0	+1.414	0
13	0	0	-1.414
14	0	0	+1.414
15	0	0	0
16	0	0	0

To model the experimental data, a full factorial response surface methodology, central composite design with three factors, five levels and one block, using the design of experiment (DOE) module of the STATISTICA 13 software package, was employed. The data were then subjected to a factorial analysis of variance (ANOVA) and tested for significance at 95% confidence level. A Pareto chart was also employed to determine the statistically significant terms.

5. RESULTS AND DISCUSSION

The findings presented in this section extend the understanding of the behaviour of the overall volumetric oxygen transfer coefficient (K_La) and the interfacial area in multiphase hydrocarbon bioprocess systems, especially in a BCR, since it is not widely reported in the available literature. As a foundation to the study of K_La behaviour in multiphase systems, it was considered critical to examine K_La in different phases. The main goal of these investigations is to confirm the impact of the superficial gas velocity, alkane concentration and yeast loading on K_La individually in a BCR.

The K_La measurement was done according to the dynamic method GOP (as discussed in Section 4.4.3) for different phase systems such as the two phase (air-water), three phase (air-water-hydrocarbons), three phase (air-water-deactivated yeast) and four phase (air-water-hydrocarbons-deactivated yeast) system. Those examinations of K_La behaviour in two phase systems and three phase systems will be further explained in the succeeding Sections5.1 and 5.2. The examinations of the interfacial area and K_La in four phase system will be also explained in Sections 5.3 and 5.4.

5.1 Examination of the K_La behaviour in two phase systems (air-water)

The following results describe the behavior of K_La in a two-phase system (air and water) in the laboratory scale BCR, determined using the 2nd order model to compute K_La. From Figure 5-1, it can be observed that an increase in the superficial gas velocity results in an increase in the K_La. An increase in the superficial gas velocity from 1 to 3 cm/sec resulted in an increase in K_La by 0.04 s^{-1}. This increase in K_La can be attributed to the increase in the amount of sparged oxygen in the system, and the improved mixing associated with increased turbulence. These findings agreed well with results available in literature. Jianlong, (2000) reported that K_La values increased with the air flow rate to a maximum of approximately 0.02 s^{-1} at 2 vvm (volume of air per volume of liquid per minute). Other researchers also confirmed the increase of K_La in ion-free water with increasing superficial gas velocity using different approaches. Calderbank, (1958 and 1959) used light transmission techniques to calculate the interfacial area. Kawecki *et al.* (1967) also measured the interfacial area using the gas hold-up and bubble size measurement techniques. Such approaches then require that K_L be determined separately, whose values have been reported to vary widely (up to a factor of six times variation) in pure

water (Calderbank and Moo-Young, 1961; Reith and Beek, 1968; Linek *et al.*, 1970; Robinson and Wilke, 1974).

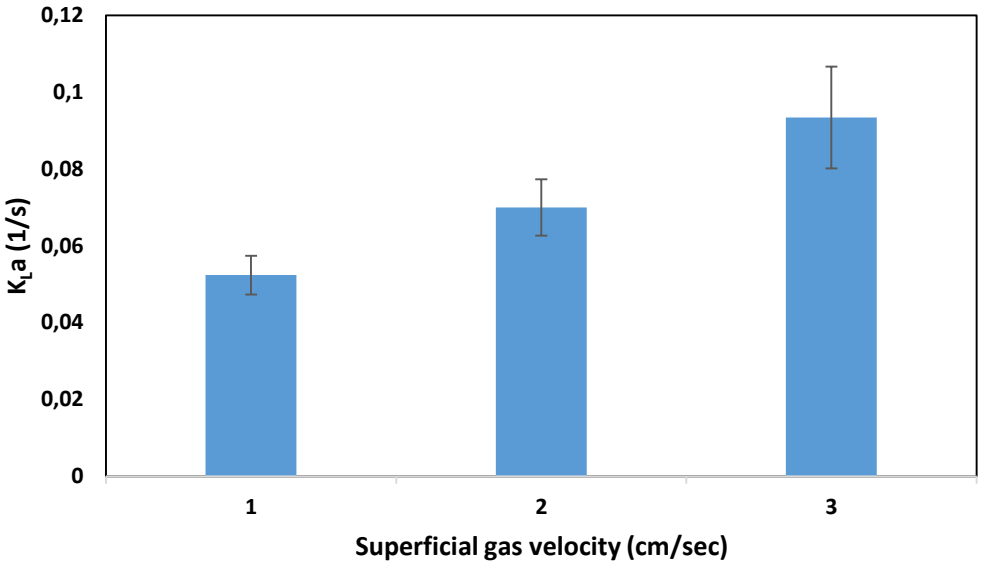

Figure 5-1: The behaviour of K_La in the two phase air-water system in the BCR under varying superficial gas velocities (1 cm/sec, 2 cm/sec and 3 cm/sec). The error bars represent the standard deviation of three replicates.

5.2 Examination of the K_La behaviour in three phase systems (air-water-hydrocarbons or air-water-microbial solids)

This section details experiments investigating K_La and liquid-phase homogeneity in two separate three-phase systems, namely: i) the air-water-hydrocarbon system and ii) the air-water-deactivated yeast system. The literature has very little information regarding the effect of hydrocarbons or deactivated yeast on the measured parameters in either of these systems, and in particular no examination of liquid-phase spatial homogeneity has been conducted previously. The spatial homogeneity of the system is particularly important for the measurements conducted in this study since an assumption of system homogeneity is implicit in the K_La equation derivation.

5.2.1 Measurement of homogeneity in three phase systems (air-water-hydrocarbons)

Industrially, it is important to achieve homogenous flow, especially when the process contains two immiscible liquids such as water and hydrocarbons. In this study, during the evaluation of the influence of hydrocarbon concentration on K_La in a three phase system (air, water and hydrocarbon) in the BCR. It was seen that the system was non-homogenous in terms of liquid-liquid flow (water and hydrocarbon), especially at low superficial gas velocities (Figure 5-2). This spatial variation is a significant limitation to the range of superficial gas velocities under which the method used in this study can determine K_La, since bulk liquid spatial homogeneity is implicit in the derivation of the equation used to compute K_La from the DO data. However, this finding has not been reported or examined in the literature and therefore required further investigation as described in Section 4.3.

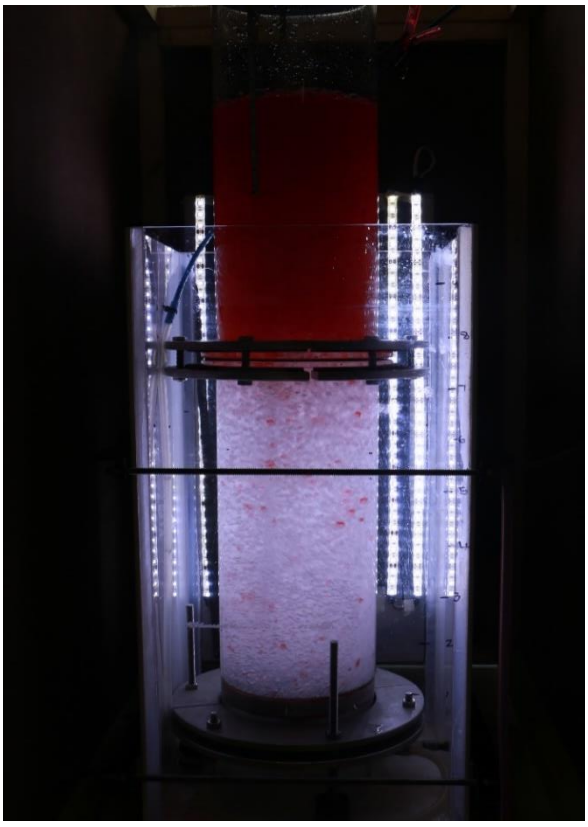

Figure 5-2: Non-homogenous flow in a three phase system (air-water-hydrocarbon) in a BCR under operation conditions of 20% v/v hydrocarbon concentration and superficial gas velocity of 1 cm/sec. The hydrocarbon phase is stained with 0.125 g/l stain for visualization.

Figure 5-3, Figure 5-4, Figure 5-5 and Figure 5-6 show the homogeneity levels at four fixed hydrocarbon concentrations (5, 10, 15 and 20% v/v respectively) at varying levels of superficial gas velocity. The graphs show that at low hydrocarbon concentrations (5 and 10% v/v), the system required high superficial gas velocity (2 cm/sec) to attain homogeneity (Figure 5-3 and Figure 5-4). However, the higher hydrocarbon concentrations (15 and 20% v/v), the system required less superficial gas velocities to achieve homogeneity (Figure 5-5 and Figure 5-6), most likely due to an increased rapidity of droplet dispersion, as viscosity increases due to droplet coalescence. At high superficial gas velocities, more oil droplets are forced to the bottom, increasing spatial homogeneity. Due to the innate variability of the measurement, some samples might register over 100% of expected hydrocarbon concentration.

The use of high superficial gas velocities to attain homogeneity may however become an operational challenge in industrial scales especially in such reactors like bubble columns. To improve the accuracy of homogeneity measurement, an image analysis methodology using MATLAB is highly recommended for further study.

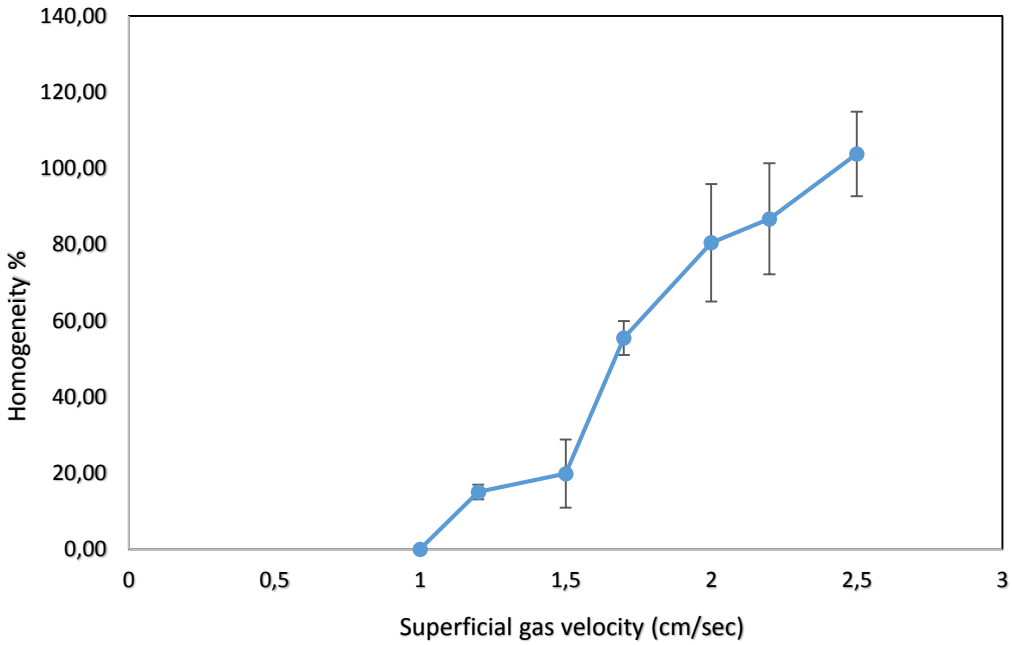

Figure 5-3: Measurement of homogeneity in a three phase system (air-water-hydrocarbons) in a BCR under varying superficial gas velocities and alkane concentrations of 5% v/v. The error bars represent the standard deviation of five replicates.

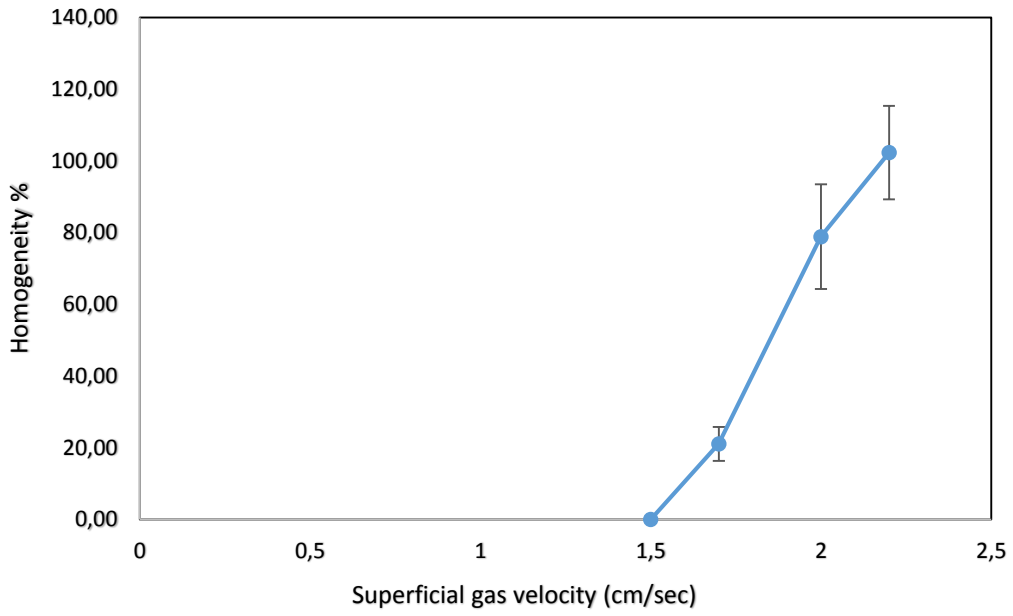

Figure 5-4: Measurement of homogeneity in a three phase system (air-water-hydrocarbons) in a BCR under varying superficial gas velocities and alkane concentrations of 10% v/v. The error bars represent the standard deviation of five replicates.

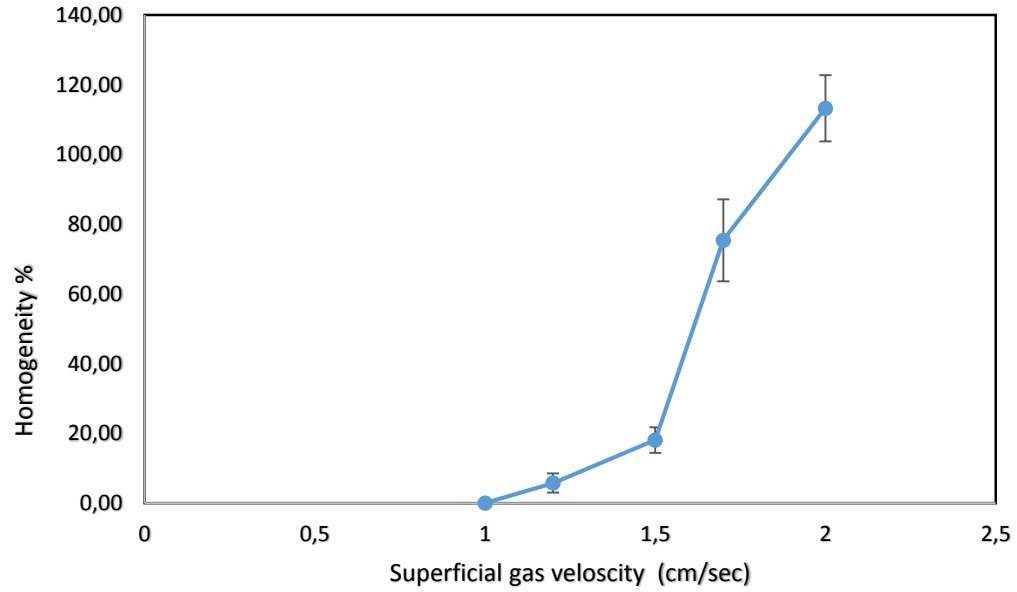

Figure 5-5: Measurement of homogeneity in a three phase system (air-water-hydrocarbons) in a BCR under varying superficial gas velocities and alkane concentrations of 15% v/v. The error bars represent the standard deviation of five replicates.

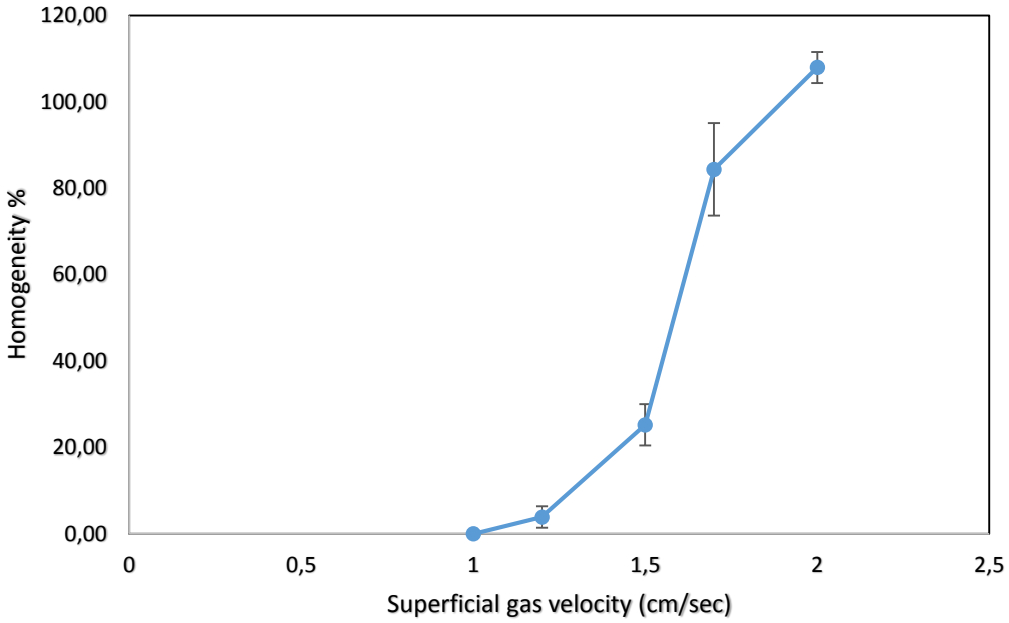

Figure 5-6: Measurement of homogeneity in a three phase system (air-water-hydrocarbons) in a BCR under varying superficial gas velocities and alkane concentrations of 20% v/v. The error bars represent the standard deviation of five replicates.

Since it was important to operate in a homogenous regime in this study, homogeneity was measured and confirmed for the four phase system (air, water, hydrocarbon and deactivated yeast) for the three independent variables (alkane concentration, yeast loading and superficial gas velocity) in a BCR. Figure 5-7, Figure 5-8, Figure 5-9 and Figure 5-10 presented the evaluation of the homogenous regime in a four phase system at different hydrocarbon concentrations (5, 10, 15 and 20% v/v respectively) and constant yeast loading of 3.25 g/l, under differing superficial gas velocities. From the graphs, it can be seen that the presence of the yeast (3.25 g/l) in the system reduced the superficial gas velocity required to attain homogeneity (1 cm/sec).

In this measurement method, a value of 75% was assumed homogenous since it is a physical method which is subject to significant measurement variation. Sampling was done in replicates of five to increase the accuracy of the measurement. Furthermore, it was confirmed that all operational conditions of this study were in the homogenous flow based on the experimental design (CCD) Table 4-4.

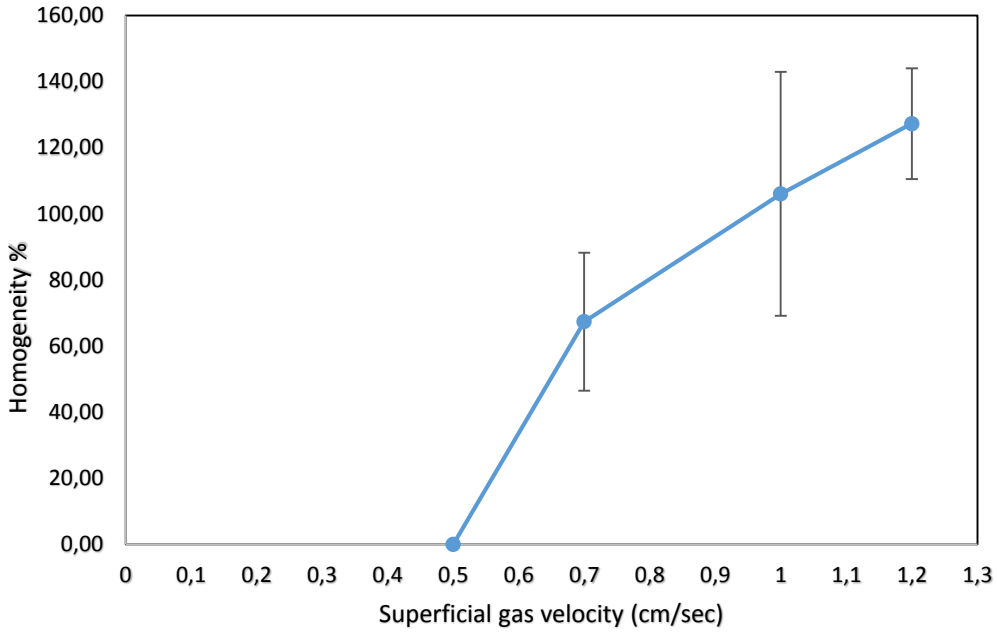

Figure 5-7: Measurement of homogeneity in a four phase system (air-water-hydrocarbon-deactivated yeast) in a BCR under varying superficial gas velocities and alkane concentrations of 5% v/v and yeast loading of 3.25 g/l. The error bars represent the standard deviation of five replicates.

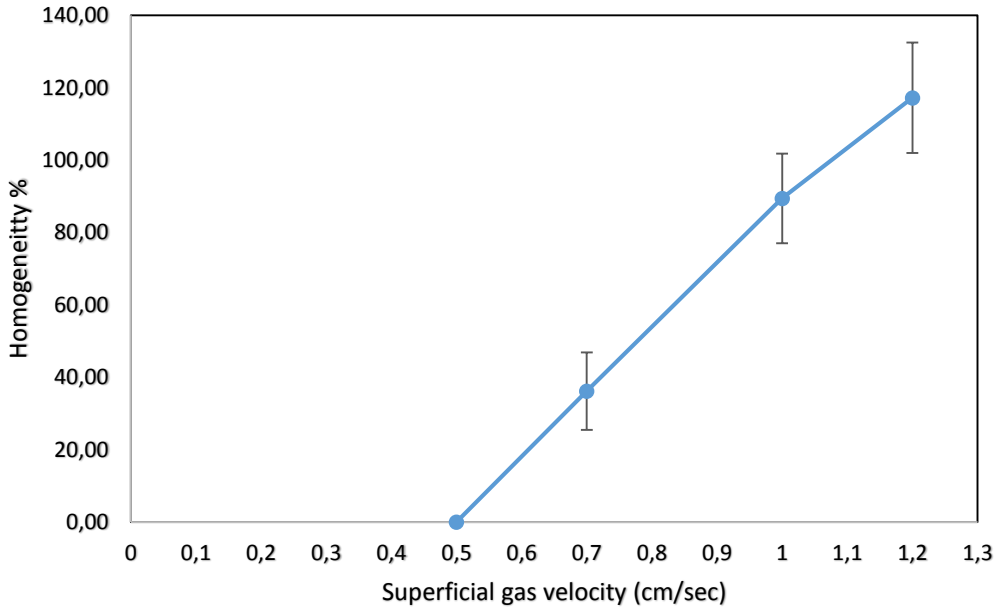

Figure 5-8: Measurement of homogeneity in a four phase system (air-water-hydrocarbon-deactivated yeast) in a BCR under varying superficial gas velocities and alkane concentrations of 10% v/v and yeast loading of 3.25 g/l. The error bars represent the standard deviation of five replicates.

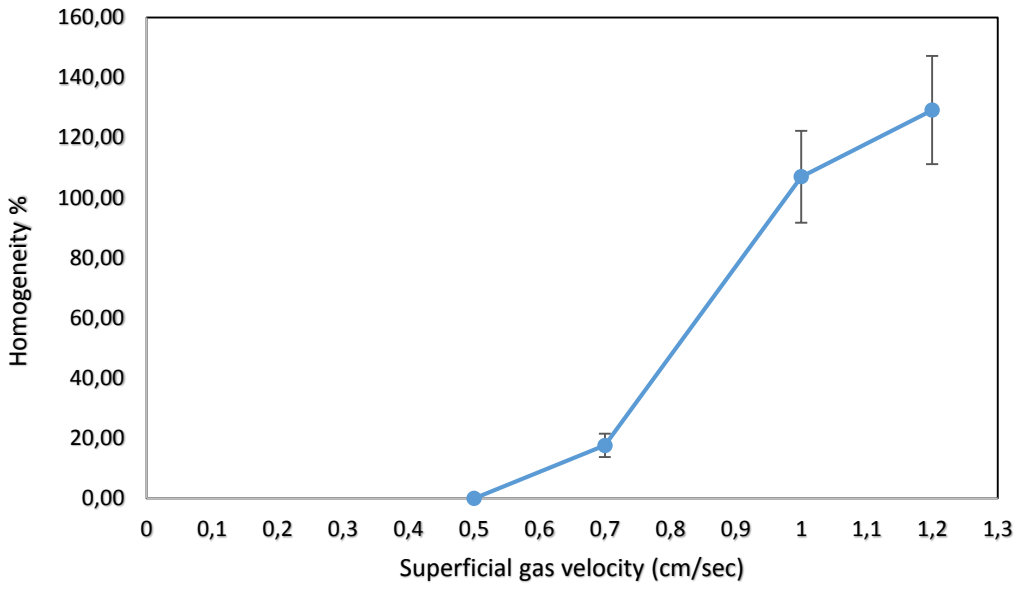

Figure 5-9: Measurement of homogeneity in a four phase system (air-water-hydrocarbon-deactivated yeast) in a BCR under varying superficial gas velocities and alkane concentrations of 15% v/v and yeast loading of 3.25 g/l. The error bars represent the standard deviation of five replicates.

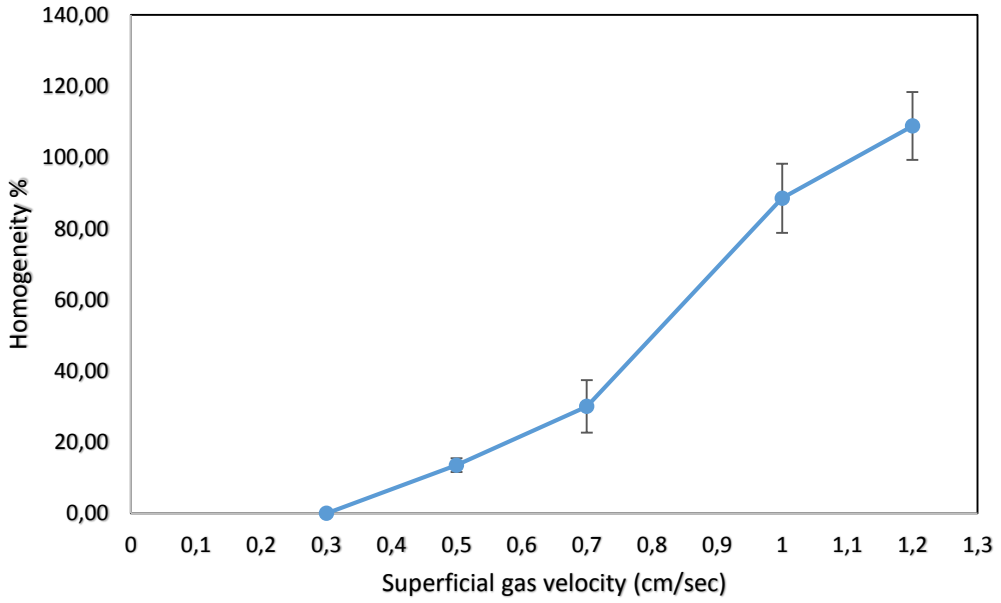

Figure 5-10: Measurement of homogeneity in a four phase system (air-water-hydrocarbon-deactivated yeast) in a BCR under varying superficial gas velocities and alkane concentrations of 20% v/v and yeast loading of 3.25 g/l. The error bars represent the standard deviation of five replicates.

Figure 5-11 shows the homogeneity of flow in the system after adding 3.25 g/l of deactivated yeast to the same system (three phase system) as of Figure 5-2 under constant superficial gas velocity (1 cm/sec) and constant hydrocarbon concentration (20% v/v). This was visible evidence to further confirm that any addition of yeast cells to the system changed the fluid properties and the flow regimes and therefore increased homogeneity. However, the effect of yeast on the homogeneity was outside the scope of this research and a recommendation is made for their investigation in further studies.

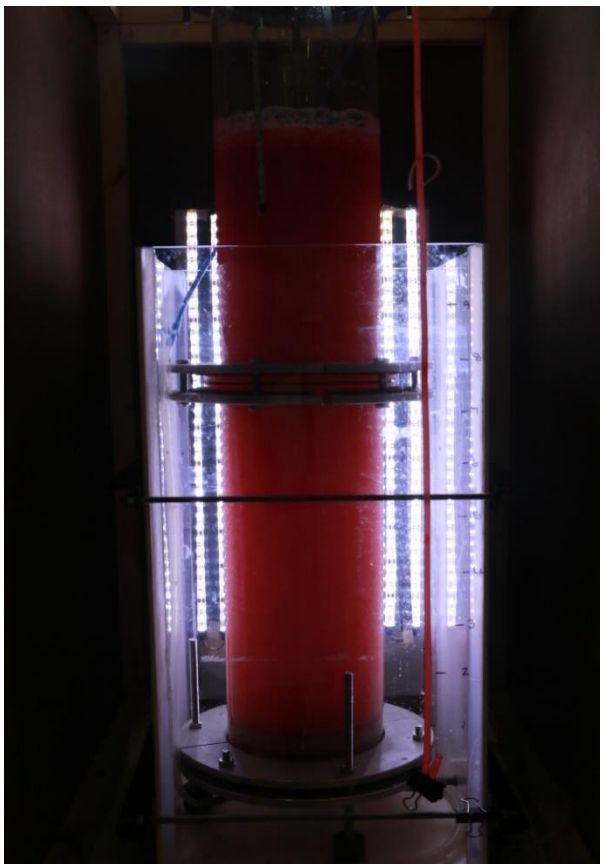

Figure 5-11: Homogenous flow in a four phase system (air-water-hydrocarbon-deactivated yeast) in a BCR under operation conditions of 20% v/v alkane concentration, 3.25 g/l yeast loading and superficial gas velocity of 1 cm/sec. The hydrocarbon phase is stained with 0.125 g/l stain for visualization.

5.2.2 Examination of the K_La behaviour in the air-water-hydrocarbon three phase system

This examination was done to confirm the effect of hydrocarbon concentration on K_La in a three phase system (air, water and hydrocarbons) in a BCR at different superficial velocities and hydrocarbon concentrations.

Figure 5-12 shows that an increase in the alkane concentration (2.5, 11.25 and 20% v/v) in the system resulted in a significant decrease in K_La at constant superficial gas velocity. However, an increase in the superficial gas velocity from 1 to 3 cm/sec had a positive influence on K_La, showing the linear relationship between the superficial gas velocity and K_La at constant alkane concentration. This is due to the increase in turbulence and increased oxygen diffusion in the system. The highest K_La (0.083 s^{-1}) was therefore found at low alkane concentration (2.5% v/v) and high superficial gas velocity (3 cm/sec), which decreased as the alkane concentration increased at constant superficial gas velocity. This is in agreement with the results of the examination that was done in two phase system (air-water) (Section 5.1), where the value of K_La was 0.1 s^{-1} at the highest superficial gas velocity (3 cm/sec). However, results obtained under the lowest superficial gas velocity (1 cm/sec) were not considered since the liquid-liquid spatial homogeneity threshold was established to be at 2 cm/sec. The value of K_La increased as the alkane concentration decreased at constant superficial gas velocity. Correia *et al.* (2010) similarly reported a decrease in K_La with an increase in the alkane concentration from 2.5 to 20% v/v. This decrease was attributed to the increase in viscosity in the bulk liquid. Adding to that, hydrocarbon type, concentration and chain length were reported in other studies to decrease the fluid tension and increase its viscosity, thereby influencing the K_La (Koide *et al.*, 1976; Freitas *et al.*, 1999; Clarke and Correia, 2008). According to Garcia-Ochoa and Gomez, (2005) as well as Yagi and Yoshida, (1974), more viscous liquids are more resistant to the gas-liquid dissolved oxygen transfer. This is due to the limited resultant gas movement within the bulk liquid phase, which in turn results in a corresponding decrease in the dissolved oxygen transfer in the system. Such findings were also reported by Juretzek *et al.* (2000) as well as Garcia-Ochoa and Gomez, (2005).

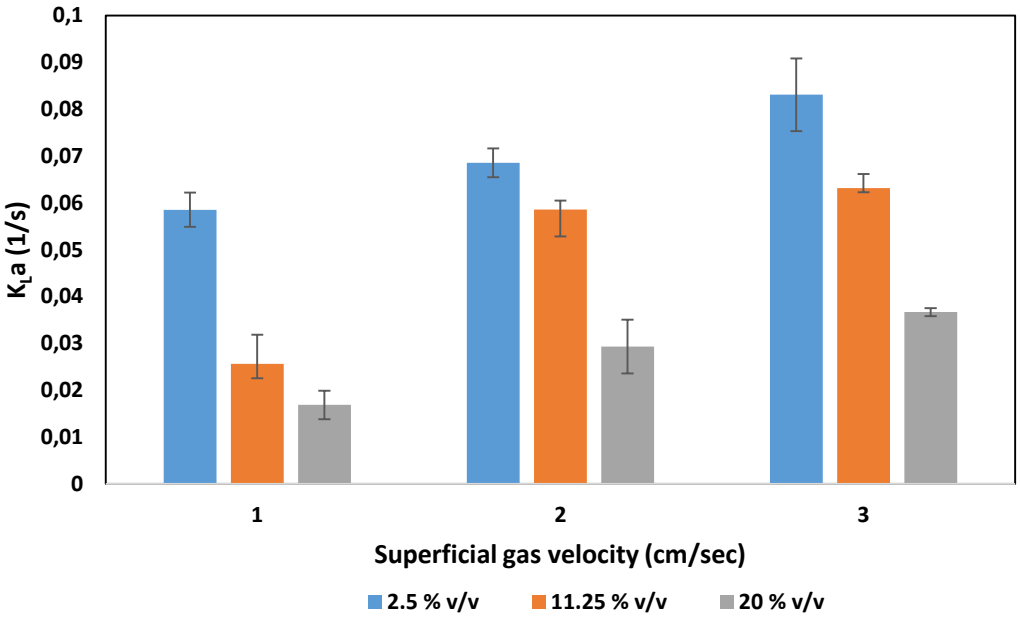

Figure 5-12: The behaviour of K_La in the three-phase air-water-hydrocarbon system in the BCR under varying superficial gas velocities (1 cm/sec, 2 cm/sec and 3 cm/sec) and alkane concentrations (2.5% v/v, 11.25% v/v and 20% v/v). The error bars represent the standard deviation of three replicates.

5.2.3 Examination of the K_La behaviour in the three-phase air-water-deactivated yeast system

This set of experiments was done to establish the influence of the yeast concentration on K_La in the three-phase system (air, water and yeast loading) in the BCR. The yeast cells were deactivated (as detailed in Section 4.1.2) and then included in the system as a solid phase. The effect of the yeast loading on K_La is not well documented in literature, especially for a BCR.

Figure 5-13 shows the effect of yeast loading on K_La under varying superficial gas velocities (1 to 3 cm/sec). It shows that an increase in the yeast loading results in a decrease in K_La at constant superficial gas velocity. On other hand, any increase in the superficial gas velocity causes a decrease in K_La at constant yeast concentrations 0.5 and 3.25 g/l. However, a different result was observed at the highest yeast concentration (6 g/l), where the K_La increased with increasing superficial gas velocity, possibly due to an increase in the fluid viscosity in the system.

Galaction *et al.* (2004) studied the use of different microorganisms such as *Propionibacterium shermanii, Saccharomyces cerevisiae* and *Penicillium chrysogenum* pellets and reported a decrease in K_La with increasing microorganism concentrations. The decrease in K_La with increasing solids concentration was suggested to be dependent on the type of the solid particle (Galaction *et al.*, 2004). Manyuchi, (2010) also reported similar findings when studying a system containing 2.5% v/v $C_{14\text{-}20}$ and different solid types in an STR.

According to Chisti and Moo-Young, (1988) as well as Moses *et al.* (1987), on investigating the effects of solids loading in a STR, the decrease in K_La was a result of the existence of diffusion blocking effects in aqueous systems. However, a separate study by Joosten *et al.* (1977) reported an initial increase followed by a steep decrease in K_La when using glass beads (53-105 mm) in an aqueous dispersion in a STR, when the solids concentration was increased. The other contributing factor to the decrease in K_La was the decreasing surface area available for oxygen transfer when solids concentration is increased (Clarke and Manyuchi, 2012).

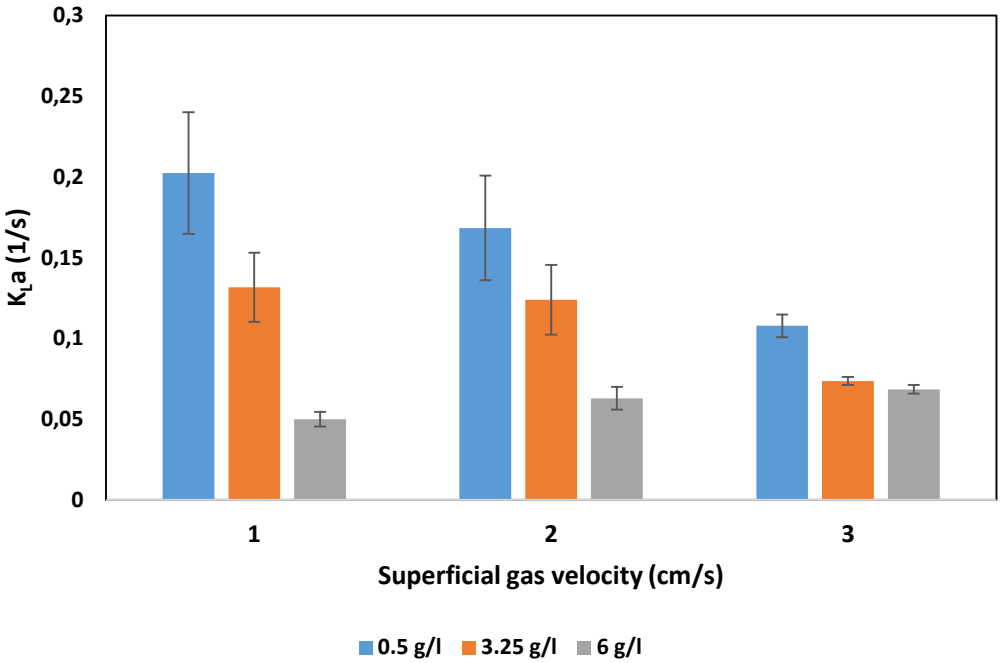

Figure 5-13: Examination of K_La in three phase systems (air-water-deactivated yeast) and different yeast loading (0.5 g/l, 3.25 g/l and 6 g/l). The error bars represent the standard deviation of three replicates.

5.3 Examination of the interfacial area in the four phase air-water-hydrocarbons-deactivated yeast system

To provide more understanding of oxygen transfer in a simulated four phase system (air, water, hydrocarbon and deactivated yeast) in the BCR, the interfacial area was determined under different parameter conditions, such as alkane concentration, superficial gas velocity and yeast loading. The interfacial area was calculated from the results of the Sauter mean diameter (D_{32}), and the gas hold up (Equation 2-7) as discussed in Section 4.5. The gas hold-up and D_{32} as well as the interfacial area data are presented in Sections 5.3.1, 5.3.2 and 5.3.3 respectively.

In this section, results of key representative data are discussed. For those effects which are consistent across a variety of parameters, only single representative graphs will be shown, with the remainder included in the appendices.

5.3.1 Influence of the system parameters on gas hold-up

Figure 5-14 is a Pareto chart showing the linear effects of superficial gas velocity and yeast loading as well as the yeast loading/alkane concentration and the superficial gas velocity/yeast loading interaction effects which have significant influence on the gas hold-up at the 95% confidence level. Positive influences were found for the linear effect of superficial gas velocity and the interaction effect of yeast loading and alkane concentration, the superficial gas velocity being the most influential. The influence of the linear effect of yeast loading and the interaction effect of superficial gas velocity and yeast loading was negative. All quadratic effects (Q) and the linear effects (L) of the alkane concentration, as well as the interaction between the superficial gas velocity and alkane concentration (1Lby3L) were not of significant influence at the 95% confidence interval. The effects of system parameters (alkane concentration, superficial gas velocity and yeast loading) on gas hold-up are presented on Figure 5-15, Figure 5-16 and Figure 5-17, respectively.

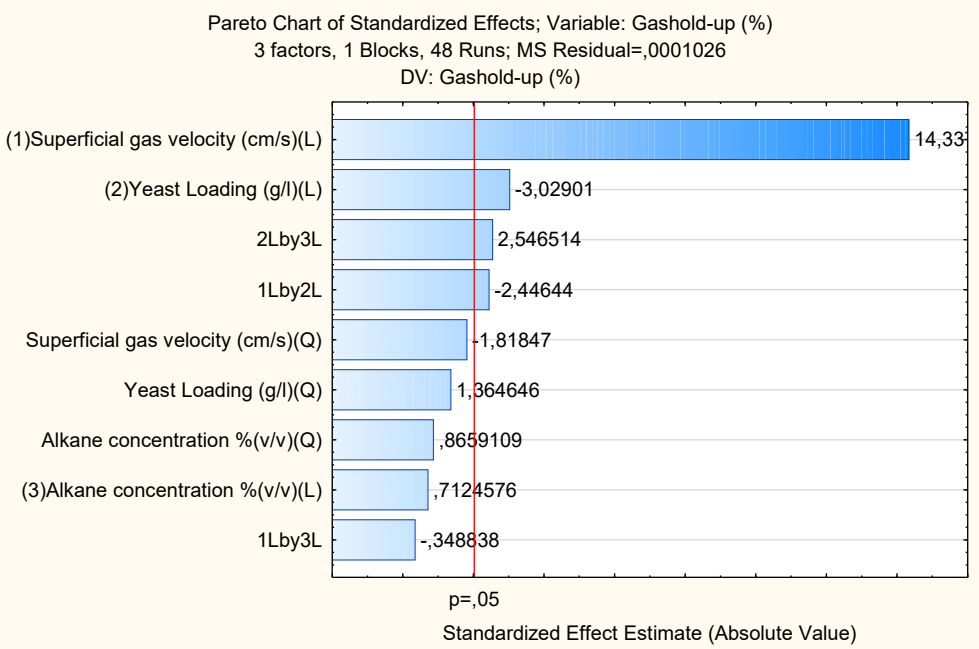

Figure 5-14: Pareto plot from statistical model for the impact of independent variables and interaction on gas hold up in a four phase model with 95% confidence level.

Figure 5-15 is a response surface graph showing the influence of superficial gas velocity and alkane concentration on the gas hold-up at constant yeast loading (at the midpoint of 3.25 g/l). The graph shown that any change in the alkane concentration does not have a significant effect on the gas holdup. It however showed a linear increase in gas hold-up with increasing superficial gas velocity, indicating that the system was operating in a homogenous flow regime, which agreed with the schematic (Figure 2-8) as drawn by Ruzicka *et al.* (2001).

Maceiras *et al.* (2010) suggested that an increase in the superficial gas velocity results in an increase in the gas hold up due to the increase in bubble break up in the homogenous flow regime. A study by Mouza *et al.* (2005a) reported that as the superficial gas velocity was increased in the homogeneous regime, the number of bubbles in the column increased which resisted the bubble rise velocity. This resistance kept the bubbles in the dispersion and increased gas hold up. The similar behaviours of gas hold-up were observed at different superficial gas velocities and alkane concentrations, and graphs are displayed in Appendix 9.2.2.

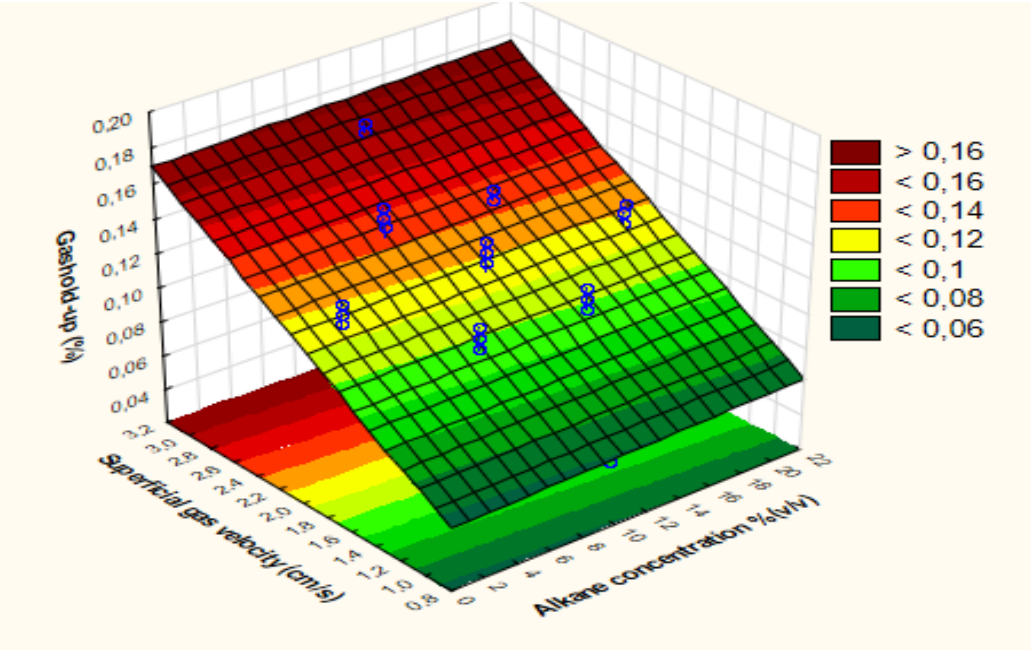

.

Figure 5-15: Effect of the alkane concentration and superficial gas velocity on gas holdup at constant solids loading (midpoint value of 3.25 g/l).

Figure 5-16 is a response surface graph showing the influence of superficial gas velocity and yeast loading on the gas hold-up at constant alkane concentration (at the midpoint of 11.25% v/v). The graph showed a linear increase in gas hold up with an increase in superficial gas velocity whilst a marginal decrease in gas hold-up with increasing yeast loading is evident. The decrease in gas hold up with increasing yeast loading can be attributed to the adhesion of particles to the bubble surface, which increased the bubble coalescence behaviour (Dietrich *et al.*, 1992).

The graph also showed that a reduced influence of the superficial gas velocity on the gas hold up when solids were added to the system. Yeast addition caused a change in flow regime from homogenous to churn-turbulent which leads to formation of large bubbles in the system as reported by Hyndman *et al.* (1997). The increase in gas hold up with increasing superficial gas velocity corroborated the findings of Gandhi *et al.* (1999), who reported that increasing superficial gas velocity resulted in a corresponding linear increase in gas hold up. Similar results were obtained at different superficial gas velocities and yeast loadings and will be provided in Appendix 9.2.1.

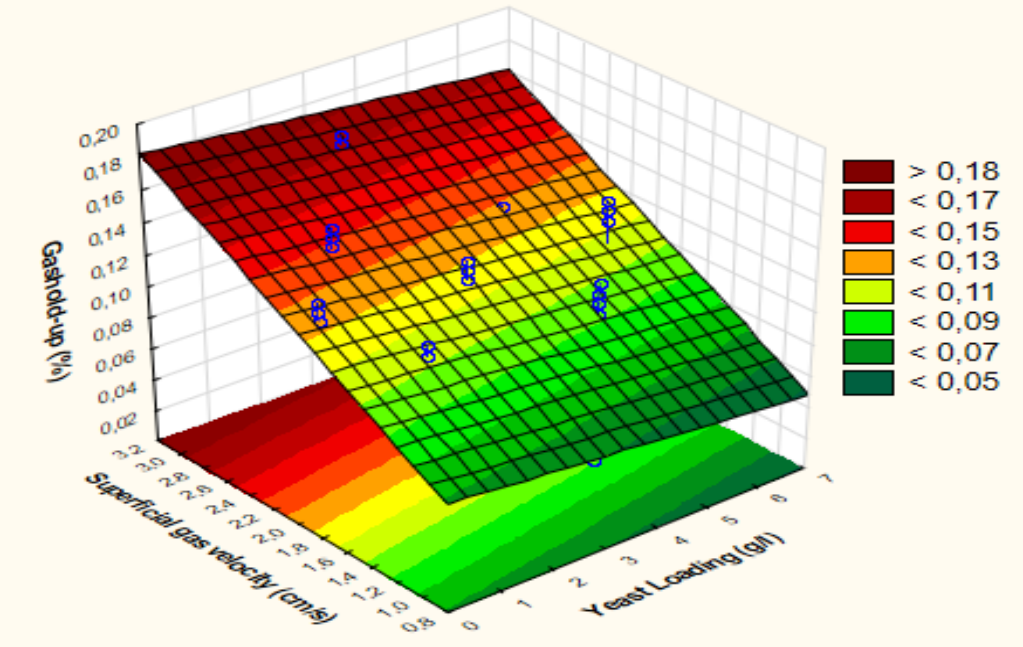

Figure 5-16: Effect of the yeast loading and superficial gas velocity on gas hold up at constant alkane concentration (midpoint value of 11.25% v/v).

Figure 5-17 is a response surface graph showing the influence of alkane concentration and yeast loading on the gas hold up at a midpoint value of superficial gas velocity (2 cm/sec). It shown that variations in alkane concentration did not affect the resultant gas hold up to a large extent, however a slight decrease in gas hold up resulted from increasing yeast loading from 0.5 to 6 g/l. It can be suggested that there is no relationship between the alkane concentration and yeast loading since the graph was flat when the superficial gas velocity was constant, as a result there was not much change in H. These findings were described previously in Figure 5-15 and Figure 5-16. Similar behaviours of gas hold up were obtained at different alkane concentrations and yeast loadings, and are provided in Appendix 9.2.1.

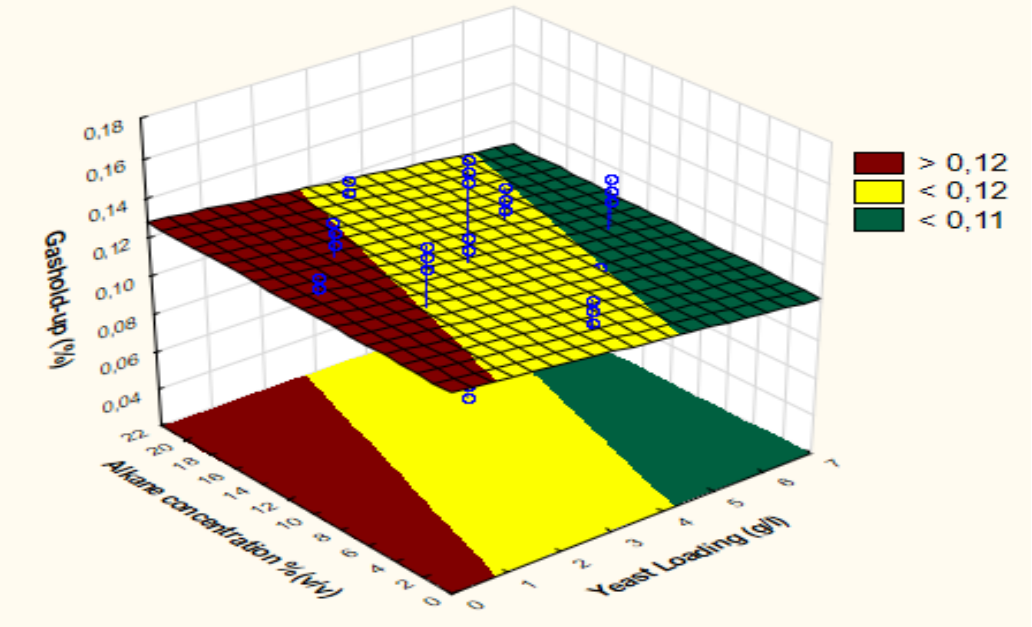

Figure 5-17: Effect of the yeast loading and alkane concentration on gas hold up at constant superficial gas velocity (midpoint value of 2 cm/sec).

5.3.2 Influence of the system parameters on the Sauter mean diameter

The Sauter mean diameter (D_{32}) for multiphase systems was obtained from the image analysis using MATLAB® (as discussed in Section 4.5.2), and then calculated from the projected bubble areas (Equation 2-7). It was thereafter statistically analysed and used to produce the Pareto chart as shown in Figure 5-18, at the 95% confidence level. The chart shows that the linear effects of superficial gas velocity, yeast loading and the interaction effect of superficial gas velocity and alkane concentration significantly affect the Sauter mean diameter (D_{32}). The linear effects of the superficial gas velocity and yeast loading are positive, with the superficial gas velocity being the most influential, whilst the interaction effect of superficial gas velocity and alkane concentration reduced D_{32}. The effects of system parameters (alkane concentration, superficial gas velocity and yeast loading) on D_{32} will be further explained in Figure 5-19, Figure 5-20 and Figure 5-21.

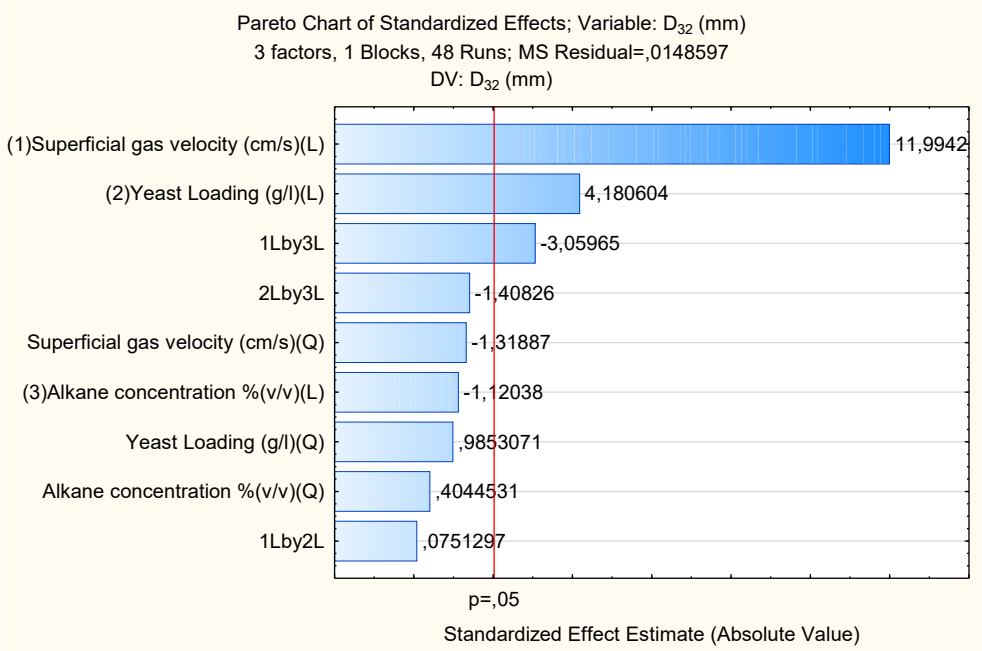

Figure 5-18: Pareto plot from basic statistical model for the impact of independent variables and interaction on D_{32} in a four phase model with 95% confidence level.

Figure 5-19 is a response surface plot showing the influence of alkane concentration and superficial gas velocity on D_{32} at constant yeast loading (midpoint). The graph shows a linear increase in D_{32} (from 2.2 mm to 3.7 mm) with increasing superficial gas velocity (1 cm/sec to 3 cm/sec). Although the alkane concentration was varied from 2.5 to 20% v/v, there was no notable change in D_{32} since at high superficial gas velocities the bubble break up and the coalescence rates are in equilibrium (Dumont *et al.*, 2006; Morao *et al.*, 1999; Kawase and Moo-Young, 1990). The increase in D_{32} with increasing superficial gas velocity corroborated the findings of Camarasa *et al.* (1999), who reported an increase in D_{32} with superficial gas velocity in a porous sparger BCR. The increase was attributed to increasing bubble formation time at the sparger which also led to an increase in the size of the bubbles developing at the sparger surface. Similar behaviours of D_{32} were observed at different alkane concentrations and superficial gas velocities as displayed in Appendix 9.2.2.

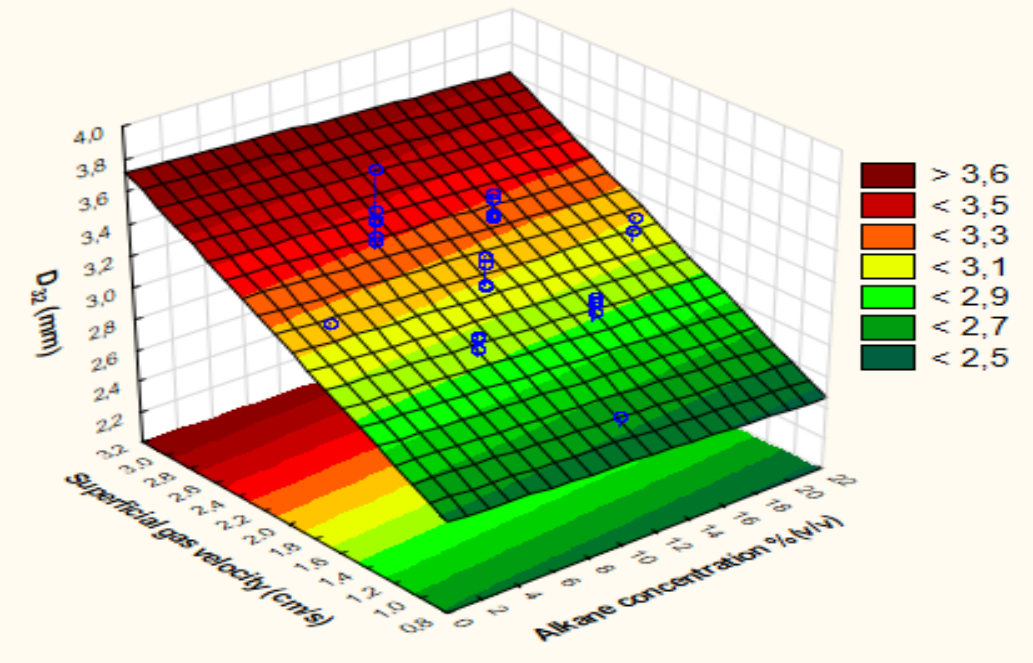

Figure 5-19: Effect of the alkane concentration and superficial gas velocity on D_{32} at constant yeast loading (midpoint value of 3.25 g/l).

Figure 5-20 is a response surface graph showing the influence of superficial gas velocity and yeast loading on D_{32} at constant alkane concentration (at the midpoint of 11.25% v/v). The graph shows the existence of a linear relationship between both input variables (yeast loading and superficial gas velocity) and the D_{32}. An increase in either of the two input variables resulted in a corresponding increase in the D_{32}, with the highest D_{32} attained (above 3.8 mm) being at the highest value of superficial gas velocity (3 cm/sec) and yeast loading (6 g/l). The findings were also consistent with reports by different researchers such as Prakash *et al.* (2001), Hyndman *et al.* (1997) and De Swart *et al.* (1996) who observed an increase in D_{32} with increasing solid concentrations and superficial gas velocities. The addition of yeast into the system changes the flow regime from homogenous to churn-turbulent, thereby increasing bubble diameters (Hyndman, Larachi and Guy, 1997). Similar results of D_{32} were found at different superficial gas velocities and yeast loadings as displayed in Appendix 9.2.2.

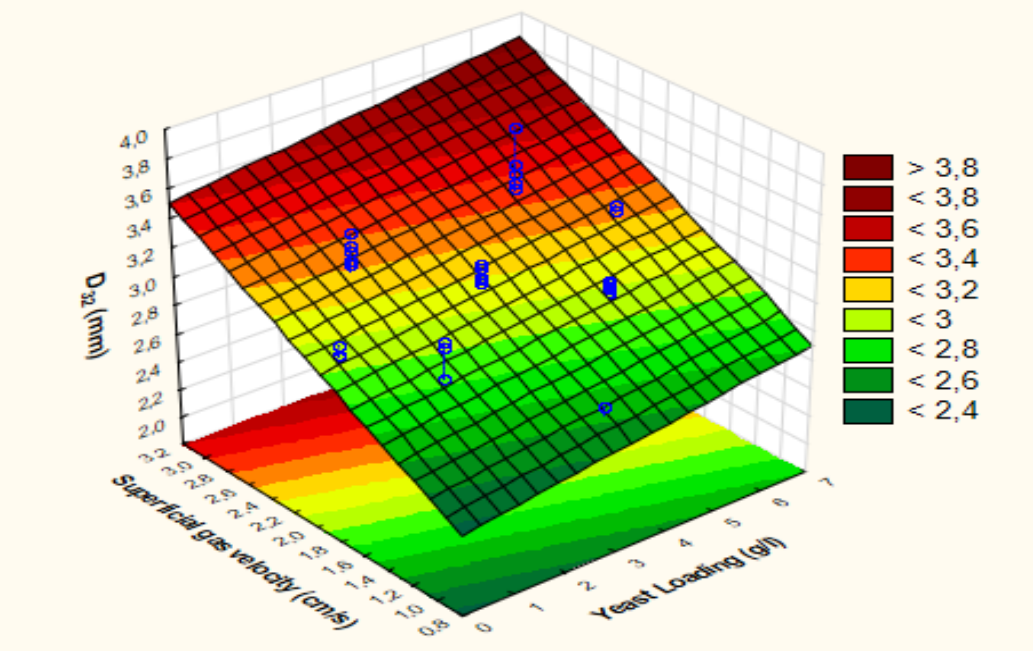

Figure 5-20: Effect of the yeast loading and superficial gas velocity on D_{32} at constant alkane concentration (midpoint value of 11.25 % v/v).

Figure 5-21 is a response surface graph showing the influence of alkane concentration and yeast loading on D_{32} at a midpoint value of superficial gas velocity (2 cm/sec). The graph showing a linear increase in D_{32} as a result of an increase in yeast loading, with a small decrease in D_{32} with increasing alkane concentration. As the solids loading is further increased, and the behaviour of non-viable yeast cells as particles ceases as the relative viscosity of the dispersion is increased, limiting the bubble breakup behaviour in the column and increasing D_{32} (Prakash *et al.*, 2001; Hyndman *et al.*, 1997; De Swart *et al.*, 1996). It confirmed the influence of the two variables (alkane concentration and yeast loading) on D_{32} as previously described on Figure 5-19 and Figure 5-20. Similar results of D_{32} were found at different alkane concentrations and yeast loadings as displayed in Appendix 9.2.2.

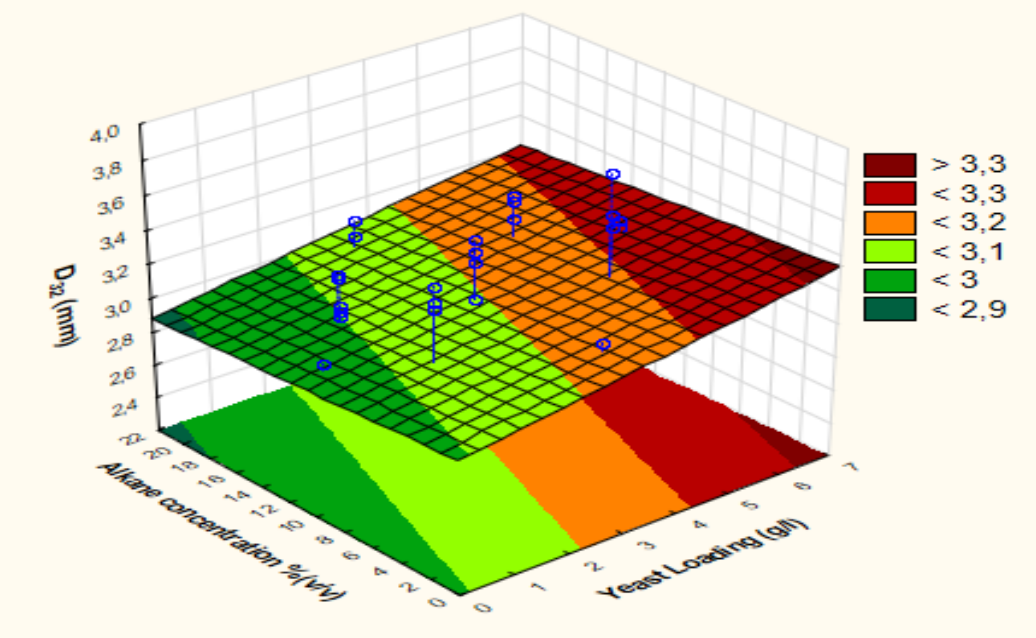

Figure 5-21: Effect of the yeast loading and alkane concentration on D_{32} at constant superficial gas velocity (midpoint value of 2 cm/sec)

5.3.3 Influence of the system parameters on the interfacial area

Figure 5-22 is a Pareto chart showing the influence of three variables (superficial gas velocity, yeast loading and alkane concentration) on the interfacial area at 95% confidence level. The chart showing that the linear effects of superficial gas velocity and yeast loading as well as the yeast loading/alkane concentration interaction effects have significant influence on the interfacial area at the 95% confidence level. Positive influences were found for the linear effect of superficial gas velocity and the interaction effect of yeast loading and alkane concentration, the superficial gas velocity being the most influential. In addition, the linear effect of yeast loading decreased the interfacial area. All quadratic effects, as well as the linear effect of the alkane concentration and the superficial gas velocity/alkane concentration interaction effects were not of significant influence. The effects of system parameters (alkane concentration, superficial gas velocity and yeast loading) on the interfacial area will be further discussed in Figure 5-23, Figure 5-24 and Figure 5-25.

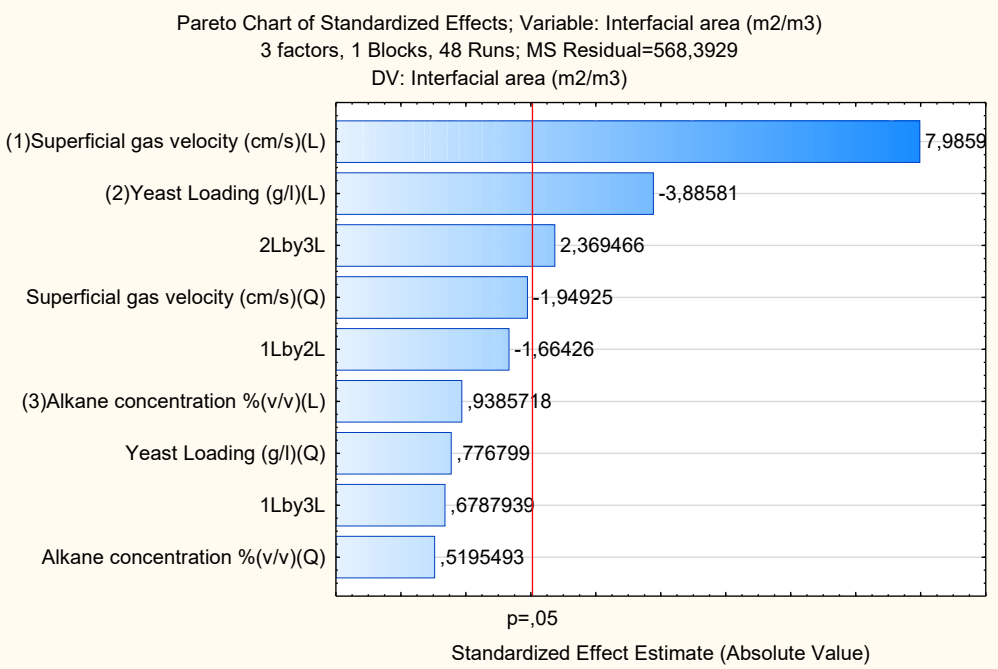

Figure 5-22: Pareto plot from basic statistical model for the impact of independent variables and interaction on interfacial area in a four phase model with 95% confidence level indicated.

Figure 5-23 is a response surface graph showing the effects of alkane concentration and superficial gas velocity on the interfacial area at constant yeast loading (at the midpoint of 3.25 g/l). A linear relationship was observed between the superficial gas velocity and the interfacial area. An increase in the superficial gas velocity from 1 to 3 cm/sec resulted in an increase in the interfacial area (120 to 290 m^2/m^3). The alkane concentration on the other hand had little impact on the interfacial area, with a marginal increase of 20 m^2/m^3 in the interfacial area when the alkane concentration was increased from 2.5 to 20 % v/v. The increase in interfacial area with increasing superficial gas velocity was due to the increase in the gas hold up as shown on Figure 5-15. This confirmed the results of study carried out by Akita and Yoshida, (1974), who reported that increase in gas hold-up will cause an increase in the interfacial area. However, a recent study in a STR by Hollis and Clarke, (2016) found a decrease in the interfacial area with an increase in the alkane concentration at constant yeast loading and high agitation rates. Those findings suggest that the mechanism of both BCR and STR are different, since the mixing in a STR has higher shear rates than in the BCR. Similar behaviours of the interfacial area were found at different alkane concentrations and superficial gas velocities as provided in Appendix 9.2.3.

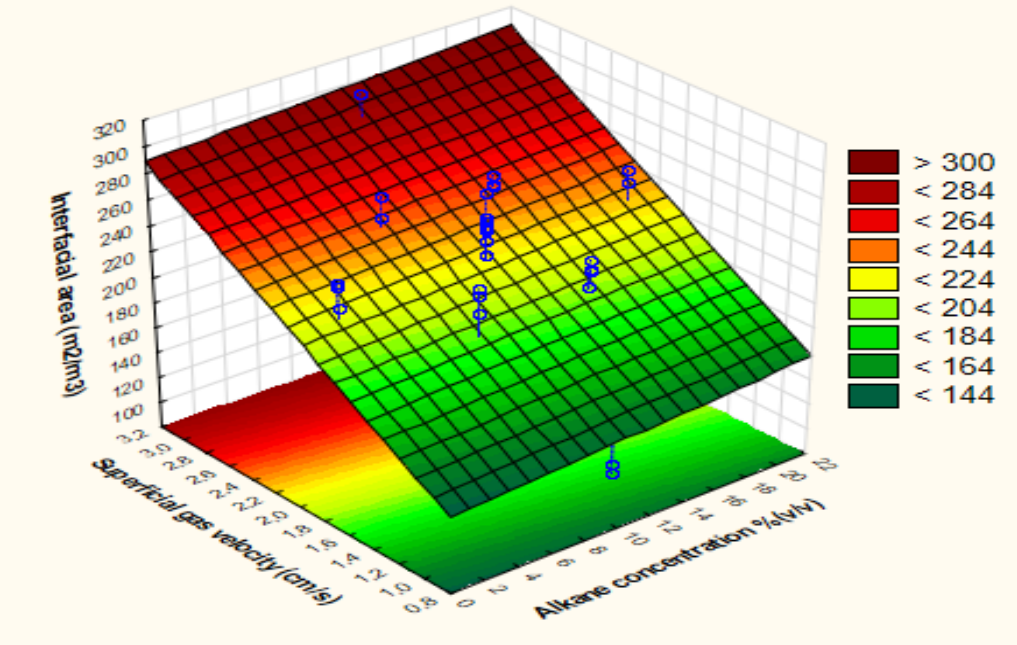

Figure 5-23: Effect of the alkane concentration and superficial gas velocity on interfacial area at constant solids loading (midpoint value of 3.25 g/l).

Figure 5-24 is a response surface graph showing the influence of yeast loading and superficial gas velocity on the interfacial area at constant alkane concentration (at the midpoint of 11.25% v/v). The interfacial area increased linearly (from 140 to 330 m^2/m^3) with increasing superficial gas velocity (from 1 to 3 cm/sec) at low yeast loading. However, increasing yeast loading from 0.5 g/l to 6 g/l saw a decrease in the interfacial area from 140 to 120 m^2/m^3 at the minimum level of superficial gas velocity (1 cm/sec). The observed decrease in the interfacial area at high yeast loadings was caused by an increase in the Sauter mean bubble diameter (Figure 5-20 and Figure 5-21), which supported the findings of Gandhi *et al.* (1999). In a similar study by Hollis and Clarke, (2016) in a STR, an increase in yeast loading resulted in a decrease in the interfacial area at constant alkane concentration under high agitation conditions, which agrees with the current findings. Similar results for the interfacial area were observed at different yeast loadings and superficial gas velocities as shown in Appendix 9.2.3.

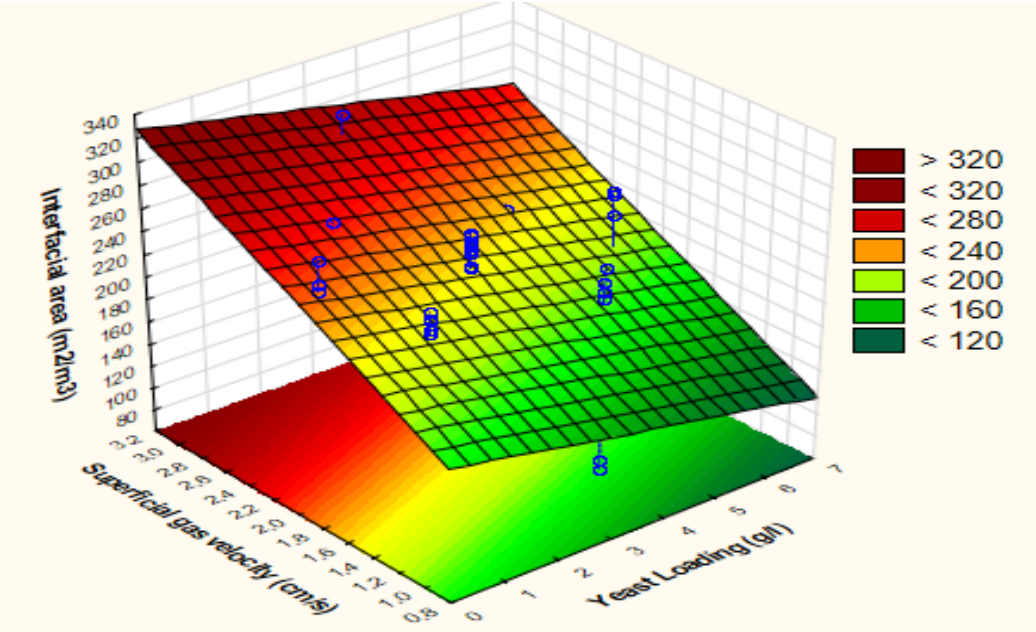

Figure 5-24: Effect of the yeast loading and superficial gas velocity on interfacial area in at constant alkane concentration (midpoint value of 11.25 % v/v).

Figure 5-25 is a response surface graph showing the influence of alkane concentration and yeast loading on the interfacial area at constant superficial gas velocity (at the midpoint of 2 cm/sec). It showing that the alkane concentration had little influence on the interfacial area (increasing by 20 m^2/m^3) when the alkane concentration was increased from 2.5 to 20% v/v, at the highest yeast loading. Increasing yeast loading however decreased the interfacial area (from 260 to 200 m^2/m^3) when it was varied from 0.5 to 6 g/l. The observed decrease in the interfacial area at high yeast loadings was caused by an increase in the D_{32} (Figure 5-20 and Figure 5-21). Similar behaviours of the interfacial area were found under different alkane concentrations and yeast loadings as displayed in Appendix 9.2.3.

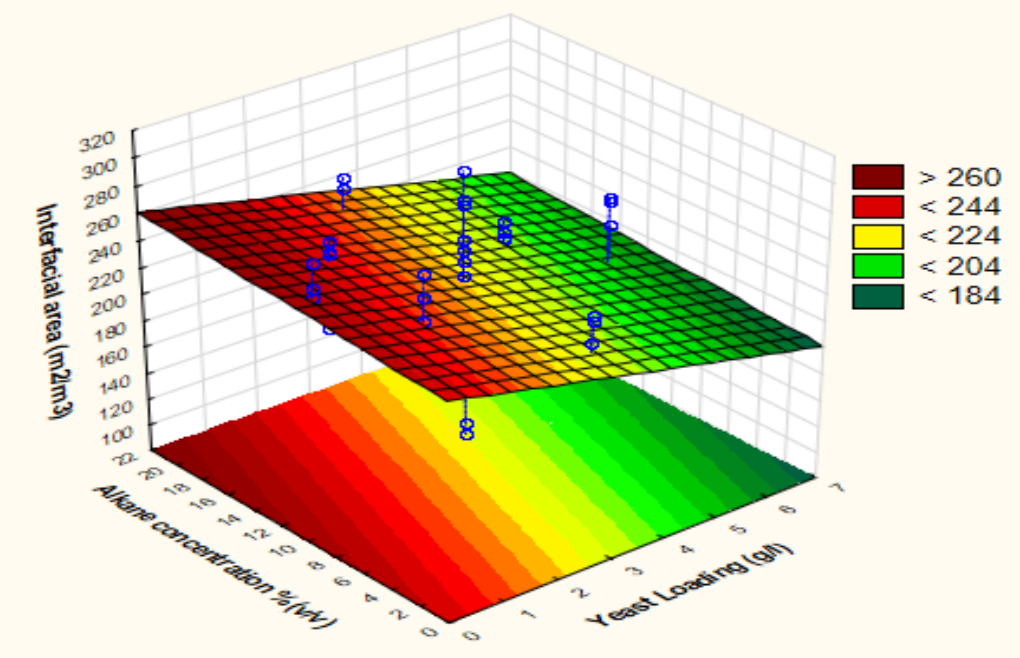

Figure 5-25: Effect of the yeast loading and alkane concentration on interfacial area at constant superficial gas velocity (midpoint value of 2 cm/sec).

It can be concluded that a high interfacial area is required for high oxygen transfer rates. From the graphs (Figure 5-23, Figure 5-24 and Figure 5-25), it was observed that the interfacial area increased mainly with increasing superficial gas velocity and decreasing yeast loading, whilst the alkane concentration had insignificant influence. The interfacial area decreased when the yeast loading increased from 0.5 to 6 g/l due to the increase in D_{32}. Therefore the system should be run at high superficial gas velocities (3 cm/sec) and low yeast loading rates (0.5 g/l) for an enhanced oxygen transfer rate. However, the implication is that D_{32} increased with increasing yeast loading and superficial gas velocity. Since the interfacial area is calculated by the gas hold up and D_{32} (Equation 2-7), a smaller D_{32} and high gas hold up are required for an increase in the mass transfer area. This calls for a balance to be made between employing high superficial gas velocities and reducing D_{32}, for the best resultant interfacial area.

5.4 Examination of the K_La behaviour in a four phase air- water- hydrocarbons- deactivated yeast system

To achieve a fundamental understanding of oxygen transfer in a simulated four-phase air, water, hydrocarbon and deactivated yeast system in the BCR, K_La was evaluated under different conditions of alkane concentration, superficial gas velocity and yeast loading. K_La was measured according to the GOP method with incorporation of the effect of the probe constant K_P as discussed in Section 4.4.3. The results of both measurements (K_P as well as K_La) are described in Sections 5.4.1 and 5.4.2 respectively.

5.4.1 Influence of system parameters on K_P

The probe constant (K_P) has to be measured for each experimental condition to ensure the accuracy of the K_La measurement. To measure the effect of the system parameters on K_P, a linear model (Equation 4-1) as described in Section 4.4.1 was employed. The measurements were done in triplicate under each condition to improve the accuracy (standard deviation of less than 0.7% of the mean) and estimate the uncertainty around K_La, when using the second order model for K_La determination (Equation 2-3).

Figure 5-26 is a Pareto chart of variables showing the influence of three variables (superficial velocity, alkane concentration and yeast loading) on K_P at 95% confidence level. The chart showing that the quadratic effect of superficial gas velocity and the linear effect of alkane concentration significantly influenced K_P. The quadratic effect of superficial gas velocity was the most positive influential of the three variables on K_P whereas the linear effect of alkane concentration reduced K_P.

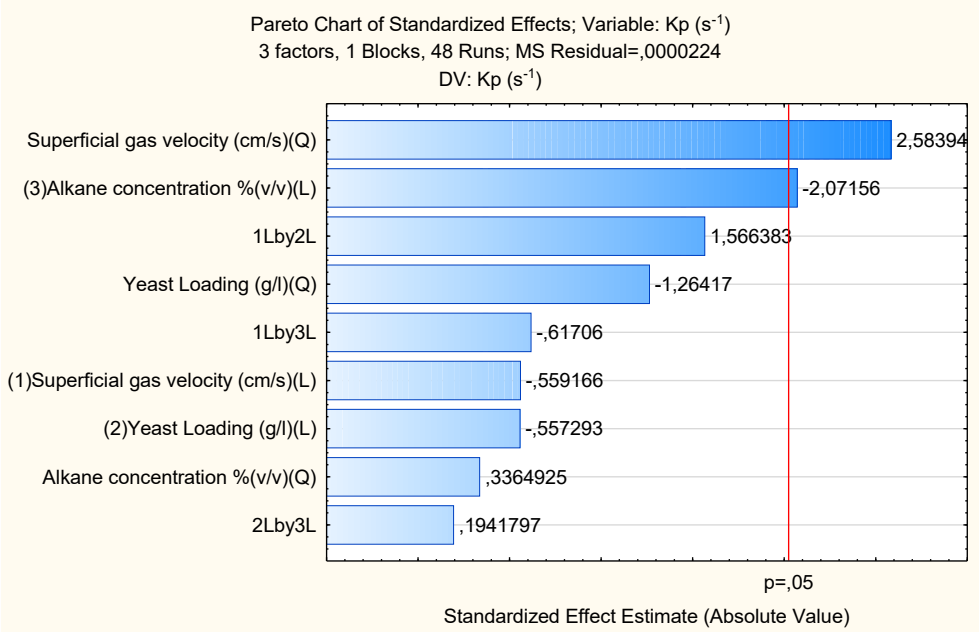

Figure 5-26: Pareto chart from statistical model for the impact of independent variables and interaction on K_P in a four phase model with 95% confidence level.

Queimada *et al.* (2003) as well as Clarke and Manyuchi, (2012), established that K_P was significantly depressed in systems containing increased alkane concentrations. Although this study did not test this, literature has also shown that an increase in the alkane chain length also decreases K_P, increasing the probe response time. Adding to this, the previous work by Hollis and Clarke, (2016) in a STR found a similar depression on K_P with increase alkane concentration and solids loading at high agitation rates. Prior to these findings, K_P had been reported to be influenced only by the properties of the probe, like membrane thickness, membrane age, membrane type and electrolyte usage (Aiba and Huang, 1969; Philichi and Stenstrom, 2009).

The response surface graphs (Figure 5-27, Figure 5-28 and Figure 5-29) also confirmed that the system parameters such as the superficial gas velocity, alkane concentration and yeast loading had an impact on K_P. Since the impact of the operational conditions on K_P is not well documented in literature especially in BCRs, it will require further investigations for the next study to establish a full understanding of K_P behaviour in BCR. Similar behaviours of K_P were found at different conditions of the system parameters (alkane concentration, yeast loading and superficial gas velocity), and are provided in Appendix 9.2.4.

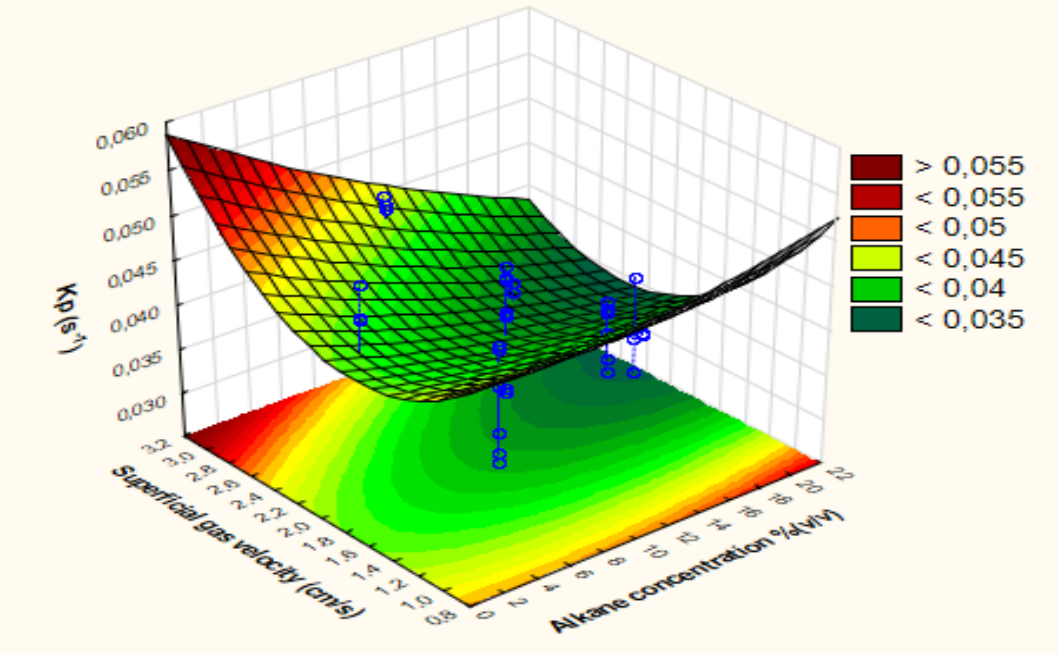

Figure 5-27: Effect of the alkane concentration and superficial gas velocity on K_P at constant solids loading (midpoint value of 3.25 g/l).

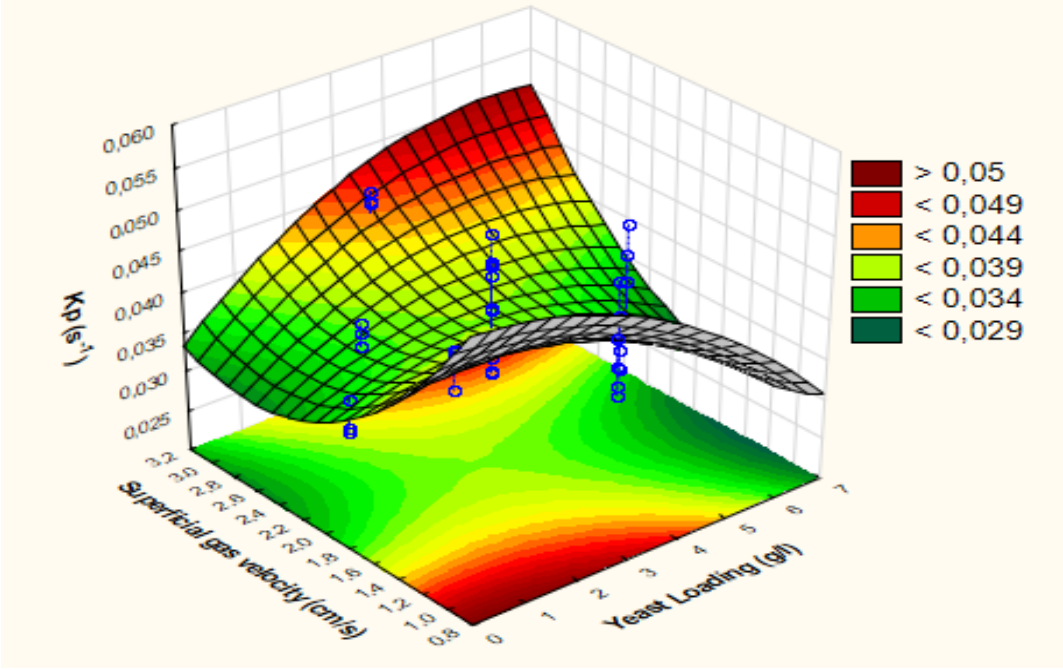

Figure 5-28: Effect of the yeast loading and superficial gas velocity on K_P at constant alkane concentration (midpoint value of 11.25% v/v).

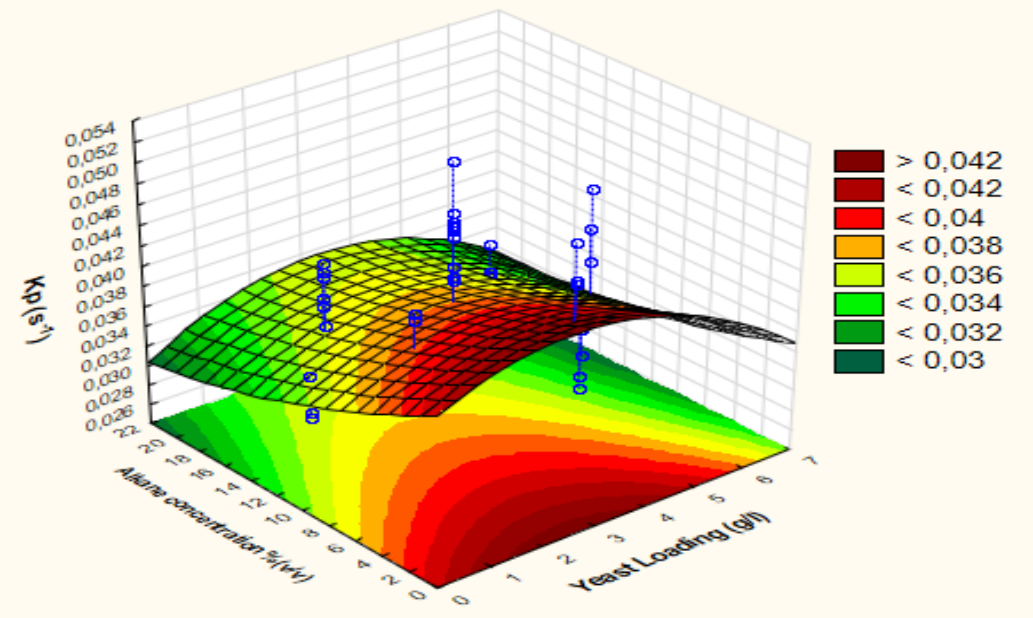

Figure 5-29: Effect of the yeast loading and alkane concentration on K_P at constant superficial gas velocity (midpoint value of 2 cm/sec).

5.4.2 Influence of system parameters on K_La

Figure 5-30 is a Pareto chart of independent variables, showing the influence of alkane concentration, yeast loading and superficial gas velocity on K_La. The quadratic effect of the alkane concentration is the only significant influence on K_La at the 95% confidence interval. All other effects were not significant at 95% confidence level. However, K_La was previously shown to be enhanced by the superficial gas velocity (as discussed in Section 5.1) and depressed by the alkane concentration and yeast loading (as discussed in Sections 5.2.2 and 5.2.3). The influence of alkane concentration, superficial gas velocity and yeast loading will be further discussed with reference to Figure 5-31, Figure 5-33 and Figure 5-37.

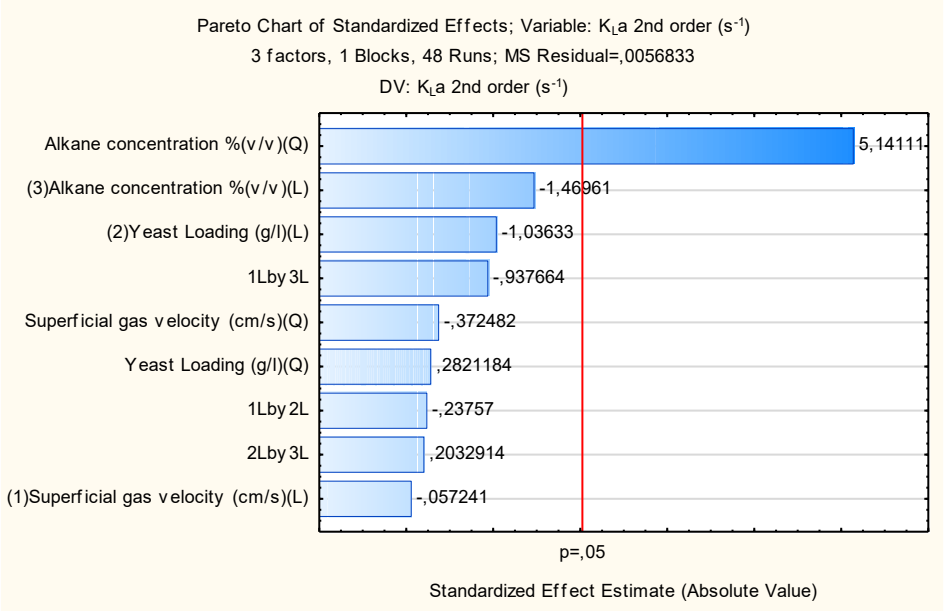

Figure 5-30: Pareto plot from statistical model for the impact of independent variables and interaction on K_La in a four phase model at 95% confidence level.

Figure 5-31 is a response surface graph showing the effects of alkane concentration and superficial gas velocity on K_La at constant yeast loading (at the midpoint of 3.25 g/l). The graph showing the existence of a minimum with a change in alkane concentration. The K_La deceased until a minimum point was reached at 10% v/v alkane concentration and then started to rise with further increases in alkane concentration up to 20% v/v. An initial decrease in the K_La value agreed with the results of investigation on K_La in three phase system (discussed in depth in Section 5.2.12). On the contrary, results reported in STRs by Hollis and Clarke, (2016) showed an initial increase in K_La with increasing alkane concentration until 11% v/v, and then a decrease in K_La value as alkane concentration further increased up to 20% v/v. The disagreement in these findings might be attributed to the differences in the reactors' geometry, sparger types as well as the mixing mechanisms, since the mixing in the BCRs depends on the aeration rate, whilst STRs have mechanical impellers.

Increasing the superficial gas velocity was observed to decrease the K_La at high alkane concentrations. At low alkane concentrations however, the opposite was observed. The decrease in K_La at high alkane concentration could be due to the increase in fluid viscosity which damped the turbulence in the system (Clarke and Manyuchi, 2012). However, this would need to be verified with further experiments examining viscosity, and other fluid parameters.

Since the K_La is product of the interfacial area and the oxygen transfer coefficient K_L and it was confirmed that the alkane concentration had insignificant impact on the interfacial area, as illustrated in Figure 5-23, whilst K_L was found to be affected by alkane concentration (Figure 5-32), it can then be inferred that the influence of alkane concentration on K_La is primarily due to K_L. This may be attributed to the change in the fluid properties and system hydrodynamics which influence K_L (Cascaval *et al.*, 2006; Chisti and Moo-Young, 1988). Similar behaviours of K_La and K_L values were observed at different alkane concentrations and superficial gas velocities and are provided in Appendix 9.2.5 and 9.2.6.

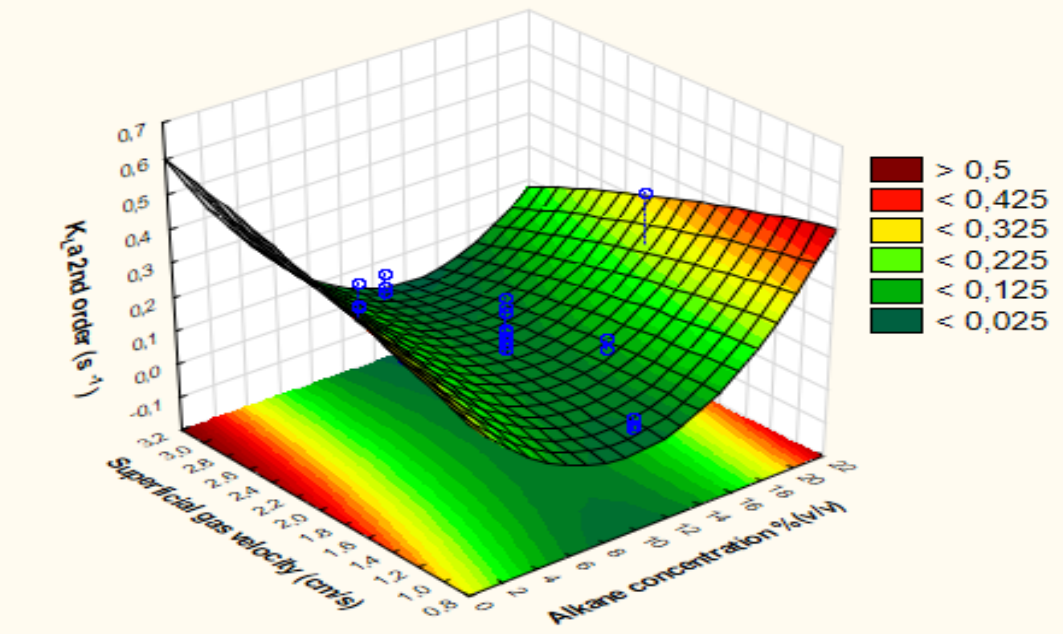

Figure 5-31: Effect of the alkane concentration and superficial gas velocity on K_La at constant solids loading (midpoint value of 3.25 g/l).

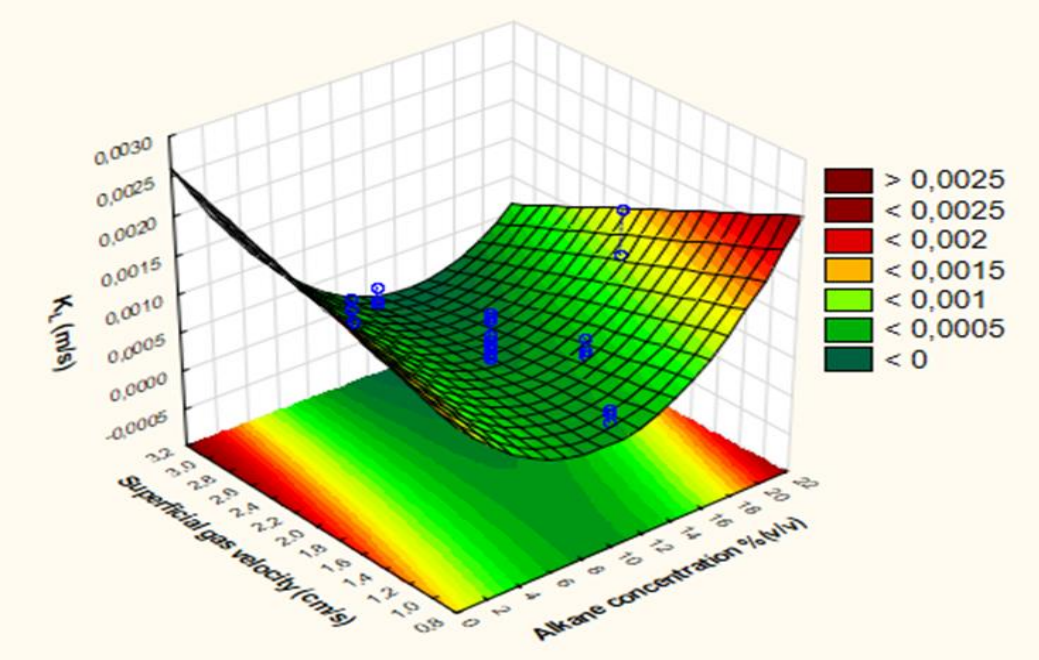

Figure 5-32: Effect of the alkane concentration and superficial gas velocity on K_L at constant solids loading (midpoint value of 3.25 g/l).

Figure 5-33 is a response surface graph showing the effects of superficial gas velocity and yeast loading on K_La at constant alkane concentration (the midpoint of 11.25% v/v). Increasing the yeast loading marginally reduced K_La at high superficial gas velocity, which agreed with the results of examination of K_La under the effect of yeast loading (as discussed in Section 5.2.3). This decrease was also observed in the interfacial area (Figure 5-24) when the yeast loading increased from 0.5 to 6 g/l. K_La increased with increasing superficial gas velocity, to give maximum value of K_La (0.49 s^1) at the highest superficial gas velocity (3 cm/sec) and low yeast loading when the alkane concentration was changed to 2.5% v/v (Figure 5-34). However, increasing the alkane concentrations to 20% v/v resulted in the K_La decreasing with increasing superficial gas velocity, resulting in a minimum value (0.15 s^{-1}) at the highest superficial gas velocity (3 cm/sec), as shown on Figure 5-35. This result might be due to increasing fluid viscosity with increasing alkane concentration, which damped the turbulence in the system and ultimately effected the K_L (Figure 5-36) (Correia *et al.*, 2010). It may as well be a result of the increasing oxygen transfer driving force, which increased the oxygen transfer rate (OTR), and therefore reduced the K_La value (Clarke and Correia, 2008). Similar behaviours of K_La and K_L were observed at different superficial gas velocities and yeast loadings and are provided in Appendix 9.2.5 and 9.2.6.

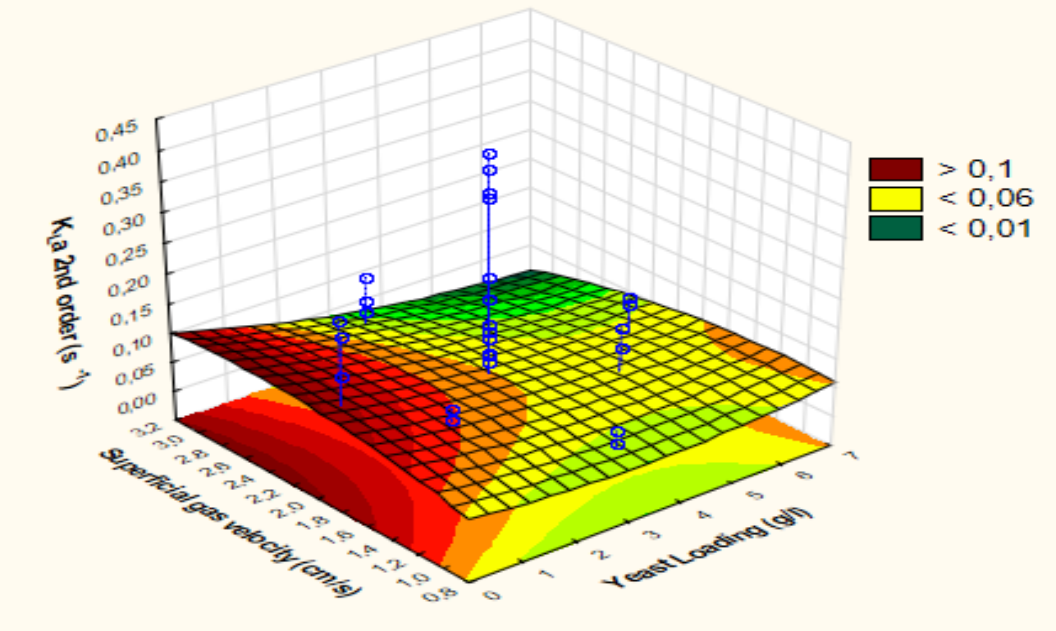

Figure 5-33: Effect of the yeast loading and superficial gas velocity on K_La at constant alkane concentration (midpoint value of 11.25% v/v).

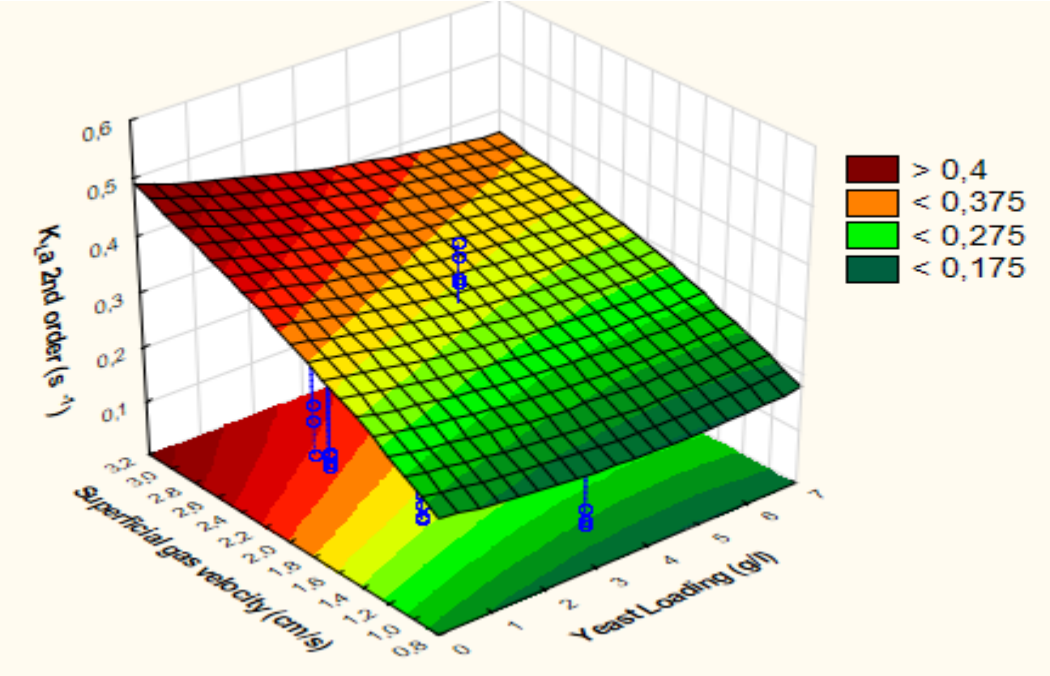

Figure 5-34: Effect of the yeast loading and superficial gas velocity on K_La at constant alkane concentration (low value of 2.5% v/v).

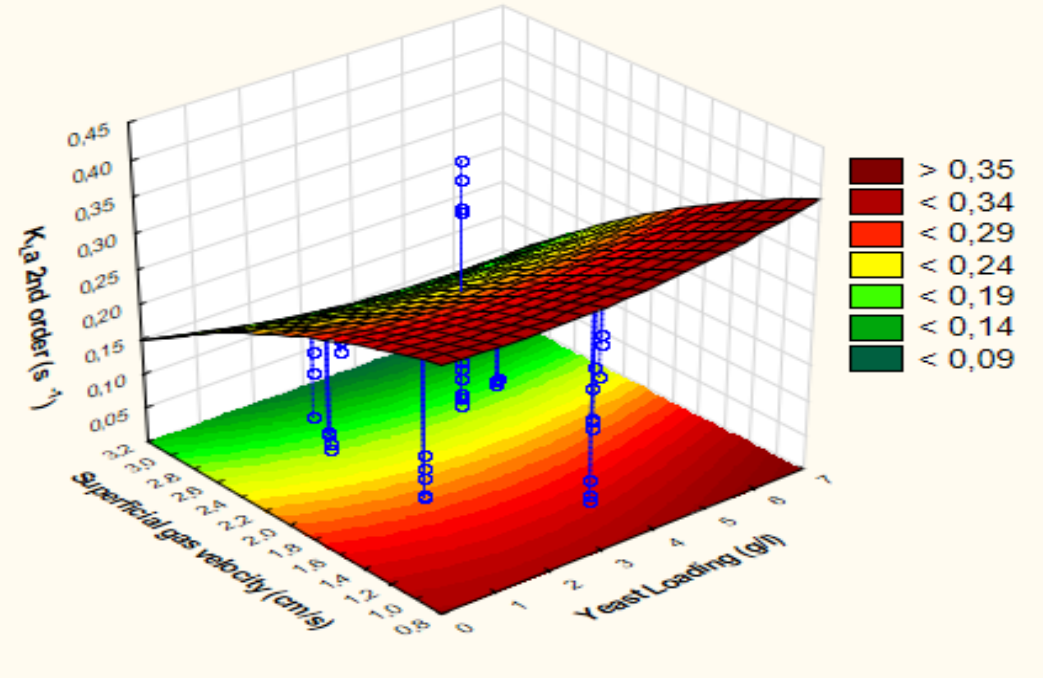

Figure 5-35: Effect of the yeast loading and superficial gas velocity on $K_L a$ at constant alkane concentration (high value of 20% v/v).

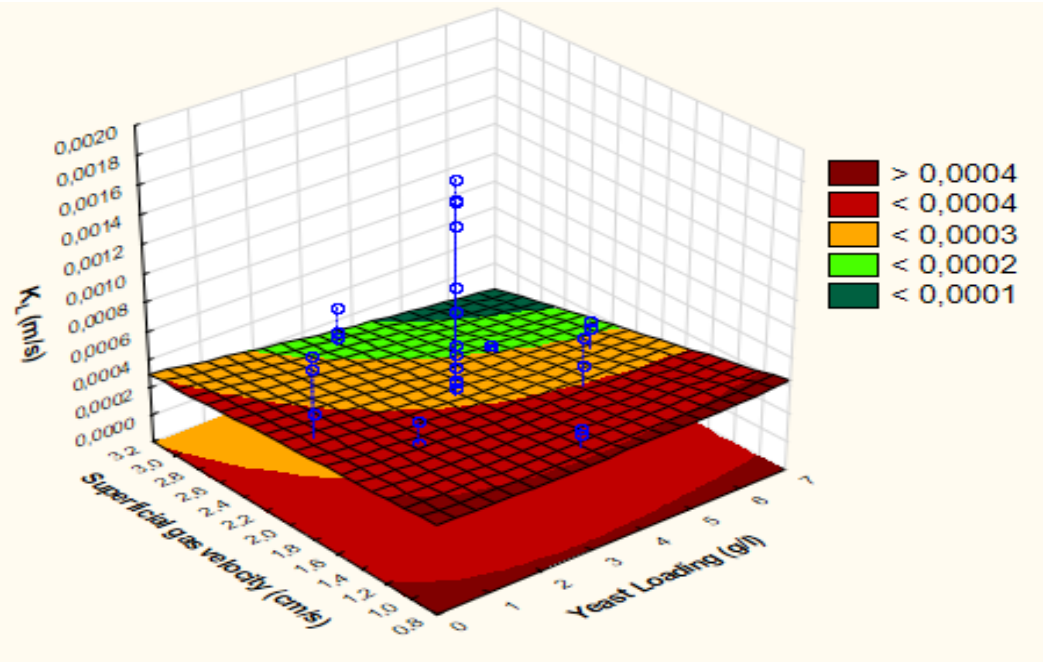

Figure 5-36: Effect of the yeast loading and superficial gas velocity on K_L at constant alkane concentration (midpoint value of 11.25% v/v).

Figure 5-37 is a response surface graph showing the influence of yeast loading and alkane concentration on K_La at constant superficial gas velocity (at the midpoint of 2 cm/sec). The graph further confirmed the existence of a minimum when the alkane concentration was increased from 2.5 to 20% v/v (Figure 5-31). However, the observed increase in K_La value above 10% v/v alkane concentration might be a result of the effect of interaction between the yeast loading and the alkane concentration, which changed the fluid properties and then influenced K_L (Figure 5-38). Since the superficial gas velocity was constant, it can also be concluded from the graph that the yeast loading did not significantly affect the K_La. Similar behaviors of K_La and K_L were found at different alkane concentrations and yeast loadings, as provided in Appendix 9.2.5 and 9.2.6.

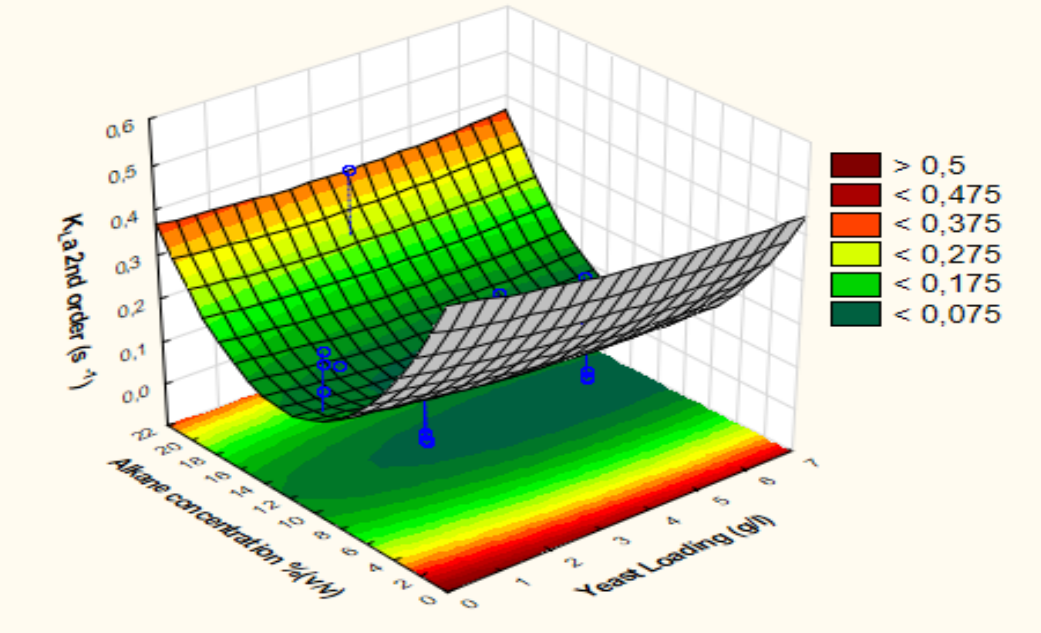

Figure 5-37: Effect of the yeast loading and alkane concentration on K_La at constant superficial gas velocity (midpoint value of 2 cm/sec).

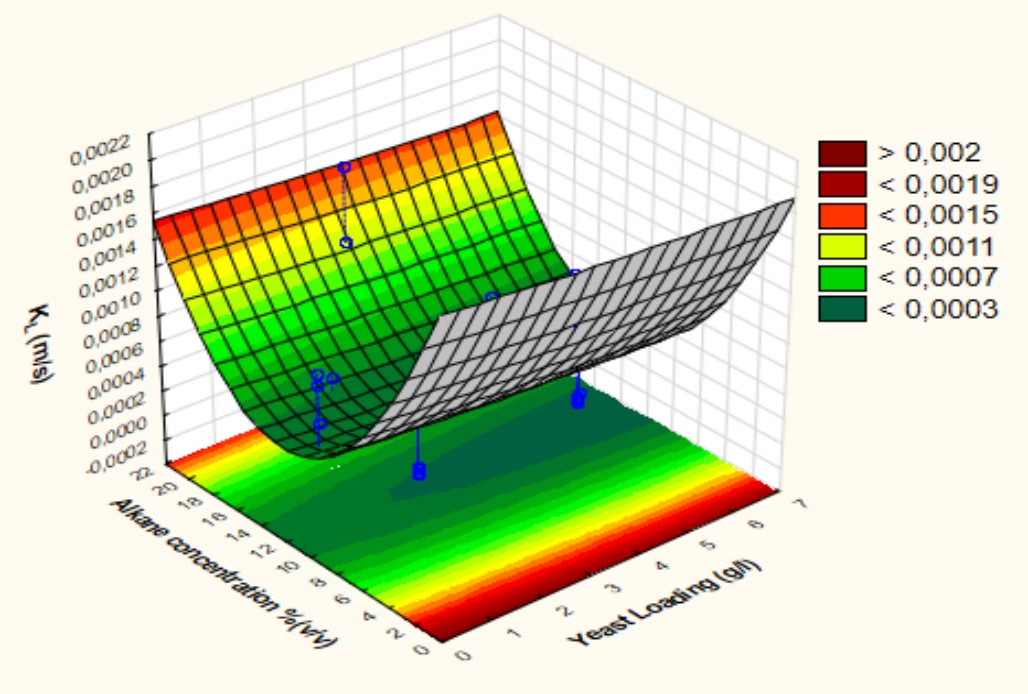

Figure 5-38: Effect of the yeast loading and alkane concentration on K_L at constant superficial gas velocity (midpoint value of 2 cm/sec).

A summary of the effects of the three parameters (superficial gas velocity, alkane concentration and yeast loading) on K_La. Figure 5-39 showing the impact of each phase combination: a) air-water, b) air-water-hydrocarbons, c) air-water-deactivated yeast and d) air-water-hydrocarbons-deactivated yeast, on the behaviour of K_La at the mid value of alkane concentration (11.25% v/v) and mid value of yeast loading (3.25 g/l) under range of superficial gas velocity (1 cm/sec, 2 cm/sec and 3 cm/sec) in the BCR. The following conclusions can be made from the graph;

a) In two phase system (air-water), the value of K_La increased when the superficial gas velocity increased from 1 to 3 cm/sec, as observed in Section 5.1.

b) In three phase system (air-water-hydrocarbons), the value of K_La also increased when the superficial gas velocity increased from 1 to 3 cm/sec at constant alkane concentration (midpoint 11.25% v/v), as discussed in Section 5.2.2.

c) In the three phase system (air-water-deactivated yeast), the value of K_La decreased when the superficial gas velocity increased from 1 cm/sec to 3 cm/sec at constant yeast loading (midpoint 3.25 g/l), as discussed in Section 5.2.3.

d) In the four phase system (air-water-hydrocarbon-deactivated yeast), the value of K_La was unstable at the given superficial gas velocities (1 cm/sec, 2 cm/sec and 3 cm/sec) at constant yeast loading (midpoint of 3.25 g/l) and constant alkane concentration (midpoint of 11.25% v/v).

It can further be concluded that the unstable trend of K_La in the four phase systems might be a result of interaction between the alkane concentration, superficial gas velocity and yeast loading, which may have changed the fluid properties and the system hydrodynamics and therefore influenced the behaviour of K_L.

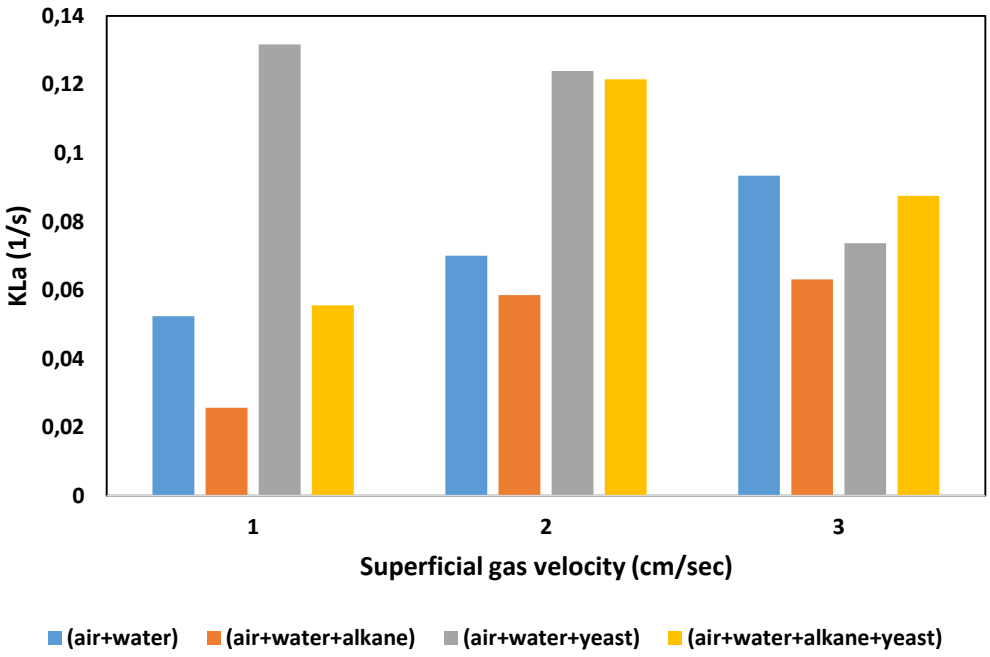

Figure 5-39: Variation of K_La behaviours with superficial gas velocity for different phases: air-water, air-water-alkane, air-water-yeast and air-water-alkane-yeast.

6. CONCLUSIONS

The conversion of alkanes through the use of microorganisms has been demonstrated by the work of many researchers. Though most of the studies were performed in stirred tank reactors, bubble column reactors are believed to be a good alternative for the bioconversion process. This study managed to provide a fundamental understanding of the impact of the alkane concentration, yeast loading and superficial gas velocity on the critical parameters (interfacial area and K_La), which underpin the oxygen transfer in a hydrocarbon-based bioprocess system in bubble column reactors.

This study was the first of its kind to focus on the behaviour of both K_La and the interfacial area in a multiphase hydrocarbon-based bioprocess system in a BCR. K_La was examined under different phase combinations (air-water, air-water-hydrocarbons and air-water-deactivated yeast) to provide an initial understanding of the impact of three factors: alkane concentration, yeast loading and superficial gas velocity on the K_La behaviours in a BCR. Eventually, the interfacial area and K_La were examined in a four phase system (air-water-hydrocarbons-deactivated yeast), to provide an understanding of their behaviours in determining the oxygen transfer rate in multiphase hydrocarbon bioprocess systems in BCRs.

The probe constant (K_P) was significantly influenced by the operational parameters (alkane concentration, yeast loading and the superficial gas velocity). For all phase conditions, it was necessary to include K_P into the measurements of K_La to enhance the reliability of the results.

Homogeneity of the system was confirmed for all experimental conditions in this study, since an assumption of homogeneity was implicated in the measurements of the interfacial area and K_La. In the three phase system (air-water-hydrocarbon), it was found that the system required a relatively high superficial gas velocity (2 cm/sec) to achieve homogeneity for different alkane concentrations (5, 10, 15 and 20% v/v). This observed result confirmed hypotheses 1. The utilization of high superficial gas velocities to achieve homogeneity may result in an increase in the power consumption, especially in industrial operation scales when the BCRs contain immiscible liquids like water and hydrocarbons. However, in the four phase system (air-water-hydrocarbon-deactivated yeast), it was seen that the addition of the yeast cells to the process changed the fluid properties and therefore increased the homogeneity, resulting in lower superficial gas velocities (1 cm/sec) required to attain sufficient homogeneity.

The impact of the yeast cells on the fluid properties and therefore on the homogeneity of the system was out of the scope of this study and requires further investigations for the next study. However, the measurement method of homogeneity was created for the first time in this study, since the homogeneity has not reported in literature, particularly in the BCRs.

In the two phase system (air-water), K_La increased with increasing superficial gas velocity (1, 2 and 3 cm/sec), which might be due to the increase in the gas hold up which increases the gas-liquid interfacial area in the system. In the three phase systems (air-water-hydrocarbon), it was observed that the values of K_La decreased when the alkane concentration increased (2.5, 11.25 and 20% v/v) at constant superficial gas velocity. The observed decrease in K_La may be due to the increase in the viscosity in the system. However, an increase was observed in the value of K_La when the superficial gas velocity increased and the alkane concentration kept constant. This might be attributed to the increased in the gas hold up which enhances the interfacial area in the system. In the three phase system (air-water-deactivated yeast), it was found that K_La also decreased with increasing yeast concentration (0.5, 3.25 and 6 g/l) at constant superficial gas velocity. Moreover, it was observed that K_La decreased when the yeast loading kept constant and the superficial gas velocity increased from 1 to 3 cm/sec. This may be due to the increase in the value of D_{32}, which then decreases the interfacial area in the system. All the results from the experiments done in two and three phase systems agree with literature, although the interfacial area was not evaluated since the camera could not capture clear images in these phases.

In the four phase system (air-water-hydrocarbons-deactivated yeast), the gas hold-up was observed to be significantly affected by the superficial gas velocity. A linear increase in the gas hold up was observed when the superficial gas velocity was increased from 1 to 3 cm/sec at constant yeast loading, while no significant effect from the alkane concentration could be established. A slight decrease in the gas hold up was found when the yeast loading was increased at high superficial gas velocities for all constant alkane concentrations. The D_{32} was also influenced by the yeast loading and the superficial gas velocity for all the alkane concentrations. A linear increase in D_{32} was also observed with increasing superficial gas velocity (1 to 3cm/sec). D_{32} increased by an average value of 0.35 mm when the yeast loading increased from 0.5 to 6 g/l at high superficial gas velocity and constant alkane concentration (11.25 % v/v).

The interfacial area was then measured from the D_{32} and the gas hold up data. The values of the interfacial area increased (from 120 to 190 m^2/m^3) with increasing superficial gas velocity (from 1 to 3 cm/sec) at low alkane concentration and constant yeast loading (midpoint of 3.25 g/l). This increase in the interfacial area was a result of the increasing gas hold up when the superficial gas velocity increased from 1 to 3 cm/sec, which confirmed hypotheses 2.

The impact of the alkane concentration on the interfacial area was insignificant since it had little influence on the gas hold up as well as D_{32}. Those results disapproved hypotheses 3 since the interfacial area was reported to be effected by the alkane concentration. On the other hand, increasing the yeast loading from 0.5 to 6 g/l resulted in a decrease in the interfacial area of approximately 60 m^2/m^3 at the highest alkane concentration (20% v/v), and constant superficial gas velocity of 2 cm/s, this decrease was a result of increasing the D_{32} when the yeast loading increased in the system. These findings agreed with literature and also confirm hypotheses 4.

In the same four phase system (air-water-hydrocarbons-deactivated yeast), K_La was observed to be mainly effected by the alkane concentration. The highest K_La (0.6 s^{-1}) occurred at the lowest alkane concentration (2.5% v/v), highest superficial gas velocity (3 cm/sec) and constant yeast loading (3.25 g/l). The K_La then decreased with an initial increase in the alkane concentration (2.5 to 10% v/v), but started to rise when the alkane concentration was further increased from 10 to 20% v/v. This result did not agree with literature and hypotheses 3, as well as the experimentation done in three phase systems (Section 5.2.2). On the other hand, increasing the yeast loading marginally reduced K_La at high superficial gas velocities, this was due to the increase in D_{32} which reduced the interfacial area in the system (hypotheses 4). In the same argument, a high value of K_La (0.49 s^{-1}) was observed at the highest superficial gas velocity and lowest yeast loading at constant alkane concentration (2.5% v/v). However, any change in the constant alkane concentrations up to 20% v/v at the same conditions resulted in a minimum value of K_La with increasing superficial gas velocity, which is likely due to the increasing viscosity of the bulk liquid in the system.

The difference behaviors between K_La and the interfacial area might be explained by the oxygen transfer coefficient K_L, which could have been affected by changes in the system hydrodynamics and fluid properties brought about by the interaction of the alkane concentration and the yeast cells (Cascaval et al. 2006; Chisti & Moo-Young 1988). In this study, the interfacial area of the bubbles was measured only at the wall of the bubble column,

which underestimates the interfacial area in the system. Based on that, the next study should verify this assumption with further work looking at the bubble regime of the system using a pressure differential.

The results provided in this study indicate that oxygen transfer is indeed dependant on the alkane concentration, yeast loading and superficial gas velocity. In addition, it was found that K_La was affected by these parameters in a way different to the results reported in STRs. In fact, this confirms that the mechanisms of both reactors are different, since the mixing in STRs is facilitated by impellers adding significant mixing energy, unlike in BCRs. On another hand, one key consideration in BCR was liquid-liquid homogeneity, since the only mixing in the system is provided by sparging which means increasing the amount of oxygen in the system. In a four phase system, the interaction between the operational conditions (yeast loading, alkane concentration and superficial gas velocity) resulted in different behavers of K_La than in two phase system and also in three phase systems. A full understanding of these parameters is a key to the successful operation of BCRs for the upgrading of linear alkanes to high value products.

7. RECOMMENDATIONS

The findings of this work highlighted some significant challenges both academically and industrially. Based on that, this work should be further expanded to understand how the operational conditions of the three factors (alkane concentration, yeast loading and the superficial gas velocity) and operational system impact the overall volumetric oxygen transfer and the interfacial area in a BCR. To establish that, some ideas and suggestions are hereby recommended for the upgrading of this project to a PhD, with some additional investigations. They include the use of alternative microbial solids, such as bacteria, and different alkane concentrations (2.5 to 10% v/v and 10 to 20% v/v) as well as conversion of the bubble column to an airlift reactor. A brief proposal of PhD study and some objectives are described in the following sections.

7.1 PhD proposal

Conversion of hydrocarbons to high value products can be performed through a biologically-mediated oxidation reaction, whereby an oxygen group is added to the alkane backbone by a micro-organism to produce a more reactive, and more valuable molecule. In order to achieve this biocatalysis, sufficient dissolved oxygen and mixing is required in the bioreactor. However, these two parameters are not well understood even in some industrially used bioreactors. This research focuses on the behaviour of the overall volumetric oxygen transfer coefficient (K_La), the interfacial area (a), and hydrodynamic mixing in a model four-phase (water, hydrocarbon, air and microbial solids) hydrocarbon bioprocess in both a bubble column bioreactor and an airlift bioreactor.

The difficulty of this system lies in the increasing complexity with the addition of each phase. Air-water, and air-water-microbe systems are well characterised while air-hydrocarbon-water systems have had some work done in the literature. However air-hydrocarbon-water-microbe systems have not been characterised in either bubble columns or airlift reactors, despite these bioreactors being excellent candidates for this biocatalysis process. In the four-phase system, the presence of the microbial cells results in significant changes in system parameters such as flow regimes, fluid properties, bubble coalescence as well as the fluid surface tension – all of which effect K_La, mixing, and the bioreactor operation.

This proposed study will give a fuller understanding of the impact of different alkane concentrations, superficial air velocity and microbial solids (as well as the type of microbe used) on the K_La, the interfacial area, and the mixing in a multiphase hydrocarbon bioprocess system in bubble column and airlift reactors. This work will form the basis for a larger project on the industrial upgrading of alkanes, when live microbial solids are employed in the process.

7.2 PhD aims and objectives

The main aim of this research is to characterise the oxygen transfer rate in a multiphase hydrocarbon based bioprocess system in bubble column and airlift reactors.

Objectives:

1) To measure the overall volumetric oxygen transfer coefficient, mixing characteristics and the interfacial area in i) a bubble column bioreactor and ii) an airlift bioreactor.

The conversion of the BCR to airlift bioreactor by adding an internal cylinder in the BCR will possibly change the recirculation behaviour of the bubbles. In addition, it will increase the homogeneity of flow in the system.

2) To evaluate the effect of the reactors' geometry (BCR and Airlift) on the key parameters.

The operational conditions such as the superficial gas velocity, yeast loading and hydrocarbon concentration could behave differently since their mixing mechanisms are not same.

3) To determine the fluid properties such as the viscosity and the surface tension under the varying 4-phase conditions and elucidate the effects seen in the bubble column results.

4) To examine the effect of microbe type (yeast versus bacteria) on the overall volumetric oxygen transfer coefficient and the interfacial area in model reactor systems.

Since the yeast size is larger than the bacteria, then their effect on K_La and the interfacial area will be different. The value of the K_La will be expected to be higher in a system containing bacteria than in a system containing yeast.

5) To use image analysis to determine the liquid-liquid spatial homogeneity in both reactors.

8. REFERENCES

Aiba, S. and Huang, S. Y. (1969). Oxygen permeability and diffusivity in polymer membranes immersed in liquids. *Chemical Engineering Science*, 24(7), pp. 1149–1159.

Akita, K. and Yoshida, F. (1974). Bubble Size, Interfacial Area, and Liquid-Phase Mass Transfer Coefficient in Bubble Columns. *Industrial and Engineering Chemistry Process Design and Development*, 13(1), pp. 84–91.

Asgharpour, M., Mehrnia, M. R. and Mostoufi, N. (2010). Effect of surface contaminants on oxygen transfer in bubble column reactors. *Biochemical Engineering Journal*, 49(3), pp. 351–360.

Bailey, M., Gomez, C. O. and Finch, J. A. (2005). Development and application of an image analysis method for wide bubble size distributions. *Minerals Engineering*, 18(12), pp. 1214–1221.

Bandyopadhyay, B., Humphrey, A. E. and Taguchi, H. (1967). Dynamic measurement of the volumetric oxygen transfer coefficient in fermentation systems. *Biotechnology and Bioengineering*, 9(4), pp. 533–544.

Benedek, A. A. and Heideger, W. J. (1970). Polarographic oxygen analyzer response: The effect of instrument lag in the non-steady state reaeration test. *Water Research*, 4(9), pp. 627–640.

Bouaifi, M., Hebrard, G., Bastoul, D. and Roustan, M. (2001). A comparative study of gas hold-up, bubble size, interfacial area and mass transfer coefficients in stirred gas–liquid reactors and bubble columns. *Chemical Engineering and Processing: Process Intensification*, 40(2), pp. 97–111.

Calderbank, P. H. (1958). Physical rate processes in industrial fermentation. Part I: The interfacial area in gas-liquid contacting with mechanical agitation. *Chemical Engineering Journal*, 36, pp. 443–459.

Calderbank, P. H. and Moo-Young, M. B. (1961). The continuous phase heat and mass-transfer properties of dispersions. *Chemical Engineering Science*, 16(1–2), pp. 39–54.

Camarasa, E., Vial, C., Poncin, S., Wild, G., Midoux, N. and Bouillard, J. (1999). Influence of

coalescence behaviour of the liquid and of gas sparging on hydrodynamics and bubble characteristics in a bubble column. *Chemical Engineering and Processing: Process Intensification*, 38(4–6), pp. 329–344.

Cascaval, D., Galaction, A.-I., Folescu, E. and Turnea, M. (2006). Comparative study on the effects of n-dodecane addition on oxygen transfer in stirred bioreactors for simulated, bacterial and yeasts broths. *Biochemical Engineering Journal*, 31(1), pp. 56–66.

Chisti, M. Y. and Moo-Young, M. (1988). Hydrodynamics and oxygen transfer in pneumatic bioreactor devices. *Biotechnology and bioengineering*, 5(31), pp. 487–494.

Christl, W., Rahmel, A. and Schütze, M. (1989). Behavior of oxide scales on 2.25Cr-1Mo steel during thermal cycling. II. Scales grown in water vapor. *Oxidation of Metals*, 31(1–2), pp. 35–69.

Clarke, K. G. and Correia, L. D. C. (2008). Oxygen transfer in hydrocarbon–aqueous dispersions and its applicability to alkane bioprocesses: A review. *Biochemical Engineering Journal*, 39(3), pp. 405–429.

Clarke, K. G. and Manyuchi, M. M. (2012). Methodology for advanced measurement accuracy of the overall volumetric oxygen transfer coefficient with application to hydrocarbon-aqueous dispersions. *Journal of Chemical Technology and Biotechnology*, 87(11), pp. 1615–1618.

Clarke, K. G., Williams, P. C., Smit, M. S. and Harrison, S. T. L. (2006). Enhancement and repression of the volumetric oxygen transfer coefficient through hydrocarbon addition and its influence on oxygen transfer rate in stirred tank bioreactors. *Biochemical Engineering Journal*, 28(3), pp. 237–242.

Colella, D., Vinci, D., Bagatin, R., Masi, M. and ABu Bakr, E. (1999). A study on coalescence and breakage mechanisms in three different bubble columns. *Chemical Engineering Science*, 54(21), pp. 4767–4777.

Correia, L. D. C., Aldrich, C. and Clarke, K. G. (2010). Interfacial gas–liquid transfer area in alkane–aqueous dispersions and its impact on the overall volumetric oxygen transfer coefficient. *Biochemical Engineering Journal*, 49(1), pp. 133–137.

Correia, L. D. and Clarke, K. G. (2009). Measurement of the overall volumetric oxygen transfer

coefficient in alkane-aqueous dispersions. *Journal of Chemical Technology & Biotechnology*, 84(12), pp. 1793–1797.

Dang, N. D. P., Karrer, D. A. and Dunn, I. J. (1977). Oxygen transfer coefficients by dynamic model moment analysis. *Biotechnology and Bioengineering*. Wiley Subscription Services, Inc., A Wiley Company, 19(6), pp. 853–865.

Daniel, L. and Correia, C. (2007). *Hydrocarbon-Aqueous Dispersions and Its Applicability To Alkane-Based Bioprocesses*. PhD. thesis. University of Stellenbosch.

Das, T. R., Bandopadhyay, A., Parthasarathy, R. and Kumar, R. (1985). Gas-liquid interfacial area in stirred vessels: The effect of an immiscible liquid phase. *Chemical Engineering Science*, 40(2), pp. 209–214.

Deckwer, Louisi, Zaldi and Ralek (1980). Hydrodynamic Properties of the Fischer-Tropsch Slurry Process. *Industrial and Engineering Chemistry, Process Design and Development*, 19(4), pp. 699–708.

Dhanasekaran, S. and Karunanithi, T. (2012). Improved gas holdup in novel bubble column. *Canadian Journal of Chemical Engineering*, 90(1), pp. 126–136.

Dietrich, E., Mathieu, C., Delmas, H. and Jenck, J. (1992). Raney-nickel catalyzed hydrogenations: Gas-liquid mass transfer in gas-induced stirred slurry reactors. *Chemical Engineering Science*, 47(13–14), pp. 3597–3604.

Doran, P. (1995). *Bioprocess engineering principles*. Academic press.

Dumont, E., Andrès, Y. and Le Cloirec, P. (2006). Effect of organic solvents on oxygen mass transfer in multiphase systems: Application to bioreactors in environmental protection. *Biochemical Engineering Journal*, 30(3), pp. 245–252.

Dumont, E. and Delmas, H. (2003). Mass transfer enhancement of gas absorption in oil-in-water systems: a review. *Chemical Engineering and Processing: Process Intensification*, 42(6), pp. 419–438.

Freitas, C., Fialová, M., Zahradnik, J. and Teixeira, J. A. (1999). Hydrodynamic model for three-phase internal- and external-loop airlift reactors. *Chemical Engineering Science*, 54(21), pp. 5253–5258.

Fukui, F. and Tanaka, A. (1980). *Production of Useful Compounds From Alkane Media in*

Japan. Springer Berlin Heidelberg.

Fukuma, M., Muroyama, K. and Yasunishi, A. (1987). Properties of Bubble Swarm in a Slurry Bubble Column. *Journal of Chemical Engineering of Japan*, 20(1), pp. 28–33.

Galaction, A.-I., Cascaval, D., Oniscu, C. and Turnea, M. (2004). Prediction of oxygen mass transfer coefficients in stirred bioreactors for bacteria, yeasts and fungus broths. *Biochemical Engineering Journal*, 20(1), pp. 85–94.

Galaction, A. I., Cascaval, D., Turnea, M. and Folescu, E. (2005). Enhancement of oxygen mass transfer in stirred bioreactors using oxygen-vectors 2. Propionibacterium shermanii broths. *Bioprocess and Biosystems Engineering*, 27(4), pp. 263–271.

Galindo, E., Larralde-Corona, C. P., Brito, T., Córdova-Aguilar, M. S., Taboada, B., Vega-Alvarado, L. and Corkidi, G. (2005). Development of advanced image analysis techniques for the in situ characterization of multiphase dispersions occurring in bioreactors. *Journal of biotechnology*, 116(3), pp. 261–70.

Gandhi, B., Prakash, A. and Bergougnou, M. A. (1999). Hydrodynamic behavior of slurry bubble column at high solids concentrations. *Powder Technology*, 103(2), pp. 80–94.

Garcia-Ochoa, F. and Gomez, E. (2005). Prediction of gas-liquid mass transfer coefficient in sparged stirred tank bioreactors. *Biotechnology and Bioengineering*, 92(6), pp. 761–772.

Garcia-Ochoa, F. and Gomez, E. (2009). Bioreactor scale-up and oxygen transfer rate in microbial processes: an overview. *Biotechnology advances*, 27(2), pp. 153–76.

Hassan, I. T. M. and Robinson, C. W. (1977). Oxygen transfer in mechanically agitated aqueous systems containing dispersed hydrocarbon. *Biotechnology and Bioengineering*. Wiley Subscription Services, Inc., A Wiley Company, 19(5), pp. 661–682.

Hesse, P. J., Battino, R. and Wilhelm, E. (1996). Solubility of Gases in Liquids . 20 . Solubility of He , Ne , Ar , Kr , N 2 , O 2 , CH 4 , CF 4 , and SF 6 in n -Alkanes n- C l H 2 l + 2 (6 e l e 16) at 298 . 15 K †. 2, pp. 195–201.

Hollis, P. G. and Clarke, K. G. (2016). A systematic quantification and correlation of oxygen transfer coefficients and interfacial area in simulated model hydrocarbon-based bioprocesses in stirred tank reactors. *Journal of Chemical Technology and Biotechnology*, (February).

Hyndman, C. L., Larachi, F. and Guy, C. (1997). Understanding gas-phase hydrodynamics in bubble columns: a convective model based on kinetic theory. *Chemical Engineering Science*, 52(1), pp. 63–77.

Jhawar, A. K. and Prakash, A. (2011). Influence of bubble column diameter on local heat transfer and related hydrodynamics. *Chemical Engineering Research and Design*. Institution of Chemical Engineers, 89(10), pp. 1996–2002.

Jianlong, W. (2000). Enhancement of citric acid production by Aspergillus niger using n-dodecane as an oxygen-vector. *Process Biochemistry*, 35(10), pp. 1079–1083.

Joosten, G. E. H., Schilder, J. G. M. and Janssen, J. J. (1977). The influence of suspended solid material on the gas-liquid mass transfer in stirred gas-liquid contactors. *Chemical Engineering Science*, 32(5), pp. 563–566.

Junker, B. (2006). Measurement of bubble and pellet size distributions: Past and current image analysis technology. *Bioprocess and Biosystems Engineering*, 29(3), pp. 185–206.

Juretzek, T., Wang, H.-J., Nicaud, J.-M., Mauersberger, S. and Barth, G. (2000). Comparison of promoters suitable for regulated overexpression of β-galactosidase in the alkane-utilizing yeastYarrowia lipolytica. *Biotechnology and Bioprocess Engineering*, 5(5), pp. 320–326.

Kantarci, N., Borak, F. and Ulgen, K. O. (2005). Bubble column reactors. *Process Biochemistry*, 40(7), pp. 2263–2283.

Kawase, Y., Halard, B. and Moo-Young, M. (1987). Theoretical prediction of volumetric mass transfer coefficients in bubble columns for Newtonian and non-Newtonian fluids. *Chemical Engineering Science*, 42(7), pp. 1609–1617.

Kawase, Y. and Moo-Young, M. (1990). Mathematical models for design of bioreactors. *The Chemical Engineering Journal*, 43(1), pp. B19–B41.

Kawecki, W., Reith, T., van Heuven, J. W. and Beek, W. J. (1967). Bubble size distribution in the impeller region of a stirred vessel. *Chemical Engineering Science*, 22(11), pp. 1519–1523.

Kazakis, N. A., Mouza, A. A. and Paras, S. V. (2008). Coalescence during bubble formation at two neighbouring pores: An experimental study in microscopic scale. *Chemical*

Engineering Science, 63(21), pp. 5160–5178.

Keil, K. and Fuchs, L. H. (1971). Hibonite [Ca2(Al, Ti)24O38] from the Leoville and Allende chondritic meteorites. *Earth and Planetary Science Letters*, 12(2), pp. 184–190.

Kohler, M. A. (1986). Comparison of mechanically agitated and bubble column slurry reactors. *Applied Catalysis*, 22(1), pp. 21–53.

Koide, K., Hayashi, T., Sumino, K. and Iwamoto, S. (1976). Mass transfer from single bubbles in aqueous solutions of surfactants. *Chemical Engineering Science*, 31(10), pp. 963–967.

Linek, V., Mayrhoferová, J. and Mošnerová, J. (1970). The influence of diffusivity on liquid phase mass transfer in solutions of electrolytes. *Chemical Engineering Science*, 25(6), pp. 1033–1045.

Lubbert, A., Paaschen, T. and Lapin, A. (1996). Fluid dynamics in bubble column bioreactors: Experiments and numerical simulations. *Biotechnology and Bioengineering*, 52, pp. 248–258.

Maceiras, R., Álvarez, E. and Cancela, M. A. (2010). Experimental interfacial area measurements in a bubble column. *Chemical Engineering Journal*, 163(3), pp. 331–336.

Makranczy, J. (1976). Solubility of gases in normal-alkanes. pp. 269–280.

Manyuchi, M. M. (2010). *Measurement and behavior of the overall volumetric oxygen transfer coefficient in aerated agitated alkane based multiphase systems*. PhD. thesis, University of Stellenbosch.

Mena, P. C., Pons, M. N., Teixeira, J. A. and Rocha, F. A. (2005). Using image analysis in the study of multiphase gas absorption. *Chemical Engineering Science*, 60(18), pp. 5144–5150.

Montes, F. J., Galan, M. A. and Cerro, R. L. (1999). Mass transfer from oscillating bubbles in bioreactors. *Chemical Engineering Science*, 54(15–16), pp. 3127–3136.

Morao, A., Maia, C. I., Fonseca, M. M. R., Vasconcelos, J. M. T. and Alves, S. S. (1999). Effect of antifoam addition on gas-liquid mass transfer in stirred fermenters. *Bioprocess Engineering*, 20(2), pp. 165–172.

Moses, C. O., Kirk Nordstrom, D., Herman, J. S. and Mills, A. L. (1987). Aqueous pyrite

oxidation by dissolved oxygen and by ferric iron. *Geochimica et Cosmochimica Acta*, 51(6), pp. 1561–1571.

Mouza, A. A., Dalakoglou, G. K. and Paras, S. V. (2005a). Effect of liquid properties on the performance of bubble column reactors with fine pore spargers. *Chemical Engineering Science*, 60(5), pp. 1465–1475.

Mouza, A. A., Dalakoglou, G. K. and Paras, S. V. (2005b). Effect of liquid properties on the performance of bubble column reactors with fine pore spargers. *Chemical Engineering Science*, 60(5), pp. 1465–1475.

Nakanoh, M. and Yoshida, F. (1980). Gas absorption by Newtonian and non-Newtonian liquids in a bubble column. *Industrial & Engineering Chemistry Process Design and Development*, pp. 190–195.

Ngo, T. H. and Schumpe, A. (2012). Oxygen absorption into stirred emulsions of n-alkanes. *International Journal of Chemical Engineering*, 2012(Table 1).

Nguyen-tien, K., Patwari, A., Schumpe, A. and Deckwer, W. (1985). Gas-liquid Mass Transfer in Fluidzed Particle Beds. *AIChE Journal*, 31, pp. 194–201.

Philichi, T. L. and Stenstrom, M. K. (2009). Effects of dissolved oxygen lag on oxygen transfer estimation probe parameter. *Water Environment Federation*, 61(1), pp. 83–86.

Pino, L. Z., Solari, R. B., Siquier, S., Antonio Estevez, L., Yepez, M. M. and Saez, A. (1992). Effect of operating conditions on gas holdup in slurry bubble columns with a foaming liquid. *Chemical Engineering Communications*, 117(1), pp. 367–382.

Prakash, A., Margaitis, A., Li, H. and Bergougnou, M. A. (2001). Hydrodynamics and local heat transfer measurements in a bubble column with suspension of yeast. *Biochemical Engineering Journal*, 9(2), pp. 155–163.

Queimada, A. J., Marrucho, I. M., Stenby, E. H. and Coutinho, J. A. P. (2004). Generalized relation between surface tension and viscosity: A study on pure and mixed n-alkanes. *Fluid Phase Equilibria*, 222–223, pp. 161–168.

Queimada, A. J., Silva, F. A., Caço, A. I., Marrucho, I. M. and Coutinho, J. A. (2003). Measurement and modeling of surface tensions of asymmetric systems: heptane, eicosane, docosane, tetracosane and their mixtures. *Fluid Phase Equilibria*, 214(2), pp.

211–221.

Reith, T. and Beek, W. . (1968). Gas holdups, interracial areas and mass transfer coefficients in gas-liquid contactors. *In 4th European Symposium on Chemical Reaction Engineering*.

Robinson, C. W. and Wilke, C. (1974). Simultaneous measurement of interfacial area and mass transfer coefficients for a well—mixed gas dispersion in aqueous electrolyte solutions. *AIChE Journal*, 2(20), pp. 285–294.

Rols, J. ., Condoret, J., Fonade, C. and Goma, G. (1990). Mecanism of enhanced oxygen transfer in fermentation using emulsified oxygen-vectors. *Biotechnology and bioengineering*, 35(4), pp. 427–435.

Rols, J. L. and Goma, G. (1989). Enhancement of oxygen transfer rates in fermentation using oxygen-vectors. *Biotechnology Advances*, 7(1), pp. 1–14.

Ruzicka, M., Zahradník, J., Drahoš, J. and Thomas, N. . (2001). Homogeneous–heterogeneous regime transition in bubble columns. *Chemical Engineering Science*, 56(15), pp. 4609–4626.

Schmid, A., Kollmer, A., Mathys, R. G. and Witholt, B. (1998). Developments toward large-scale bacterial bioprocesses in the presence of bulk amounts of organic solvents. *Extremophiles*, 2(3), pp. 249–256.

Schugerl, S. (1980). Oxygen transfer into highly viscous media. *Verfahrenstechnik*, 4(11), pp. 727–730.

Shennan, J. and Levi, J. (1973). The growth of yeasts on hydrocarbons. *Progress in Industrial Microbiology*, 13, pp. 1–57.

Shennan, J. and Levi, J. . (1974). The growth of yeasts on hydrocarbons. *Progress in Industrial Microbiology*, 13, pp. 1–57.

Shuler, M. and Kargi, F. (2009). *Bioprocess Engineering: Basic Concepts*. 2nd edn.

da Silva, T. L., Calado, V., Silva, N., Mendes, R. L., Alves, S. S., Vasconcelos, J. M. T. and Reis, A. (2006). Effects of hydrocarbon additions on gas-liquid mass transfer coefficients in biphasic bioreactors. *Biotechnology and Bioprocess Engineering*, 11(3), pp. 245–250.

De Swart, J. W. A., van Vliet, R. E. and Krishna, R. (1996). Size, structure and dynamics of

"large" bubbles in a two-dimensional slurry bubble column. *Chemical Engineering Science*, 51(20), pp. 4619–4629.

Tobajas, M., García-Calvo, E., Siegel, M. H. and Apitz, S. E. (1999). Hydrodynamics and mass transfer prediction in a three-phase airlift reactor for marine sediment biotreatment. *Chemical Engineering Science*, 54(21), pp. 5347–5354.

Vandu, C. O., Koop, K. and Krishna, R. (2004). Volumetric mass transfer coefficient in a slurry bubble column operating in the heterogeneous flow regime. *Chemical Engineering Science*, 59(22–23), pp. 5417–5423.

Walker, G. . (1998). Yeast: Physiology and Biotechnology. *John Wiley and Sons*.

Wentzel, A., Ellingsen, T. E., Kotlar, H. K., Zotchev, S. B. and Throne-Holst, M. (2007). Bacterial metabolism of long-chain n-alkanes. *Applied Microbiology and Biotechnology*, 76(6), pp. 1209–1221.

Wilkinson, P. M., Haringa, H. and Van Dierendonck, L. L. (1994). Mass transfer and bubble size in a bubble column under pressure. *Chemical Engineering Science*, 49(9), pp. 1417–1427.

Yagi, H. and Yoshida, F. (Kyoto U. (Japan). F. of E. (1974). Oxygen absorption in fermenters: Effects of surfactants, antifoaming agents, and sterilized cells. *Journal of Fermentation Technology (Japan)*, 52(12), pp. 905–916.

9. APPENDICES

9.1 Experimental data obtained in BCR for K_La in two and three phase systems as well as, K_P, K_La, gas hold up, D_{32} and interfacial area in four phase system

Table 9-1: K_La (s^{-1}) data in two phase (air-water) system.

Run	Superficial gas velocity (cm/s)	K_la (1/s) Replicate 1	Kla (1/s) Replicate 2	Kla (1/s) Replicate 3	Average
1	1	0,046	0,053	0,058	0,052
2	2	0,062	0,069	0,080	0,070
3	3	0,100	0,106	0,075	0,093

Table 9-2: K_La (s^{-1}) data in three phase (air-water-alkane) system.

Run	Superficial gas velocity (cm/s)	Alkane concentration (% v/v)	Kla (1/s) Replicate 1	Kla (1/s) Replicate 2	Kla (1/s) Replicate 3	Average
1	1	2,5	0,059	0,062	0,055	0,059
2	2	2,5	0,067	0,072	0,067	0,069
3	3	2,5	0,085	0,089	0,074	0,083
4	1	11,25	0,028	0,030	0,019	0,026
5	2	11,25	0,061	0,058	0,057	0,059
6	3	11,25	0,066	0,064	0,060	0,063
7	1	20	0,018	0,013	0,019	0,017
8	2	20	0,028	0,024	0,036	0,029
9	3	20	0,036	0,037	0,037	0,037

Table 9-3: K_La (s^{-1}) data in three phase (air-water-deactivated yeast) system.

Run	Superficial gas velocity (cm/s)	Yeast concentration (g/l)	Kla (1/s) Replicate 1	Kla (1/s) Replicate 2	Kla (1/s) Replicate 3	Average
1	1	0,5	0,229	0,229	0,149	0,202
2	2	0,5	0,214	0,145	0,146	0,168
3	3	0,5	0,117	0,107	0,100	0,108
4	1	3,25	0,121	0,112	0,162	0,132
5	2	3,25	0,149	0,097	0,126	0,124
6	3	3,25	0,076	0,075	0,070	0,074
7	1	20	0,056	0,050	0,044	0,050
8	2	20	0,055	0,061	0,072	0,063
9	3	20	0,068	0,072	0,066	0,069

Table 9-4: K_P (s^{-1}) data measured in a four phase (air-water-alkane-deactivated yeast) system.

Run	Alkane concentration (% v/v)	Yeast concentration (g/l)	Superficial gas velocity (cm/s)	Take 1	Take 2	Take 3	Average
1	7,88	1,62	1,62	0,037	0,041	0,042	0,040
2	7,88	1,62	2,38	0,035	0,035	0,034	0,035
3	7,88	4,88	1,62	0,030	0,032	0,029	0,030
4	7,88	4,88	2,38	0,035	0,035	0,035	0,035
5	14,62	1,62	1,62	0,041	0,042	0,041	0,042
6	14,62	1,62	2,38	0,039	0,036	0,038	0,038
7	14,62	4,88	1,62	0,034	0,036	0,039	0,036
8	14,62	4,88	2,38	0,035	0,034	0,034	0,034
9	2,5	3,25	2	0,046	0,049	0,046	0,047
10	20	3,25	2	0,032	0,034	0,032	0,033
11	11,25	0,5	2	0,032	0,032	0,036	0,033
12	11,25	6	2	0,037	0,041	0,044	0,041
13	11,25	3,25	1	0,052	0,041	0,045	0,046
14	11,25	3,25	3	0,045	0,047	0,046	0,046
15	11,25	3,25	2	0,040	0,035	0,037	0,037
16	11,25	3,25	2	0,040	0,044	0,046	0,043

Table 9-5: K_La (s^{-1}) data measured in a four phase (air-water-alkane-deactivated yeast) system.

Run	Alkane concentration (% v/v)	Yeast concentration (g/l)	Superficial gas velocity (cm/s)	Take 1	Take 2	Take 3	Average
1	7,88	1,62	1,62	0,036	0,034	0,033	0,034
2	7,88	1,62	2,38	0,051	0,048	0,047	0,049
3	7,88	4,88	1,62	0,039	0,037	0,051	0,042
4	7,88	4,88	2,38	0,037	0,038	0,038	0,037
5	14,62	1,62	1,62	0,060	0,075	0,094	0,076
6	14,62	1,62	2,38	0,033	0,025	0,026	0,028
7	14,62	4,88	1,62	0,127	0,096	0,051	0,092
8	14,62	4,88	2,38	0,035	0,030	0,038	0,034
9	2,5	3,25	2	0,352	0,359	0,422	0,377
10	20	3,25	2	0,093	0,223	0,396	0,237
11	11,25	0,5	2	0,232	0,141	0,205	0,193
12	11,25	6	2	0,094	0,108	0,047	0,083
13	11,25	3,25	1	0,073	0,051	0,042	0,056
14	11,25	3,25	3	0,080	0,062	0,121	0,088
15	11,25	3,25	2	0,187	0,096	0,081	0,122
16	11,25	3,25	2	0,143	0,119	0,132	0,131

Table 9-6: Gas hold-up data mesured in a four phase (air-water-alkane-deactivated yeast) system.

Run	Alkane concentration (% v/v)	Yeast concentration (g/l)	Superficial gas velocity (cm/s)	Take 1	Take 2	Take 3	Average
1	7,88	1,62	1,62	0,103	0,110	0,097	0,103
2	7,88	1,62	2,38	0,145	0,150	0,139	0,145
3	7,88	4,88	1,62	0,091	0,085	0,097	0,091
4	7,88	4,88	2,38	0,110	0,097	0,103	0,103
5	14,62	1,62	1,62	0,103	0,110	0,097	0,103
6	14,62	1,62	2,38	0,128	0,133	0,139	0,133
7	14,62	4,88	1,62	0,097	0,110	0,103	0,103
8	14,62	4,88	2,38	0,116	0,122	0,128	0,122
9	2,5	3,25	2	0,122	0,116	0,128	0,122
10	20	3,25	2	0,122	0,116	0,128	0,122
11	11,25	0,5	2	0,128	0,133	0,122	0,127
12	11,25	6	2	0,128	0,133	0,122	0,127
13	11,25	3,25	1	0,058	0,044	0,051	0,051
14	11,25	3,25	3	0,167	0,156	0,161	0,161
15	11,25	3,25	2	0,110	0,128	0,122	0,120
16	11,25	3,25	2	0,110	0,128	0,122	0,120

Table 9-7: D_{32} (mm) data measured in a four phase (air-water-alkane-deactivated yeast) system.

Run	Alkane concentration (% v/v)	Yeast concentration (g/l)	Superficial gas velocity (cm/s)	Take 1	Take 2	Take 3	Average
1	7,88	1,62	1,62	2,717	2,810	2,713	2,747
2	7,88	1,62	2,38	3,462	3,371	3,331	3,388
3	7,88	4,88	1,62	3,051	2,973	3,043	3,022
4	7,88	4,88	2,38	3,535	3,778	3,467	3,593
5	14,62	1,62	1,62	2,745	3,017	3,052	2,938
6	14,62	1,62	2,38	3,082	3,243	3,266	3,197
7	14,62	4,88	1,62	2,959	3,006	3,021	2,995
8	14,62	4,88	2,38	3,258	3,396	3,365	3,340
9	2,5	3,25	2	3,003	3,100	3,187	3,097
10	20	3,25	2	2,869	3,203	3,119	3,063
11	11,25	0,5	2	3,007	2,926	2,939	2,957
12	11,25	6	2	3,098	3,269	3,229	3,199
13	11,25	3,25	1	2,478	2,500	2,694	2,557
14	11,25	3,25	3	3,301	3,364	3,436	3,367
15	11,25	3,25	2	3,012	3,029	2,979	3,007
16	11,25	3,25	2	2,914	3,031	3,083	3,009

Table 9-8: Interfacial area (m^2/m^3) data measured in a four phase (air-water-alkane-deactivated yeast) system.

Run	Alkane concentration (% v/v)	Yeast concentration (g/l)	Superficial gas velocity (cm/s)	Take 1	Take 2	Take 3	Average
1	7,88	1,62	1,62	228,48	234,03	214,98	225,83
2	7,88	1,62	2,38	250,87	267,57	250,50	256,32
3	7,88	4,88	1,62	178,79	170,56	191,73	180,36
4	7,88	4,88	2,38	186,02	154,42	179,02	173,16
5	14,62	1,62	1,62	226,14	217,96	191,13	211,74
6	14,62	1,62	2,38	248,24	246,68	255,53	250,15
7	14,62	4,88	1,62	197,16	218,72	205,43	207,10
8	14,62	4,88	2,38	212,99	214,85	227,38	218,41
9	2,5	3,25	2	243,01	223,86	240,06	235,64
10	20	3,25	2	254,36	216,63	245,34	238,78
11	11,25	0,5	2	254,46	273,41	248,26	258,71
12	11,25	6	2	246,94	244,69	225,97	239,20
13	11,25	3,25	1	140,36	105,87	113,82	120,01
14	11,25	3,25	3	302,98	278,00	281,62	287,53
15	11,25	3,25	2	218,32	252,59	244,95	238,62
16	11,25	3,25	2	225,68	252,42	236,73	238,28

Table 9-9: K_L (m/s) data measured in a four phase (air-water-alkane-deactivated yeast) system.

Run	Alkane concentration (% v/v)	Yeast concentration (g/l)	Superficial gas velocity (cm/s)	Take 1	Take 2	Take 3	Average
1	7,88	1,62	1,62	0,0002	0,0001	0,0002	0,0002
2	7,88	1,62	2,38	0,0002	0,0002	0,0002	0,0002
3	7,88	4,88	1,62	0,0002	0,0002	0,0003	0,0002
4	7,88	4,88	2,38	0,0002	0,0002	0,0002	0,0002
5	14,62	1,62	1,62	0,0003	0,0003	0,0005	0,0004
6	14,62	1,62	2,38	0,0001	0,0001	0,0001	0,0001
7	14,62	4,88	1,62	0,0006	0,0004	0,0003	0,0004
8	14,62	4,88	2,38	0,0002	0,0001	0,0002	0,0002
9	2,5	3,25	2	0,0014	0,0016	0,0018	0,0016
10	20	3,25	2	0,0004	0,0010	0,0016	0,0010
11	11,25	0,5	2	0,0009	0,0005	0,0008	0,0008
12	11,25	6	2	0,0004	0,0004	0,0002	0,0003
13	11,25	3,25	1	0,0005	0,0005	0,0004	0,0005
14	11,25	3,25	3	0,0003	0,0002	0,0004	0,0003
15	11,25	3,25	2	0,0009	0,0004	0,0003	0,0005
16	11,25	3,25	2	0,0006	0,0005	0,0006	0,0006

9.2 Statistical graphs (3D) obtained in a four phase (air-water-alkane-deactivated yeast) system.

9.2.1 Behaviour of gas hold-up in a four phase system.

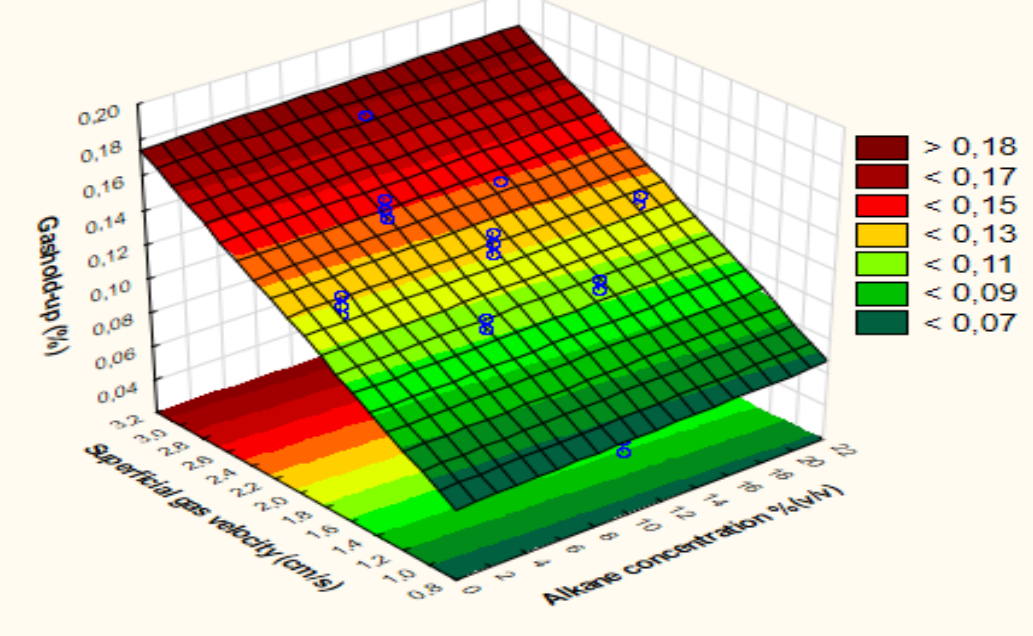

Figure 9-1: Influence of alkane concenatrtion and superficial gas velocity on Gas hold-up at constant yeast loading (1.62 g/l).

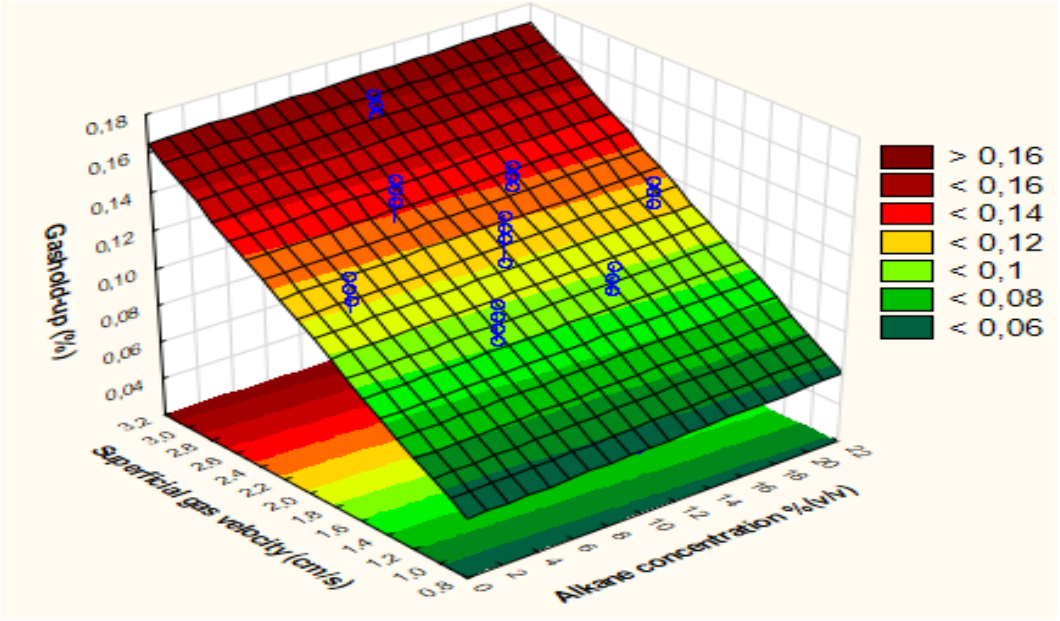

Figure 9-2: Influence of alkane concenatrtion and superficial gas velocity on Gas hold-up at constant yeast loading (4.88 g/l).

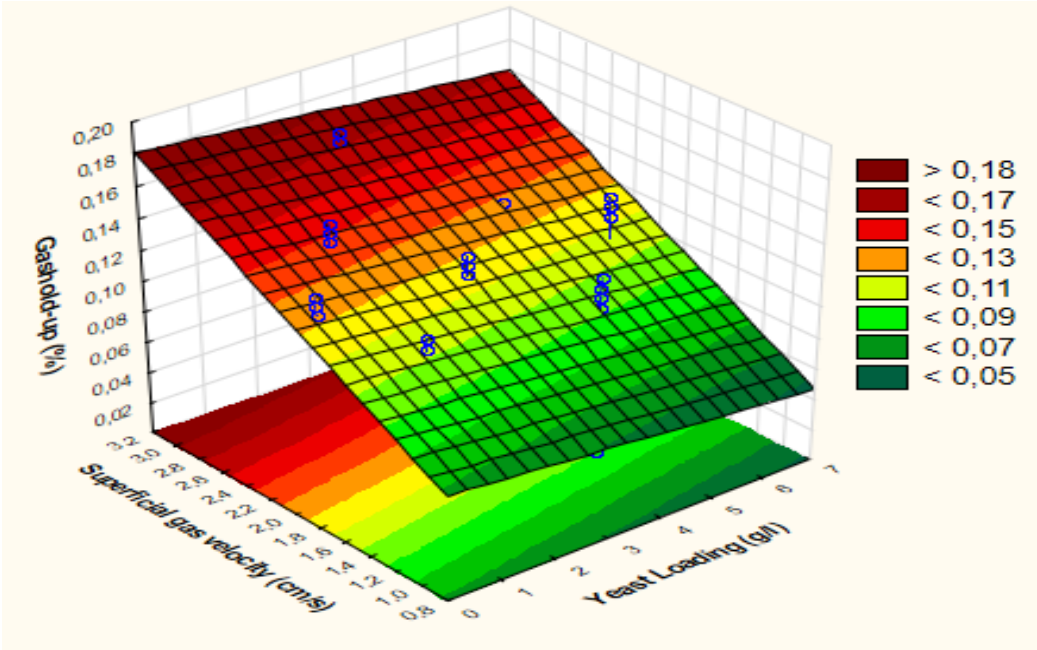

Figure 9-3: Influence of yeast loading and superficial gas velocity on Gas hold-up at constant alkane concenatrtion (7.88% v/v).

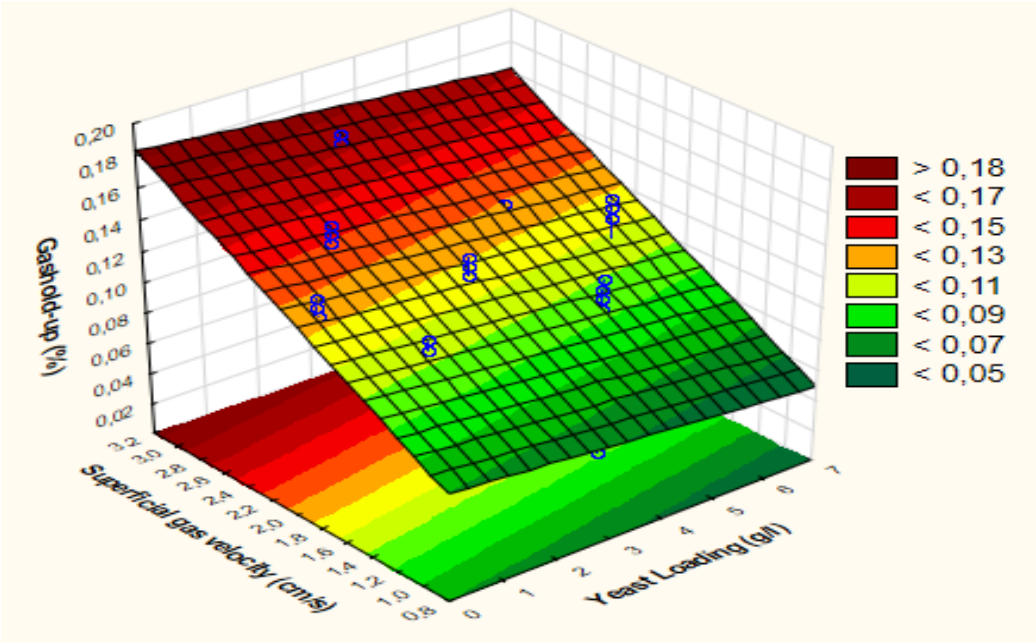

Figure 9-4: Influence of yeast loading and superficial gas velocity on Gas hold-up at constant alkane concenatrtion (14.62% v/v).

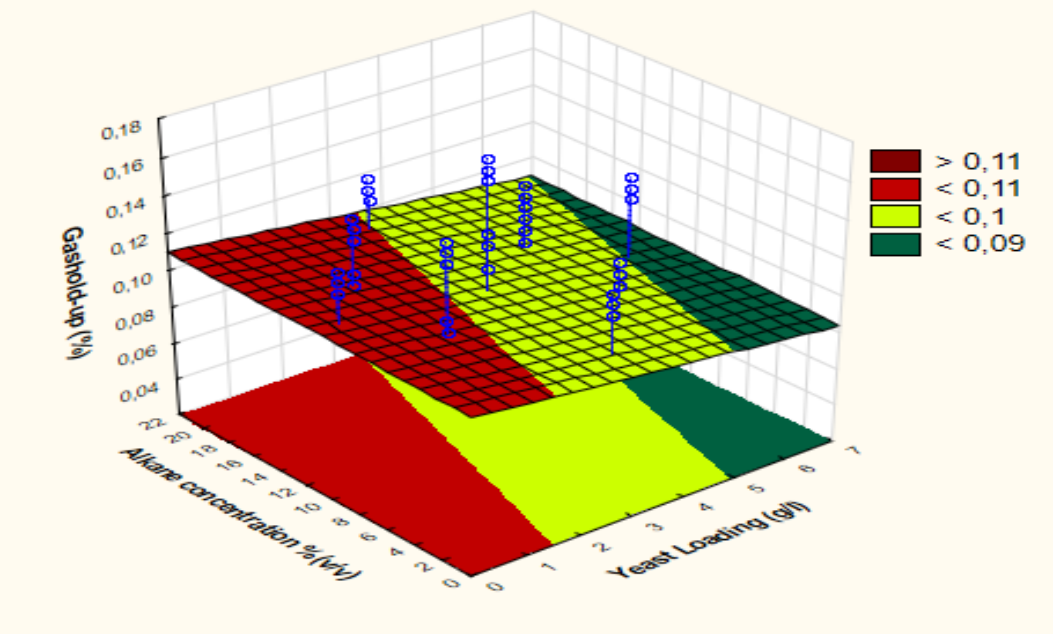

Figure 9-5: Influence of yeast loading and alkane concenatrtion on Gas hold-up at constant superficial gas velocity (1.62 cm/sec).

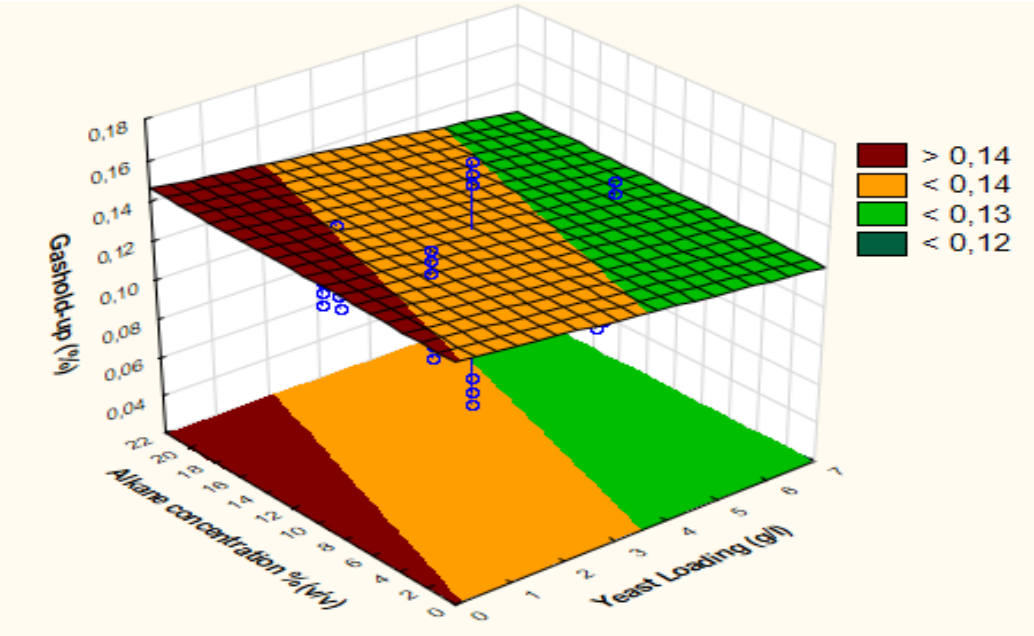

Figure 9-6: Influence of yeast loading and alkane concenatrtion on Gas hold-up at constant superficial gas velocity (2.38 cm/sec).

9.2.2 Behaviour of D32 in a four phase system

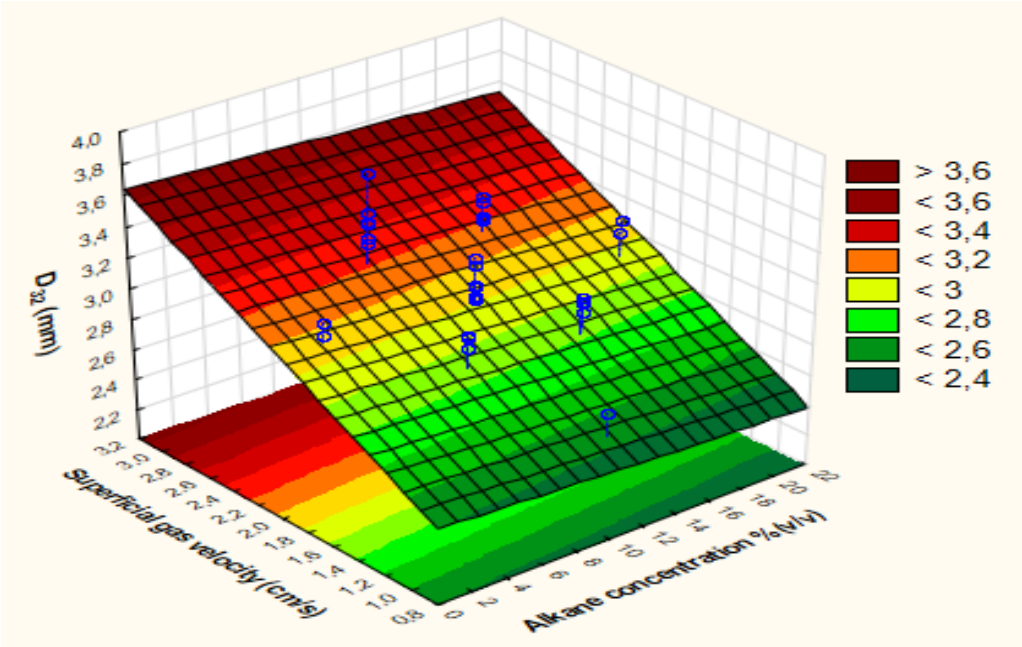

Figure 9-7: Influence of alkane concenatrtion and superficial gas velocity on D_{32} at constant yeast loading (1.62 g/l).

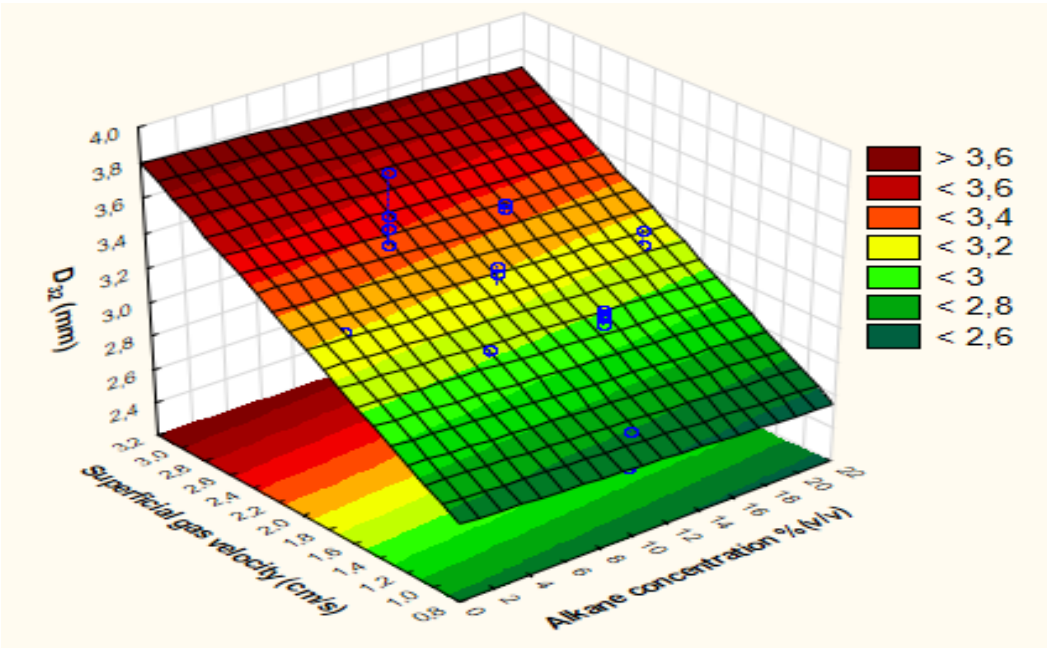

Figure 9-8: Influence of alkane concenatrtion and superficial gas velocity on D_{32} at constant yeast loading (4.88 g/l).

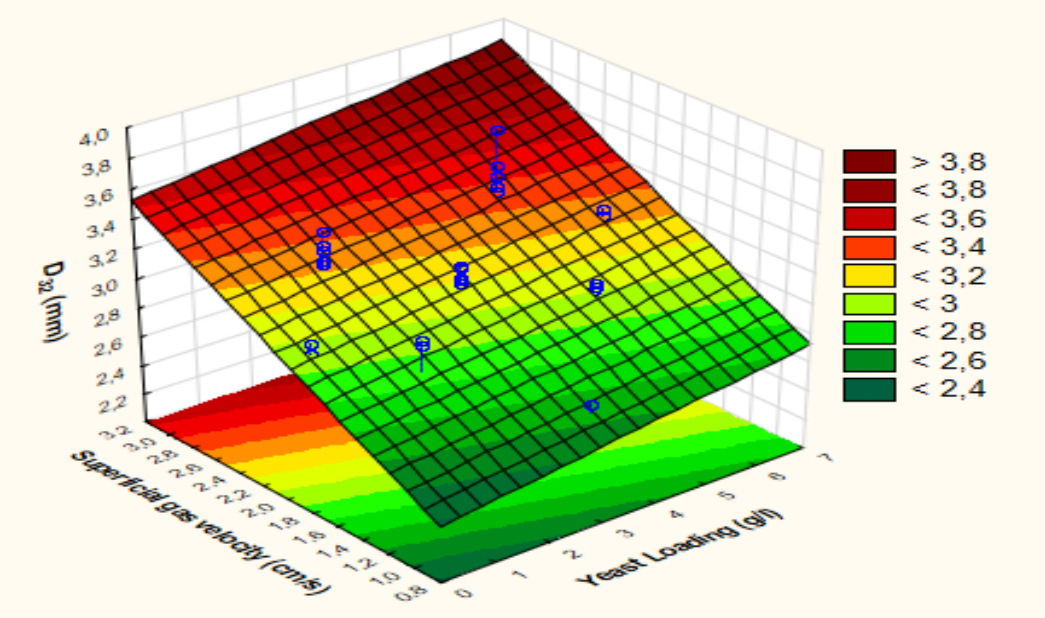

Figure 9-9: Influence of yeast loading and superficial gas velocity on D_{32} at constant alkane concenatrtion (7.88% v/v).

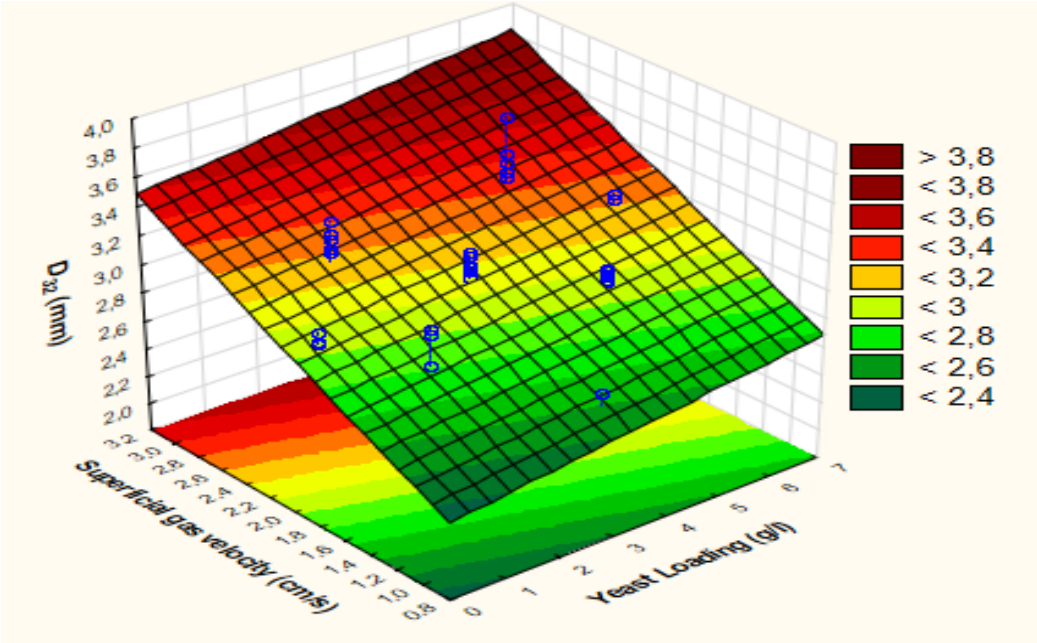

Figure 9-10: Influence of yeast loading and superficial gas velocity on D_{32} at constant alkane concenatrtion (14.62% v/v).

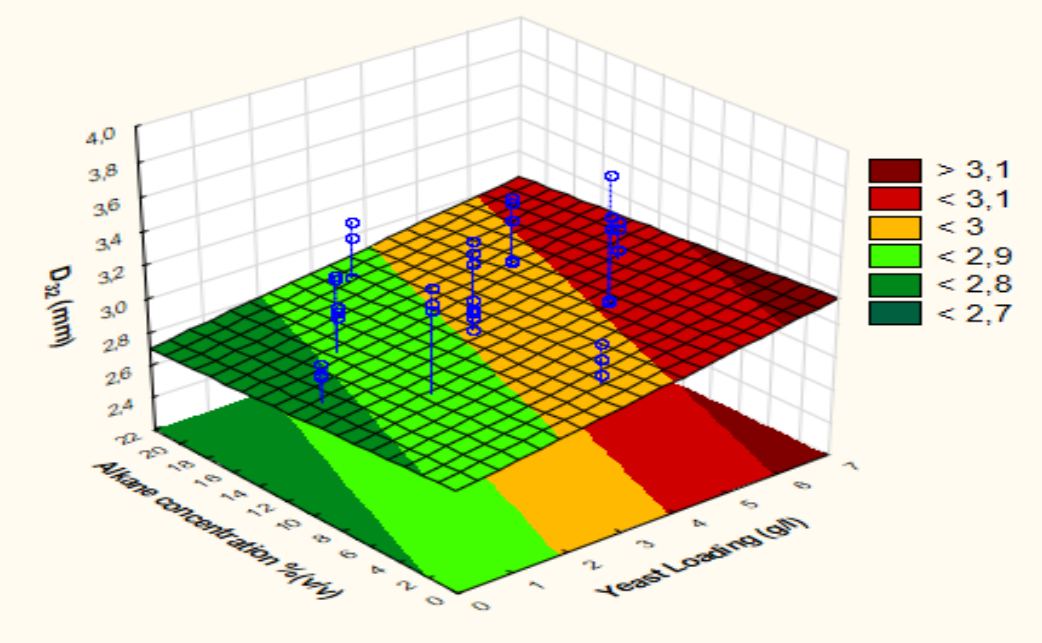

Figure 9-11: Influence of yeast loading and alkane concenatrtion on D_{32} at constant superficial gas velocity (1.62 cm/sec).

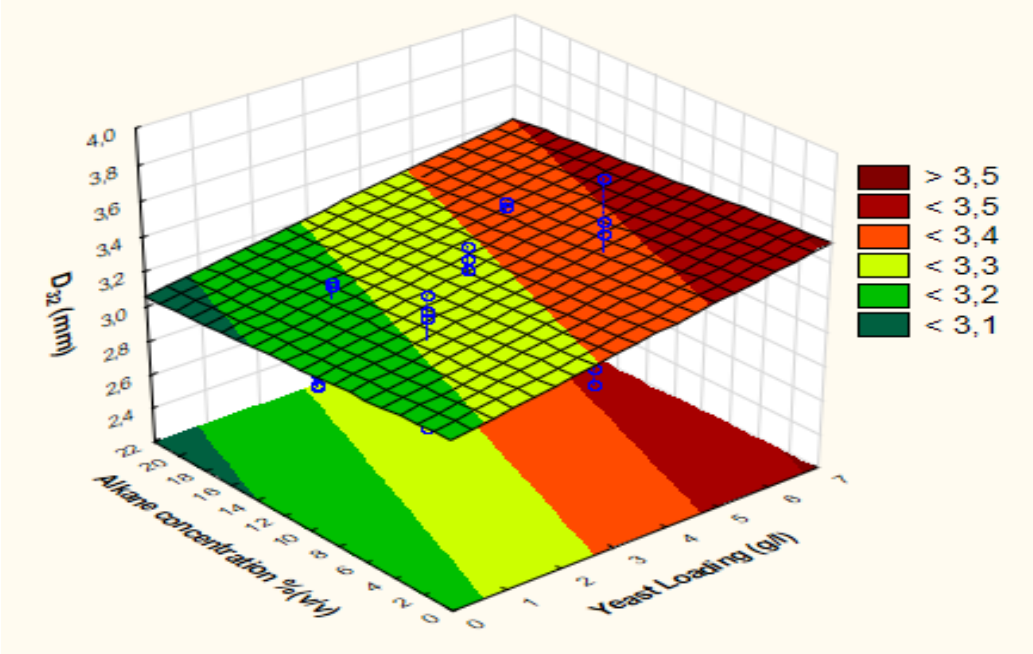

Figure 9-12: Influence of yeast loading and alkane concenatrtion on D_{32} at constant superficial gas velocity (2.38 cm/sec).

9.2.3 Behaviour of the interfacial area in a four phase system

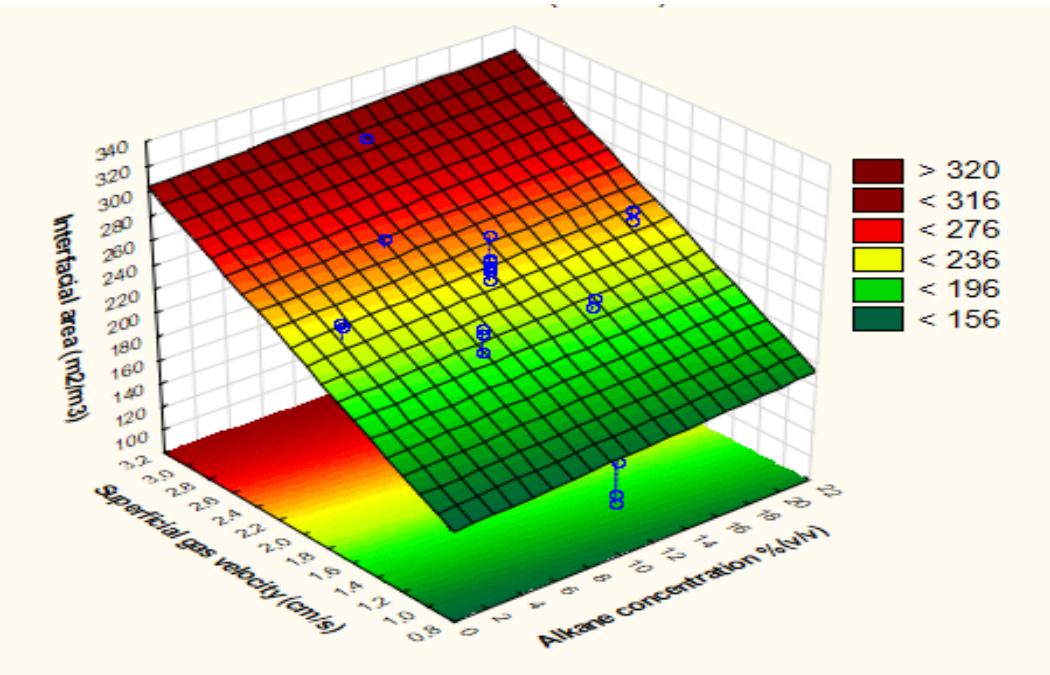

Figure 9-13: Influence of alkane concenatrtion and superficial gas velocity on the interfacial area at constant yeast loading (1.62 g/l).

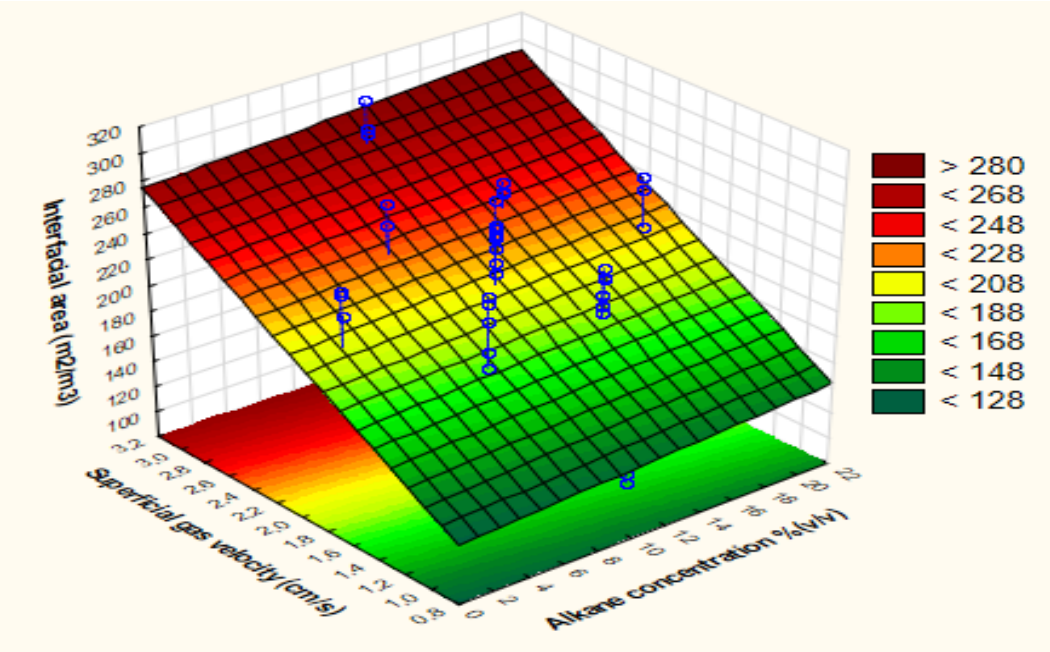

Figure 9-14: Influence of alkane concenatrtion and superficial gas velocity on the interfacial area at constant yeast loading (4.88 g/l).

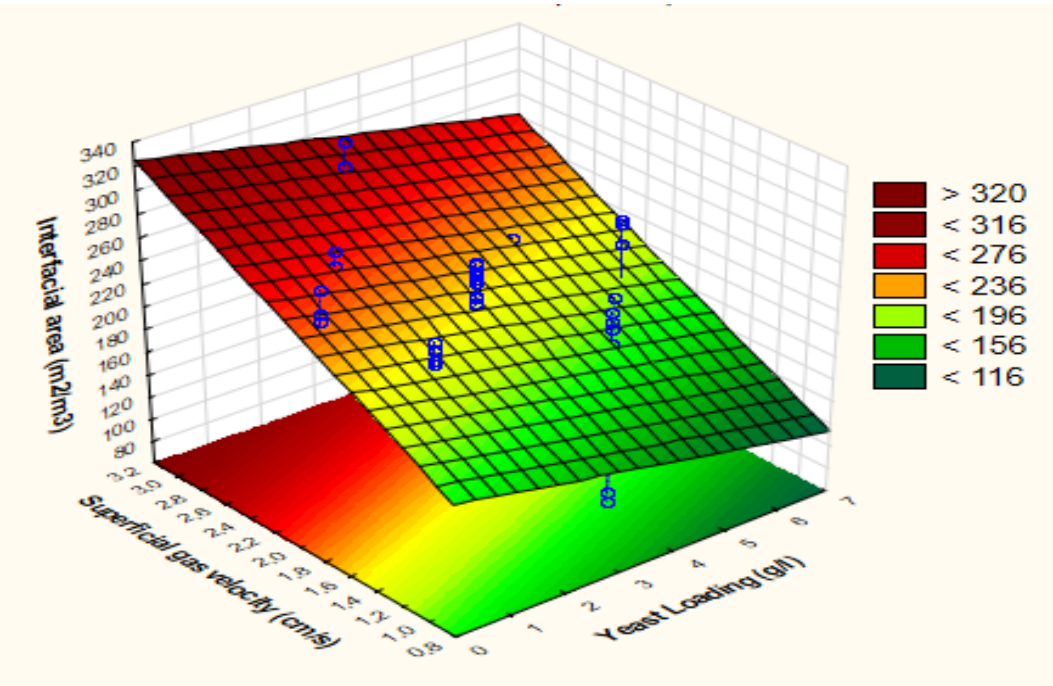

Figure 9-15: Influence of yeast loading and superficial gas velocity on the interfacial area at constant alkane concenatrtion (7.88% v/v).

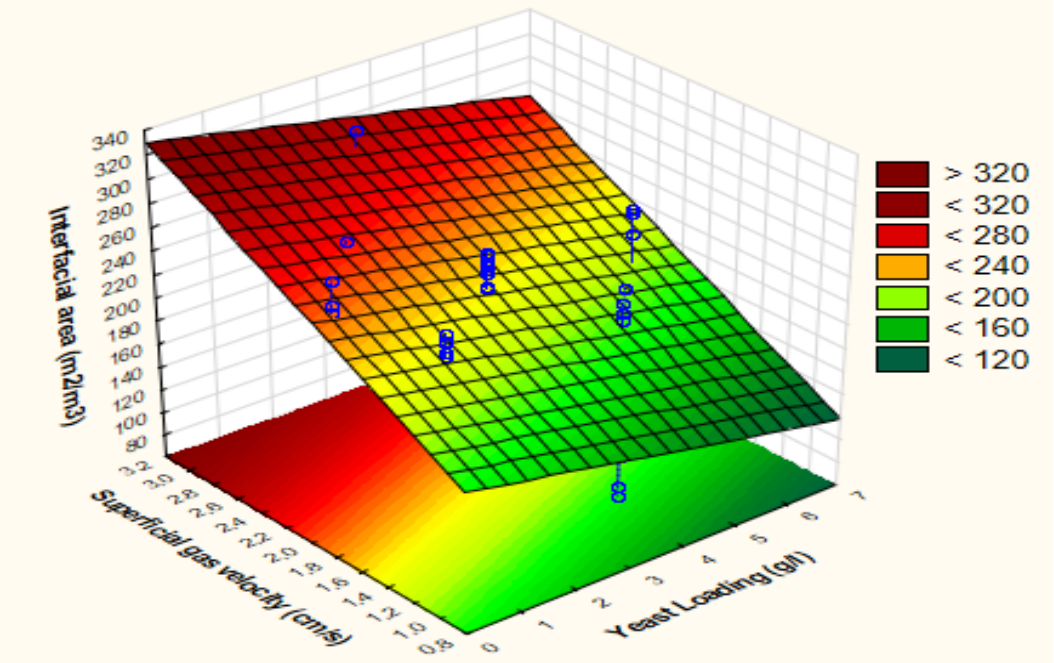

Figure 9-16: Influence of yeast loading and superficial gas velocity on the interfacial area at constant alkane concenatrtion (14.62% v/v).

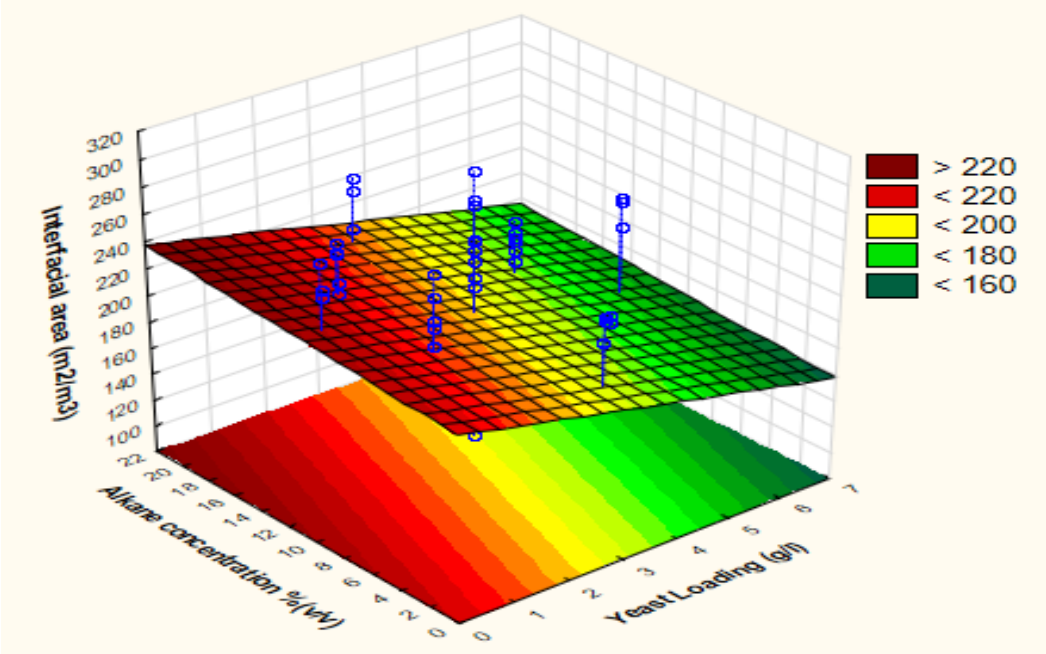

Figure9-17: Influence of yeast loading and alkane concenatrtion on the interfacial area at constant superficial gas velocity (1.62 cm/sec).

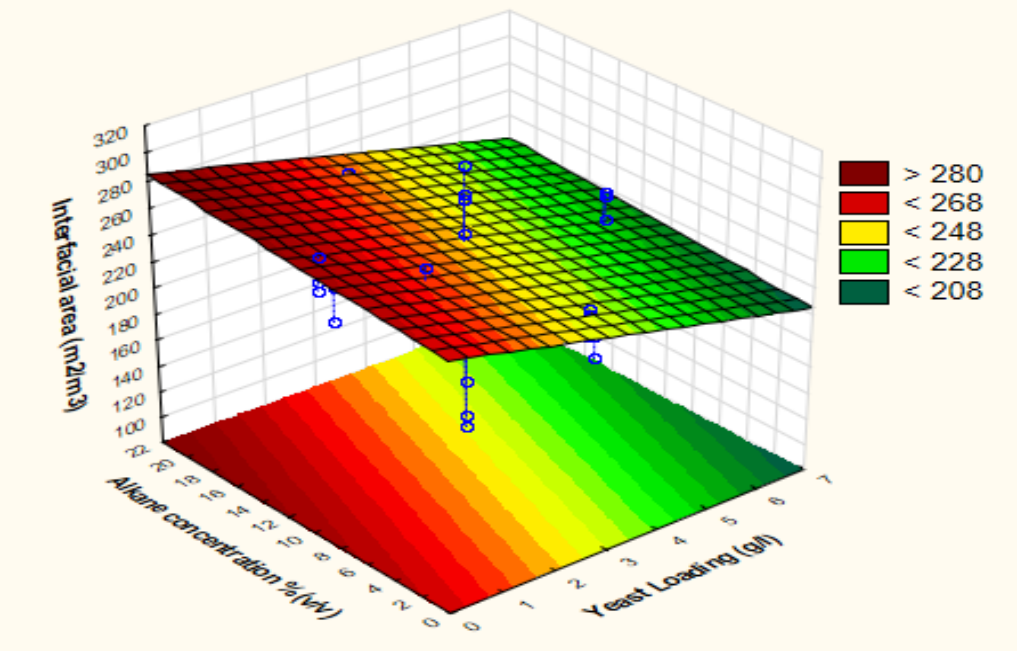

Figure 9-18: Influence of yeast loading and alkane concenatrtion on the interfacial area at constant superficial gas velocity (2.38 cm/sec).

9.2.4 Behaviour of K_P in a four phase system

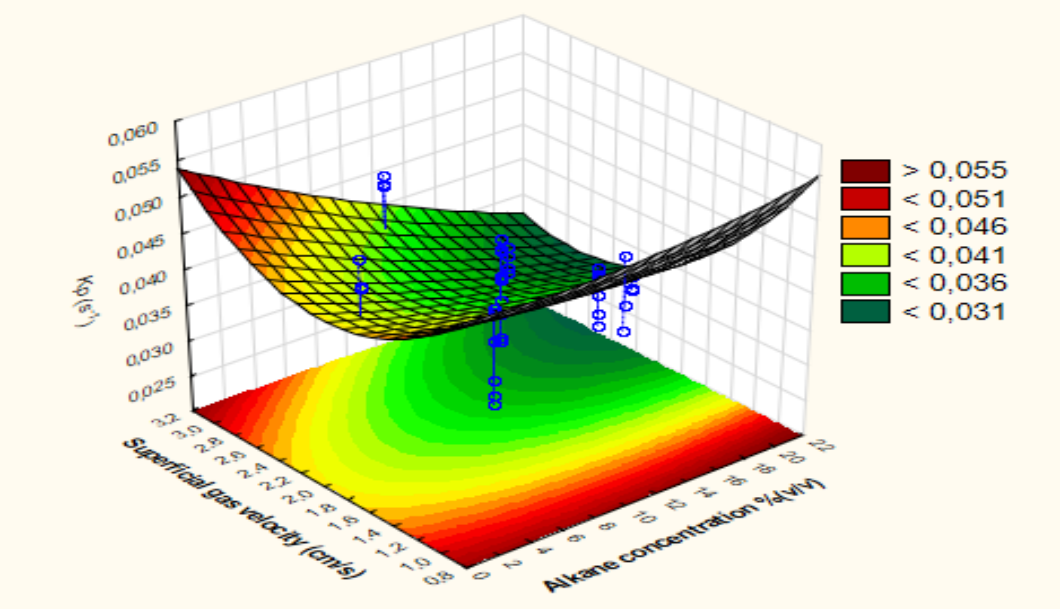

Figure 9-19: Influence of alkane concenatrtion and superficial gas velocity on K_P at constant yeast loading (1.62 g/l).

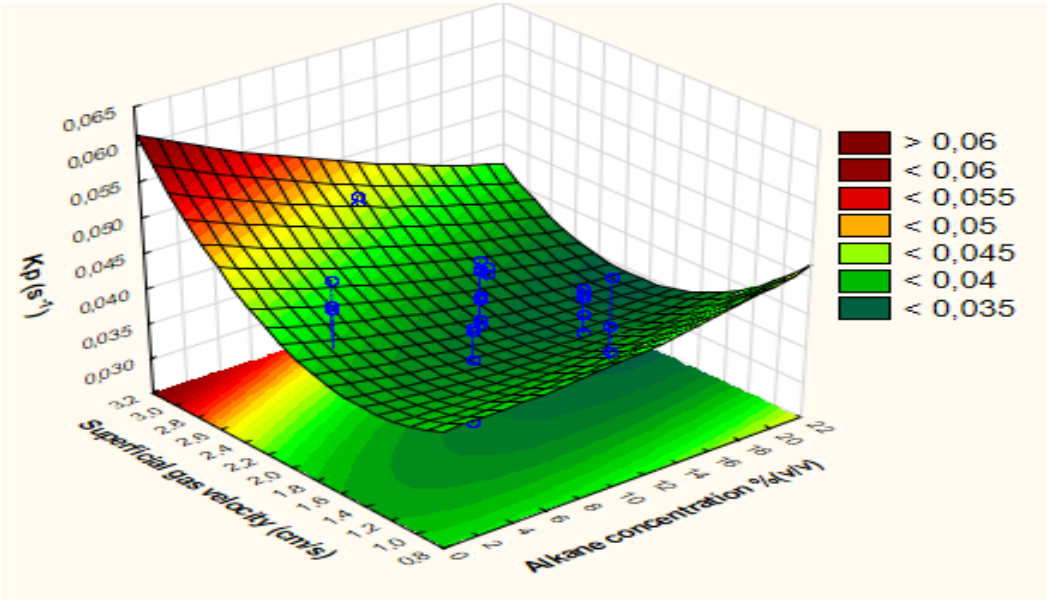

Figure 9-20: Influence of alkane concenatrtion and superficial gas velocity on K_P at constant yeast loading (4.88 g/l).

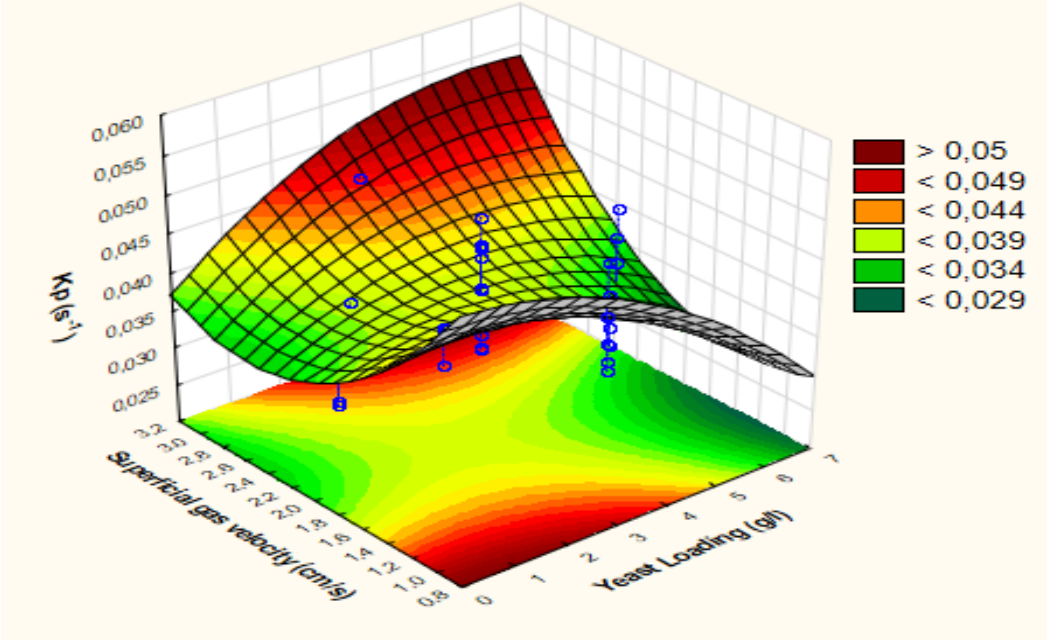

Figure 9-21: Influence of yeast loading and superficial gas velocity on K_P at constant alkane concenatrtion (7.88% v/v).

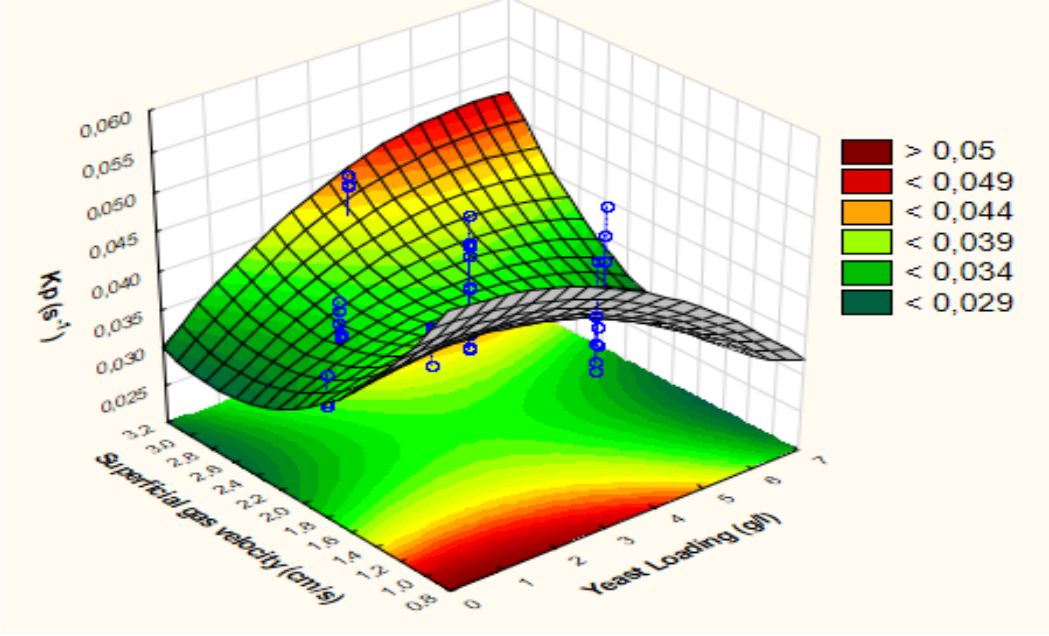

Figure 9-22: Influence of yeast loading and superficial gas velocity on K_P at constant alkane concenatrtion (14.62% v/v).

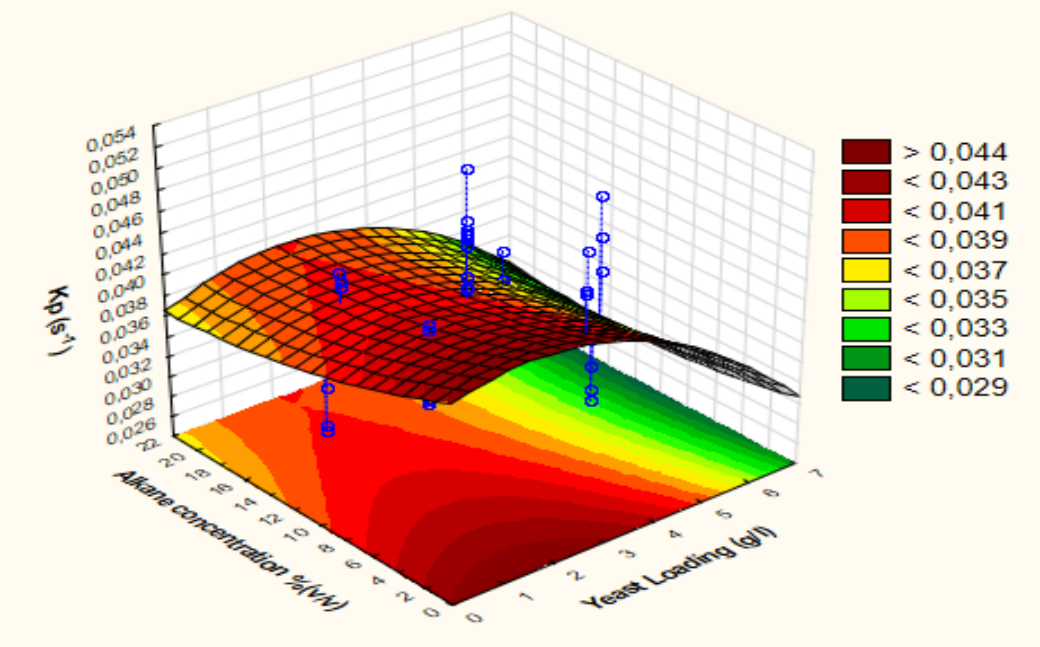

Figure 9-23: Influence of yeast loading and alkane concenatrtion on K_P at constant superficial gas velocity (1.62 cm/sec).

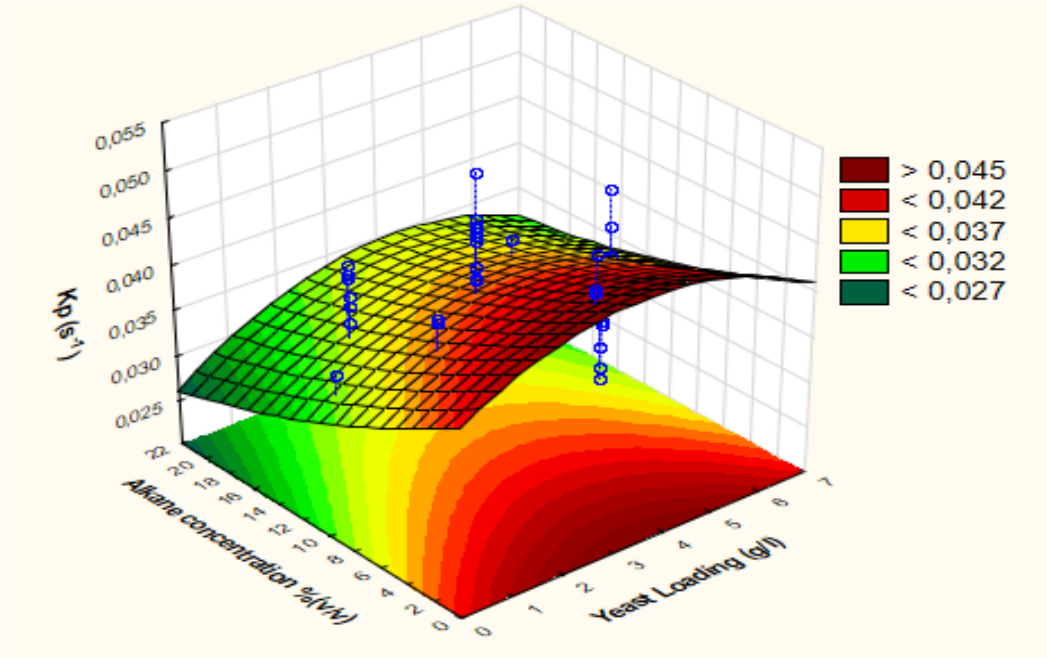

Figure 9-24: Influence of yeast loading and alkane concenatrtion on K_P at constant superficial gas velocity (2.38 cm/sec).

9.2.5 Behaviour of K_La in a four phase system.

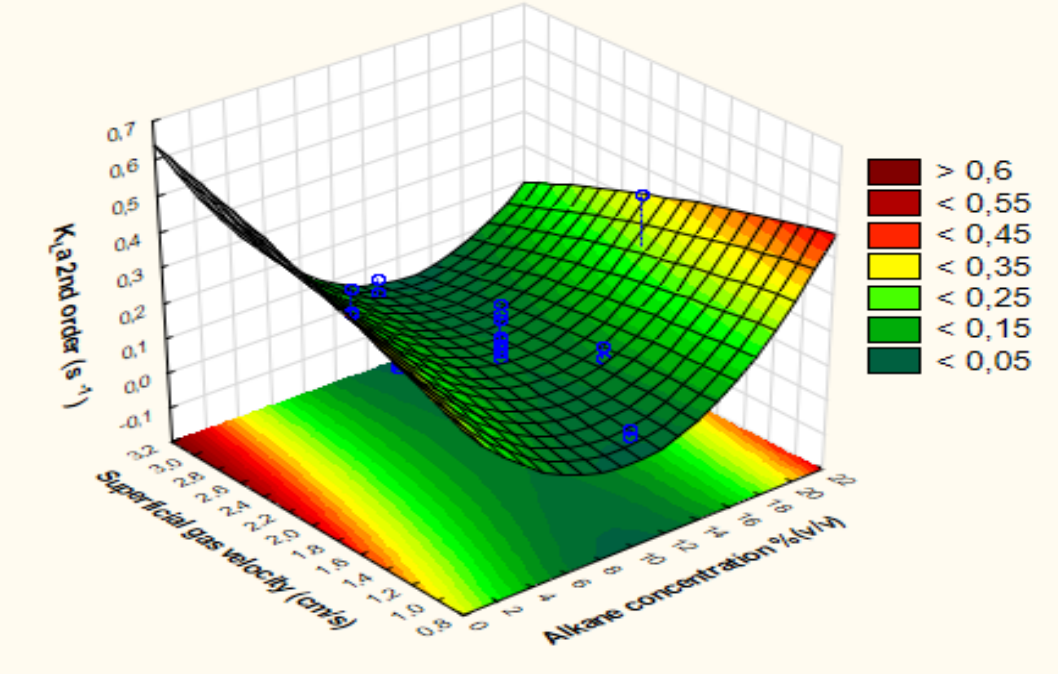

Figure 9-25: Influence of alkane concenatrtion and superficial gas velocity on K_La at constant yeast loading (1.62 g/l).

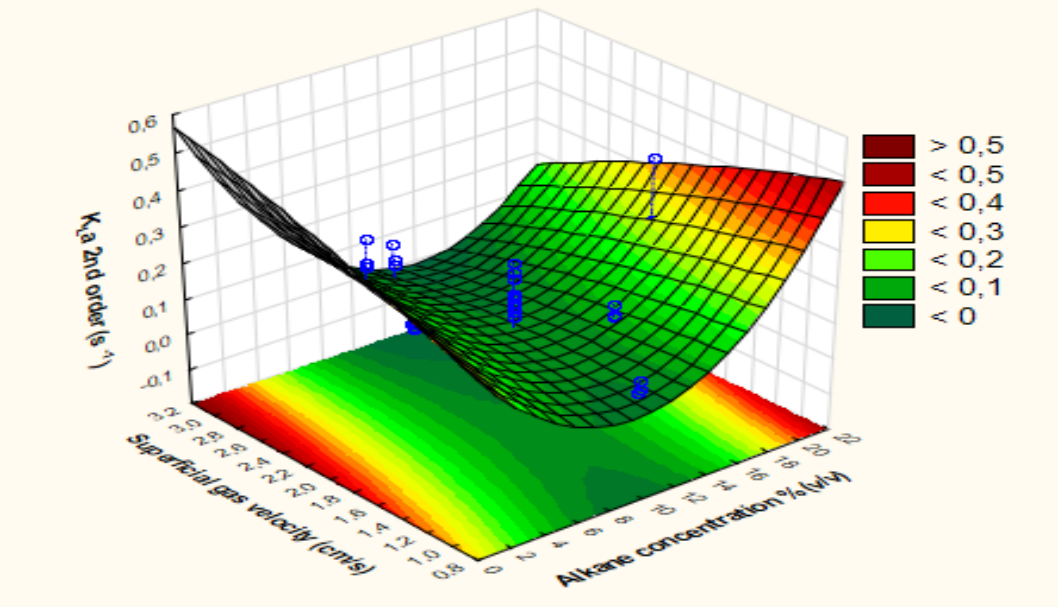

Figure 9-26: Influence of alkane concenatrtion and superficial gas velocity on K_La at constant yeast loading (4.88 g/l).

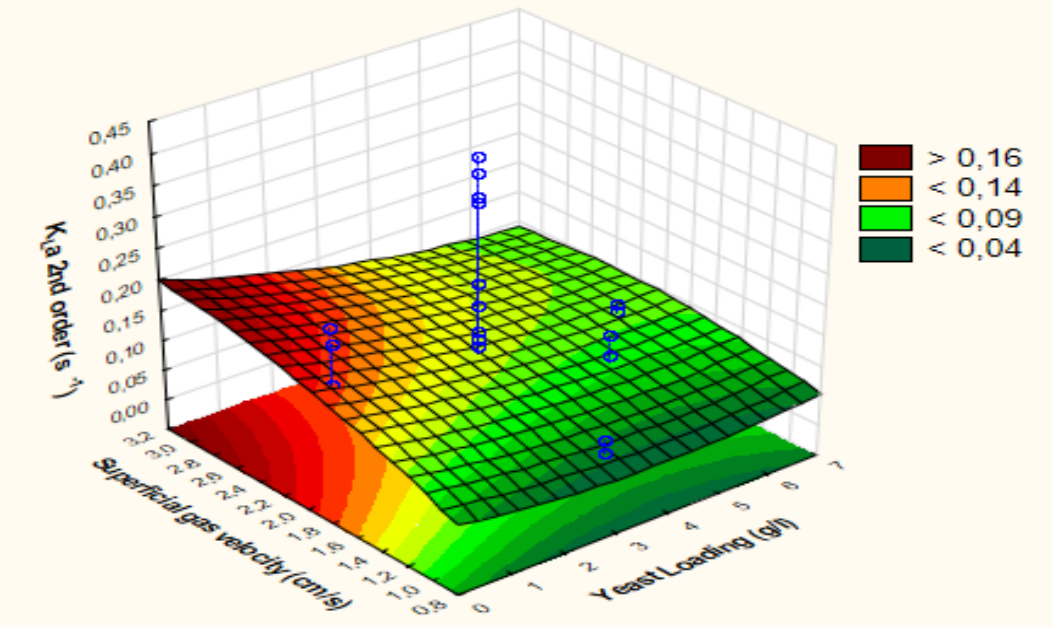

Figure 9-27: Influence of yeast loading and superficial gas velocity on K_La at constant alkane concenatrtion (7.88% v/v).

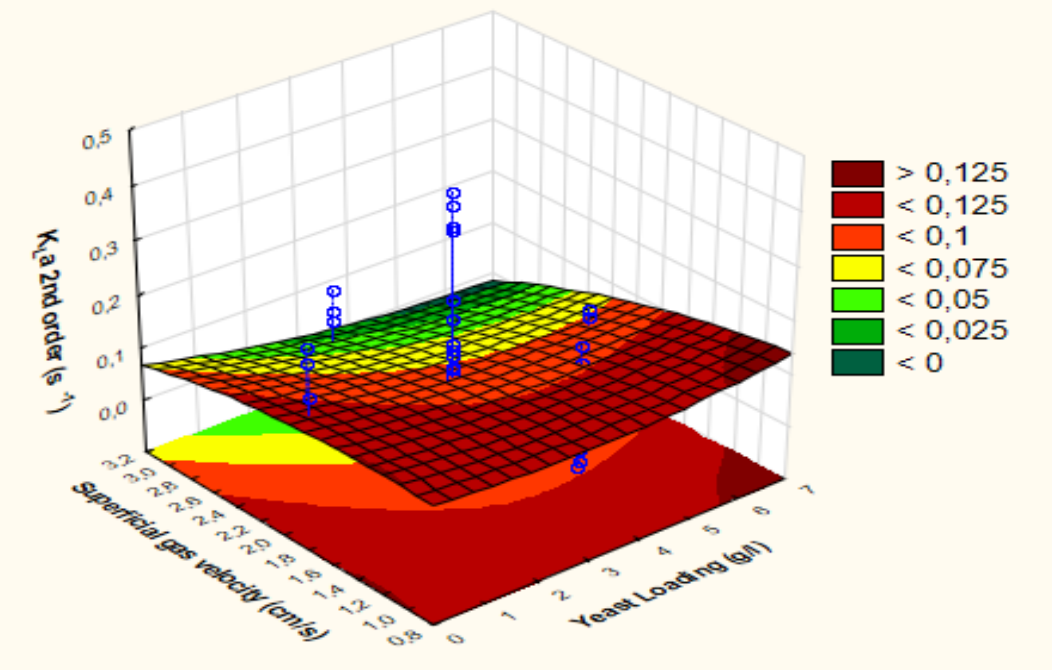

Figure 9-28: Influence of yeast loading and superficial gas velocity on K_La at constant alkane concenatrtion (14.88% v/v).

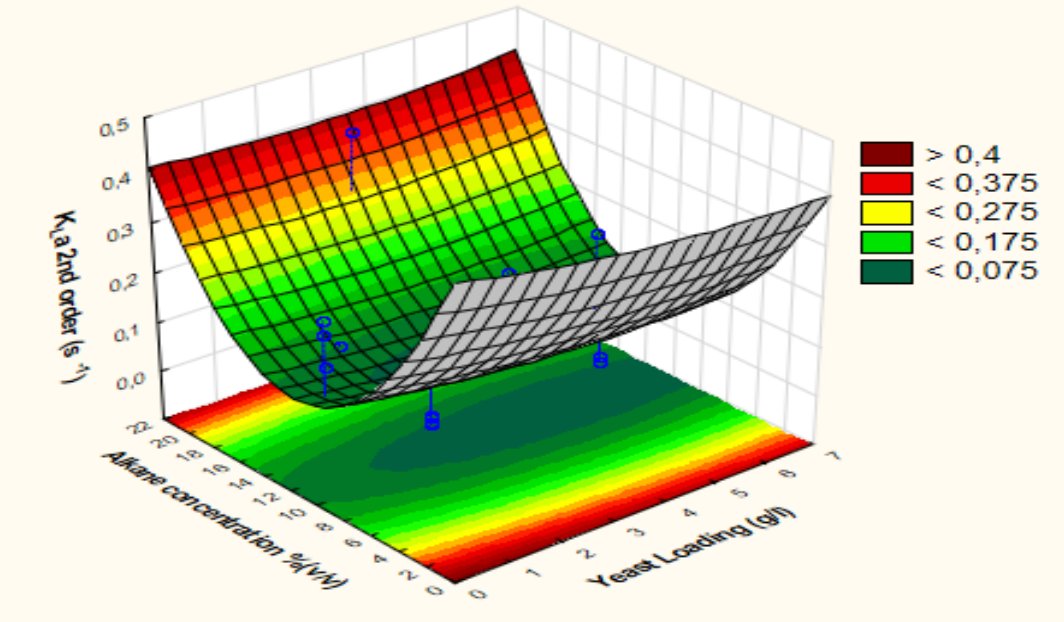

Figure 9-29: Influence of yeast loading and alkane concenatrtion on K_La at constant superficial gas velocity (1.62 cm/sec).

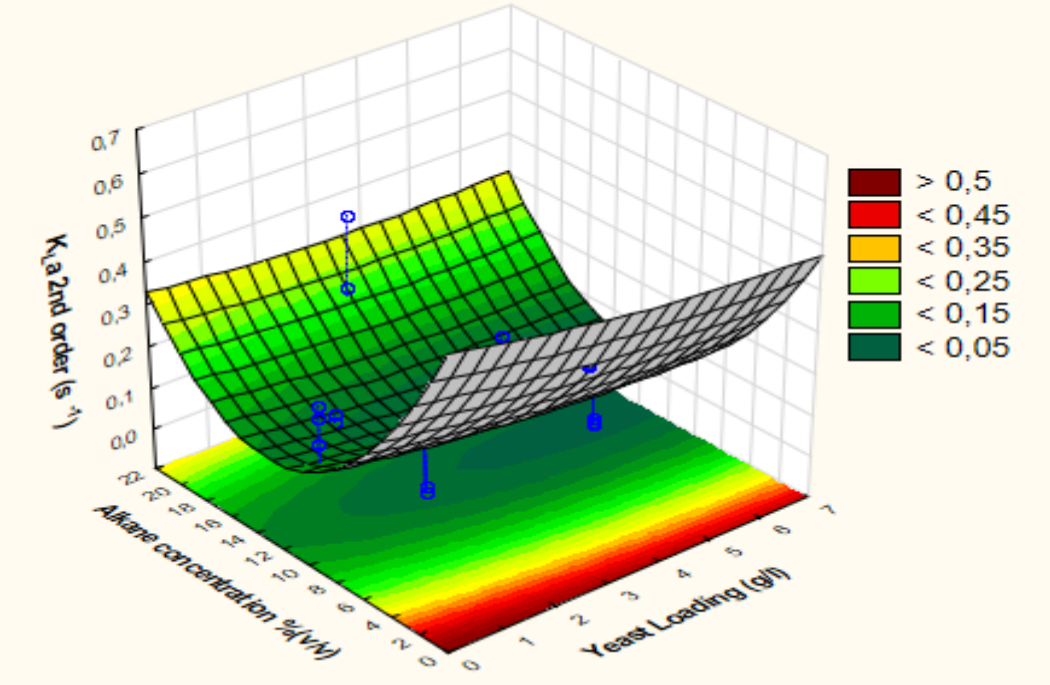

Figure 9-30: Influence of yeast loading and alkane concenatrtion on K_La at constant superficial gas velocity (2.38 cm/sec).

9.2.6 Behaviour of the K_L in a four phase system.

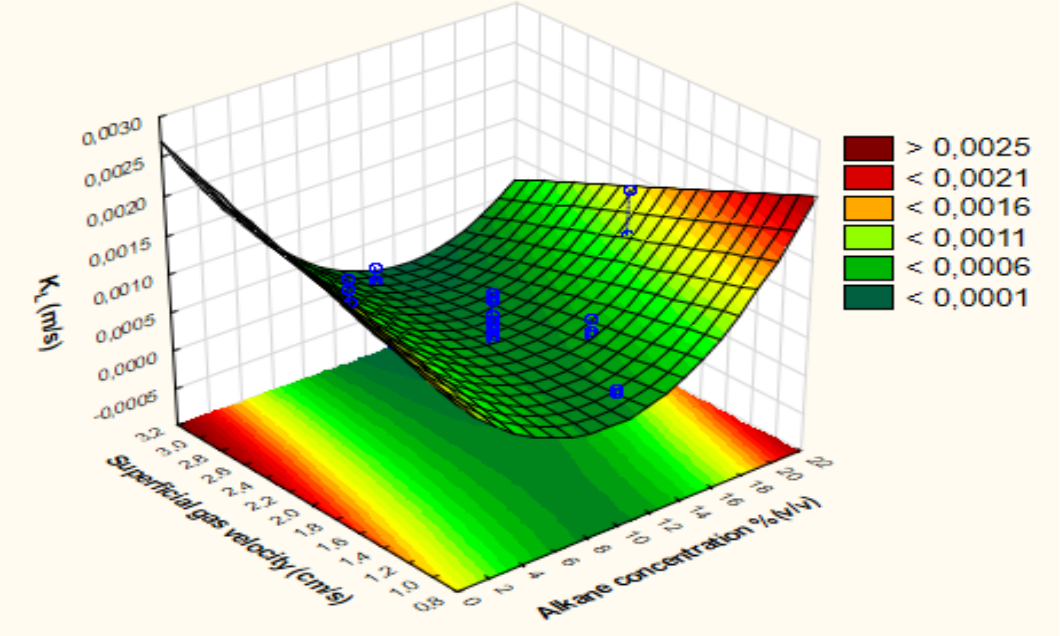

Figure 9-31: Influence of alkane concenatrtion and superficial gas velocity on K_L at constant yeast loading (1.62 g/l).

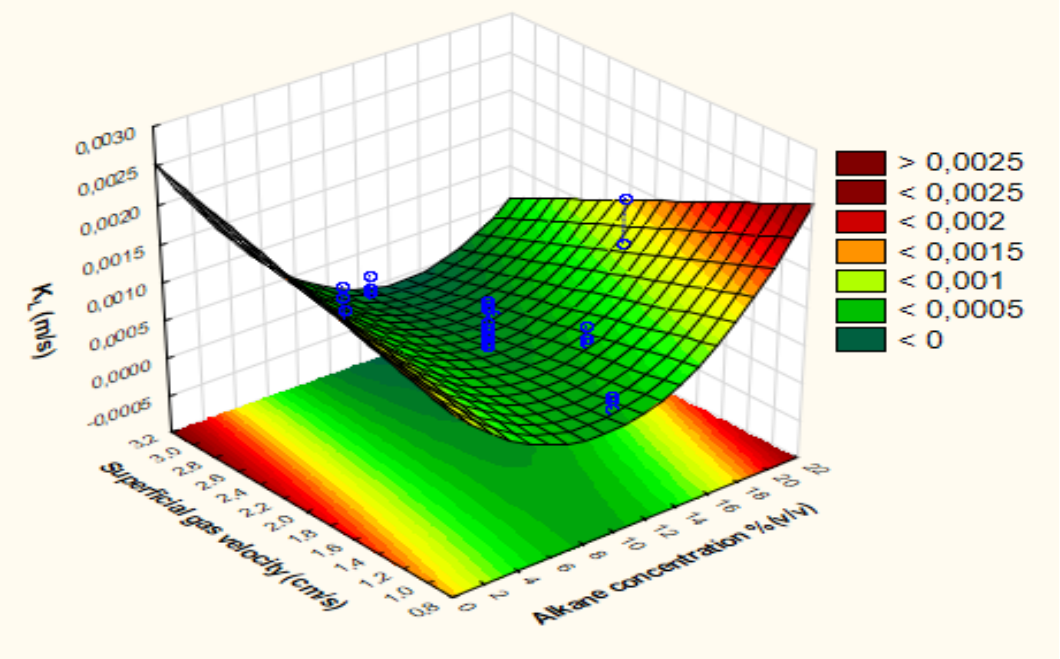

Figure 9-32: Influence of alkane concenatrtion and superficial gas velocity on K_L at constant yeast loading (4.88 g/l).

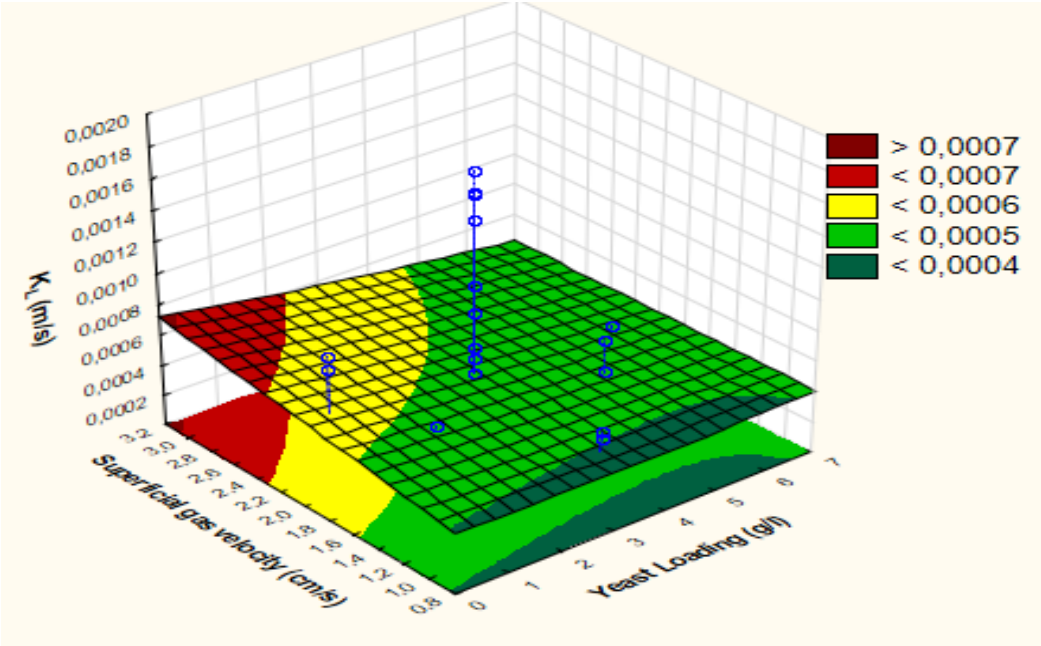

Figure 9-33: Influence of yeast loading and superficial gas velocity on K_L at constant alkane concenatrtion (7.88% v/v).

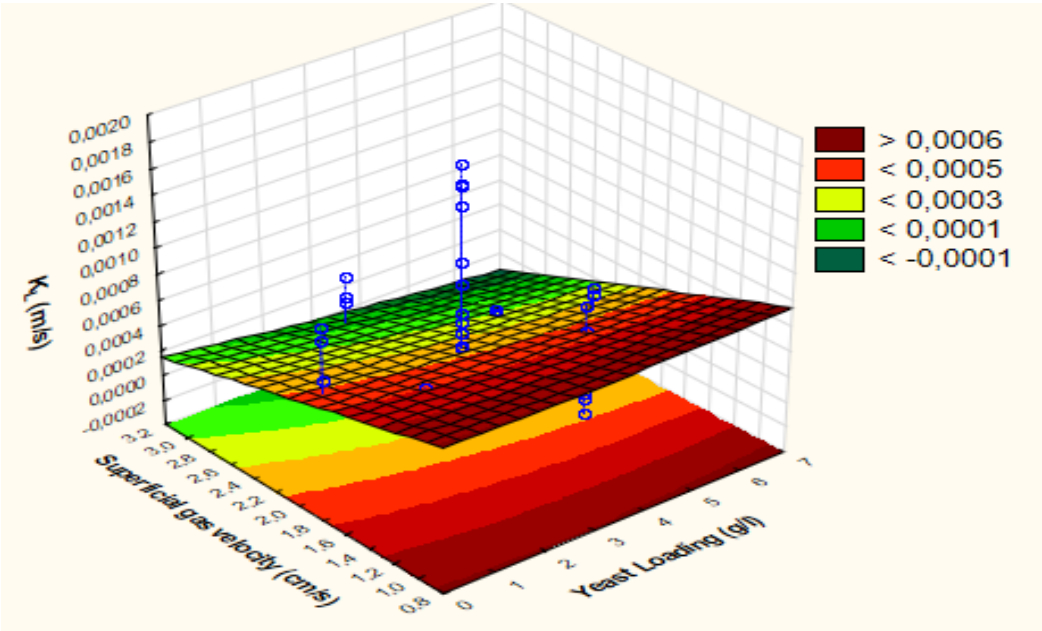

Figure 9-34: Influence of yeast loading and superficial gas velocity on K_L at constant alkane concenatrtion (14.62% v/v).

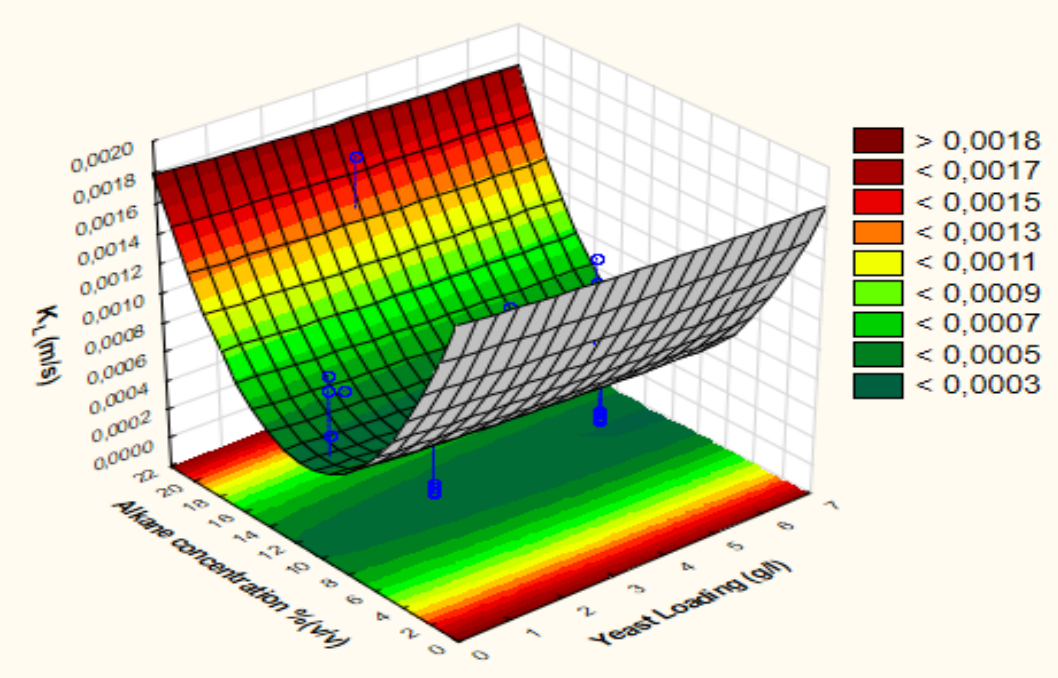

Figure 9-35: Influence of yeast loading and alkane concenatrtion on K_L at constant superficial gas velocity (1.62 cm/sec).

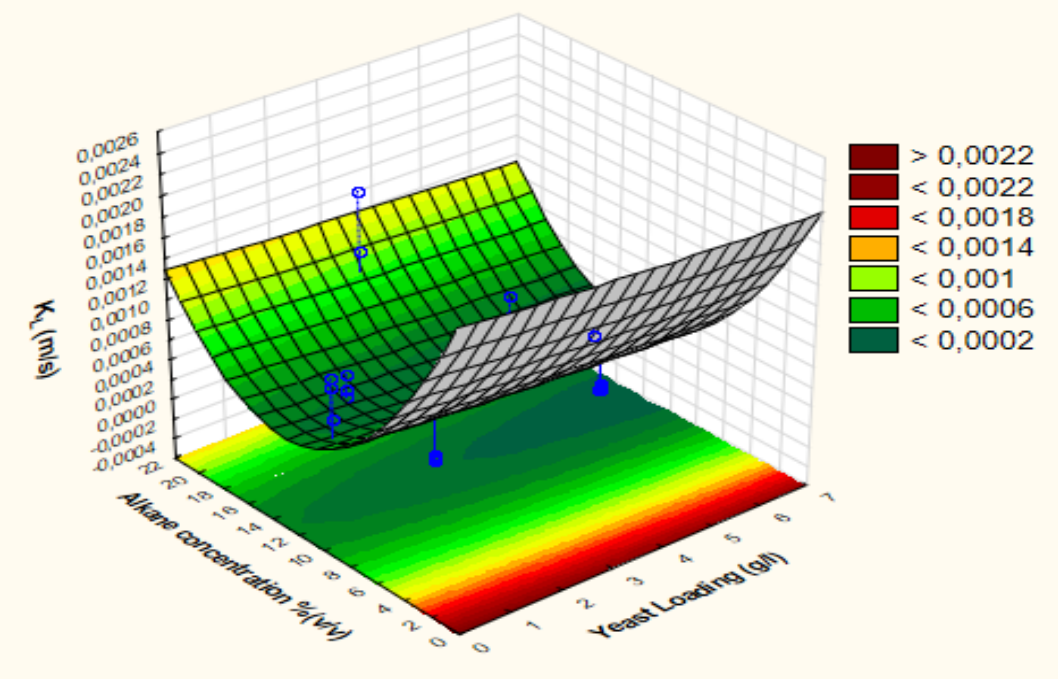

Figure 9-36: Influence of yeast loading and alkane concenatrtion on K_L at constant superficial gas velocity (2.38 cm/sec).

9.3 MATLAB code for image analysis

MATLAB code was used to measure the bubble diameter and therefore the interfacial area in the system. The code was developed by Clarke and Correia, (2008) and Hollis and Clarke, (2016). In this study, it was modified by Matt Molteno (personal communication), in order to enhance its accuracy and reduce the processing time.

```
function
[data,headers,scale]=measurebubbles(A,calibrate,thresh,bubsize
_range,pcent_border,circularity,medf,joinpixels,inc_background
,medf_background)
% MEASUREBUBBLES Version 2 5/15/2017 Uses image filtering to
get bubbles in
% binary image form and integrates pixel perimeter and areas.
% Also fits an ellipse to each one. Then line and area
integrals are
% computed with scale factore: calibrate.
% DESCRIPTION OF INPUTS:
% A: must be UINT8 as given by A =
imread('IMAGE5.jpg');A=rgb2gray(A);
% CALIBRATE: if logical (i.e. true/false), then runs
calibration,
% otherwise if numeric then the value is used to calibrate.
% THRESH: a threshold to detect bubble edges.
% BUBSIZE_RANGE: is a vector of [minimum acceptable bubble,
maximum acceptable bubble] in
% pixels.
% PCENT_BORDER: a fraction of the image between 0 and 1 which
excludes the
% outer image border of size(A)*PCENT_BORDER/2 pixels.
% DESCRIPTION OF OUTPUTS:
% DATA: is the data output in which each row is a bubble, each
column is a
% bubble characteristic. The column names are stored in
headers.
% HEADERS: contains column names in DATA.
% SCALE contains the mm/pixel conversion obtained from
calibration (if
% CALIBRATE=true.
% The last few columns of data provide the analytical formulas
for ellipse area and
% perimeter are used to determine projected bubble
circumference.
% The ellipse is fitted with linear least squares, with
automatic rejection
% of hyperbolic or parabolic functions.
% Written by Matt Molteno for Dr Robert Pott/
```

```
% For support contact mattmolteno@gmail.com or call 0745224455


fit_ellipses=true;
plotstages=true; % plot all stages of filtering and bubbles

if size(A,3)==3
    A=rgb2gray(A);
end

%% Uses Matlabs image toolbox
%% Default inputs
if nargin<10
    medf_background=5;
if nargin<9
        inc_background=5;
if nargin<8
            joinpixels=3;
if nargin<7
                medf=3;
if nargin<6
                    circularity=0.2;
if nargin<5
                        pcent_border=0.2;
if nargin<4
                            bubsize_range=[2,numel(A)/10]; %
min and max bubble sizes in pixels
if nargin<3
                                thresh=0.2;
if nargin<2
                                    calibrate=true;
end
end
end
end
end
end
end
end
end

if islogical(calibrate)&&calibrate
    figure('Units','normalized','Position',[0 0 1 1])
if ndims(A)==3
if size(A,3)==3
            imshow(rgb2gray(A));
end
else
        imshow(A);
end
```

```
    title('click and drag calibration line')
    refH = imline(gca);
    position = wait(refH);
    close(gcf)
    dposition=abs(position(1,:)-position(2,:));

%     pixLength = max(position(3),position(4));
    pixLength = max(dposition);

    answer = inputdlg({'Reference length(mm)'},...
'Reference measurements',1,{'10'});
    mmLength = str2double(answer{1});

    scale = mmLength/pixLength;%mm/pix;
    disp(['Calibration factor is: ',num2str(scale),'
[mm/pixel]'])
else
    scale = calibrate;
end



%% Section 1: highlight bubbles (subtract background)
A=double(A);
Aref=A;
A = medfilt3(A,[3,3]);


%% get background
B=A;
[bb,aa]=size(B);
linxs=round(linspace(1,aa,round(aa/inc_background)));
linys=round(linspace(1,bb,round(bb/inc_background)));
[xxs,yys]=meshgrid(linxs,linys);
Bs=B(linys,linxs);
Bsmed=medfilt3(Bs,[medf_background,medf_background]);

linx=1:aa;
liny=1:bb;
[xx,yy]=meshgrid(linx,liny);
underlying_shape=interp2(xxs,yys,double(Bsmed),xx,yy,'linear')
;
B=underlying_shape-B;
B(B<0)=0;
bvec=B(:);
bvec=bvec(~isnan(bvec));
B=(B-mean(bvec))/(std(bvec)); % normalise
imi=1;
imi=imi+1;lkim_fif(Aref,plotstages,'original');
imi=imi+1;lkim_fif(B,plotstages,'backgnd sub');
```

```
%% make bw image
bw=B>thresh;
imi=imi+1;lkim_fif(bw,plotstages,['# ',num2str(imi),':
thresh']);

bw=medfilt2(bw,[medf,medf]);
imi=imi+1;lkim_fif(bw,plotstages,['# ',num2str(imi),':
medf']);


bw=imdilate(bw,strel('disk',joinpixels)); % join lost pixels
with dilate ? erode operation
bw=imerode(bw,strel('disk',joinpixels));
imi=imi+1;lkim_fif(bw,plotstages,['# ',num2str(imi),':
joinpixels']);

bw=imdilate(bwmorph(bw,'skel',inf),strel('square',2));
bwh= imfill(bw,'holes');
bw=bwh-bw;
bwborder=imdilate(bw,strel('disk',2))-bw;
imi=imi+1;lkim_fif(bwborder,plotstages,['# ',num2str(imi),':
final edges']);

bwholes=medfilt2(bw);
imi=imi+1;lkim_fif(bw,plotstages,['# ',num2str(imi),':
final']);

[GL,L] = bwboundaries(bwholes,'noholes');
numbubs=max(L(:));
[X,Y]=meshgrid(1:size(L,2),1:size(L,1));

% create border
pcent_border=pcent_border/2; % because it will operate on both
borders
ignore_edge=round(pcent_border*mean(size(L)));
minx=ignore_edge;
maxx=max(X(:))-ignore_edge;
miny=ignore_edge;
maxy=max(Y(:))-ignore_edge;


figure
subplot(1,2,1),imagesc(1:size(L,2),1:size(L,1),Aref);
hold on
subplot(1,2,2),imagesc(1:size(L,2),1:size(L,1),logical(bw));co
lormap gray
hold on

bubbles=1:numbubs;
```

```
dl=scale;
da=scale^2;
count=0;
disp(['Measuring ',num2str(numbubs),' bubbles
>>>>>>>>>>>>>>>> started. Will print exceptions in command
window'])
data='no data was saved';
headers={'scale','bubble number (ii)','perimeter
length','projected area',...
'ellipse perimeter','ellipse
area','ellipse_centre_position_x','ellipse_centre_position_y',
'ellipse_average_diameter','ellipse_a','ellipse_b'};

for ii=bubbles

    Lid=(L==ii);
if any(Lid(:))

        elx=X(Lid);
        ely=Y(Lid);
        midbubx=mean(elx);
        midbuby=mean(ely);
        perimx=GL{ii}(:,2);
        perimy=GL{ii}(:,1);
        perim_i=integrate_border_fif(perimx,perimy)*dl;
        area_i=sum(Lid(:))*da;
        circularity_i=4*pi()*area_i/(perim_i^2); % defined as
shape factor - circle is 1

        dothisbubble=true;
if (area_i<(bubsize_range(1)*da))
            dothisbubble=false;
            disp(['bubble ',num2str(ii),' was outside size
range: too small'])
elseif (area_i>(bubsize_range(2)*da))
            dothisbubble=false;
            disp(['bubble ',num2str(ii),' was outside size
range: too big'])
end

if
~((midbubx>minx)&&(midbubx<maxx)&&(midbuby>miny)&&(midbuby<max
y))
            dothisbubble=false;
            disp(['bubble ',num2str(ii),' outside position
range'])
end

if circularity_i<circularity
            dothisbubble=false;
```

```
            disp(['bubble ',num2str(ii),' circularity
',num2str(circularity_i),' was smaller than set circularity
',num2str(circularity)])
end

if dothisbubble
            count=count+1;

            data_i=[scale,ii,perim_i,area_i]; % see
data_ellipse_i

% plot stuff

subplot(1,2,1),text(midbubx,midbuby,num2str(ii),'Color','b');
            subplot(1,2,1),plot(midbubx,midbuby,'k+');


subplot(1,2,2),fill(perimx,perimy,[0,0,1]*0.5,'facealpha',0.5)
;

subplot(1,2,2),text(midbubx,midbuby,num2str(ii),'Color','b');



            data_ellipse_i=[];
if fit_ellipses
try
                    [ellipse_t,ellipse_plot] =
fit_ellipse_fif(perimx,perimy);
                    ai=ellipse_t.a;
                    bi=ellipse_t.b;
                    ellipse_area_i=pi()*ai*bi*scale^2;
                    hh=(ai-bi)^2/(ai+bi)^2;

ellipse_perim_i=pi()*(ai+bi)*(1+(3*hh)/(10+sqrt(4-
3*hh)))*scale;

ellipse_centre_position_xy=mean([ellipse_plot.xr(:),ellipse_pl
ot.yr(:)]);
                    ellipse_a=ai; % ellipse parameter 1
                    ellipse_b=bi; % ellipse parameter 2 ...
for more, see ellipse_t.
                    ellipse_average_diameter=(ai+bi)/2*scale;

data_ellipse_i=[ellipse_perim_i,ellipse_area_i,ellipse_centre_
position_xy,ellipse_average_diameter,ellipse_a,ellipse_b];

% plot stuff

subplot(1,2,2),plot(ellipse_plot.xr,ellipse_plot.yr,'r-');
```

```
subplot(1,2,2),plot(ellipse_plot.new_ver_line(1,:),ellipse_plo
t.new_ver_line(2,:),'r-');

subplot(1,2,2),plot(ellipse_plot.new_horz_line(1,:),ellipse_pl
ot.new_horz_line(2,:),'r-');

catch

                    warning on;
                    warning('ellipse was not fitted')
end
end
            rowdata=[data_i,data_ellipse_i];
if count==1
                data=nan(numbubs,length(rowdata));
end
            data(ii,1:length(rowdata))=rowdata;
else
%             subplot(1,2,2),hold on

subplot(1,2,2),text(midbubx,midbuby,num2str(ii),'EdgeColor','g
','Color','g');
%             subplot(1,2,2),hold off

%             subplot(1,2,1),hold on

subplot(1,2,1),text(midbubx,midbuby,num2str(ii),'Color','g');
            subplot(1,2,1),plot(midbubx,midbuby,'k+');
%             subplot(1,2,1),hold off
end

end
end

subplot(1,2,2),title({['outer ',num2str(pcent_border*100*2),'
% image ignored'];'ignored bubbles (green), measured bubbles
(blue)'})
hold off
drawnow;
end

function lkim_fif(A,plotiftrue,titletext)
if plotiftrue
    figure;
    imagesc(A);
    axis square;
    title(titletext);
end
end
```

```
function L=integrate_border_fif(perimx,perimy)
nn=length(perimx);
perimx=[perimx(:)',perimx(1)];
perimy=[perimy(:)',perimy(1)];
L=0;
for ii=1:nn
    dx=(perimx(ii+1)-perimx(ii));
    dy=(perimy(ii+1)-perimy(ii));
    dL=sqrt(dx^2+dy^2);
    L=L+dL;
end
end

function [ellipse_t,ellipse_plot] = fit_ellipse_fif(
x,y,axis_handle)
%
% fit_ellipse - finds the best fit to an ellipse for the given
set of points.
%
% Format:   ellipse_t = fit_ellipse( x,y,axis_handle )
%
% Input:    x,y         - a set of points in 2 column vectors.
AT LEAST 5 points are needed !
%           axis_handle - optional. a handle to an axis, at
which the estimated ellipse
%                         will be drawn along with it's axes
%
% Output:   ellipse_t - structure that defines the best fit to
an ellipse
%                       a           - sub axis (radius) of the
X axis of the non-tilt ellipse
%                       b           - sub axis (radius) of the
Y axis of the non-tilt ellipse
%                       phi         - orientation in radians
of the ellipse (tilt)
%                       X0          - center at the X axis of
the non-tilt ellipse
%                       Y0          - center at the Y axis of
the non-tilt ellipse
%                       X0_in       - center at the X axis of
the tilted ellipse
%                       Y0_in       - center at the Y axis of
the tilted ellipse
%                       long_axis   - size of the long axis of
the ellipse
%                       short_axis  - size of the short axis
of the ellipse
%                       status      - status of detection of
an ellipse
```

```
%
% Note:     if an ellipse was not detected (but a parabola or
hyperbola), then
%           an empty structure is returned

%
=============================================================
=======================
%                   Ellipse Fit using Least Squares criterion
%
=============================================================
=======================
% We will try to fit the best ellipse to the given
measurements. the mathematical
% representation of use will be the CONIC Equation of the
Ellipse which is:
%
%    Ellipse = a*x^2 + b*x*y + c*y^2 + d*x + e*y + f = 0
%
% The fit-estimation method of use is the Least Squares method
(without any weights)
% The estimator is extracted from the following equations:
%
%    g(x,y;A) := a*x^2 + b*x*y + c*y^2 + d*x + e*y = f
%
%    where:
%       A   - is the vector of parameters to be estimated
(a,b,c,d,e)
%       x,y - is a single measurement
%
% We will define the cost function to be:
%
%   Cost(A) := (g_c(x_c,y_c;A)-f_c)'*(g_c(x_c,y_c;A)-f_c)
%            = (X*A+f_c)'*(X*A+f_c)
%            = A'*X'*X*A + 2*f_c'*X*A + N*f^2
%
%   where:
%       g_c(x_c,y_c;A) - vector function of ALL the
measurements
%                        each element of g_c() is g(x,y;A)
%       X              - a matrix of the form: [x_c.^2,
x_c.*y_c, y_c.^2, x_c, y_c ]
%       f_c            - is actually defined as
ones(length(f),1)*f
%
% Derivation of the Cost function with respect to the vector
of parameters "A" yields:
%
%   A'*X'*X = -f_c'*X = -f*ones(1,length(f_c))*X = -f*sum(X)
%
```

```
% Which yields the estimator:
%
%
~~~~~~~~~~~~~~~~~~~~~~~~~~~~~~~~~~~~~~~~~~~~~~~~~~~~~~~~~~~~~~~~~~~~~~~~
~~~~~~~~~~~~~~
%       |  A_least_squares = -f*sum(X)/(X'*X) ->(normalize by
-f) = sum(X)/(X'*X)   |
%
~~~~~~~~~~~~~~~~~~~~~~~~~~~~~~~~~~~~~~~~~~~~~~~~~~~~~~~~~~~~~~~~~~~~~~~~
~~~~~~~~~~~~~~
%
% (We will normalize the variables by (-f) since "f" is
unknown and can be accounted for later on)
%
% NOW, all that is left to do is to extract the parameters
from the Conic Equation.
% We will deal the vector A into the variables: (A,B,C,D,E)
and assume F = -1;
%
%    Recall the conic representation of an ellipse:
%
%       A*x^2 + B*x*y + C*y^2 + D*x + E*y + F = 0
%
% We will check if the ellipse has a tilt (=orientation). The
orientation is present
% if the coefficient of the term "x*y" is not zero. If so, we
first need to remove the
% tilt of the ellipse.
%
% If the parameter "B" is not equal to zero, then we have an
orientation (tilt) to the ellipse.
% we will remove the tilt of the ellipse so as to remain with
a conic representation of an
% ellipse without a tilt, for which the math is more simple:
%
% Non tilt conic rep.:  A`*x^2 + C`*y^2 + D`*x + E`*y + F` = 0
%
% We will remove the orientation using the following
substitution:
%
%   Replace x with cx+sy and y with -sx+cy such that the conic
representation is:
%
%   A(cx+sy)^2 + B(cx+sy)(-sx+cy) + C(-sx+cy)^2 + D(cx+sy) +
E(-sx+cy) + F = 0
%
%   where:      c = cos(phi)    ,   s = sin(phi)
%
%   and simplify...
%
```

```
%       x^2(A*c^2 - Bcs + Cs^2) + xy(2A*cs +(c^2-s^2)B -2Ccs)
+ ...
%           y^2(As^2 + Bcs + Cc^2) + x(Dc-Es) + y(Ds+Ec) + F =
0
%
%   The orientation is easily found by the condition of
(B_new=0) which results in:
%
%   2A*cs +(c^2-s^2)B -2Ccs = 0  ==> phi = 1/2 * atan( b/(c-a)
)
%
%   Now the constants   c=cos(phi)  and  s=sin(phi)  can be
found, and from them
%   all the other constants A`,C`,D`,E` can be found.
%
%   A` = A*c^2 - B*c*s + C*s^2                   D` = D*c-E*s
%   B` = 2*A*c*s +(c^2-s^2)*B -2*C*c*s = 0       E` = D*s+E*c
%   C` = A*s^2 + B*c*s + C*c^2
%
% Next, we want the representation of the non-tilted ellipse
to be as:
%
%       Ellipse = ( (X-X0)/a )^2 + ( (Y-Y0)/b )^2 = 1
%
%       where:  (X0,Y0) is the center of the ellipse
%               a,b     are the ellipse "radiuses" (or sub-
axis)
%
% Using a square completion method we will define:
%
%       F`` = -F` + (D`^2)/(4*A`) + (E`^2)/(4*C`)
%
%       Such that:    a`*(X-X0)^2 = A`(X^2 + X*D`/A` +
(D`/(2*A`))^2 )
%                     c`*(Y-Y0)^2 = C`(Y^2 + Y*E`/C` +
(E`/(2*C`))^2 )
%
%       which yields the transformations:
%
%           X0  =   -D`/(2*A`)
%           Y0  =   -E`/(2*C`)
%           a   =   sqrt( abs( F``/A` ) )
%           b   =   sqrt( abs( F``/C` ) )
%
% And finally we can define the remaining parameters:
%
%   long_axis   = 2 * max( a,b )
%   short_axis  = 2 * min( a,b )
%   Orientation = phi
%
```

```
%

% initialize
orientation_tolerance = 1e-3;

% empty warning stack
warning( '' );

% prepare vectors, must be column vectors
x = x(:);
y = y(:);

% remove bias of the ellipse - to make matrix inversion more
accurate. (will be added later on).
mean_x = mean(x);
mean_y = mean(y);
x = x-mean_x;
y = y-mean_y;

% the estimation for the conic equation of the ellipse
X = [x.^2, x.*y, y.^2, x, y ];
a = sum(X)/(X'*X);

% check for warnings
if ~isempty( lastwarn )
    disp( 'stopped because of a warning regarding matrix
inversion' );
    ellipse_t = [];
return
end

% extract parameters from the conic equation
[a,b,c,d,e] = deal( a(1),a(2),a(3),a(4),a(5) );

% remove the orientation from the ellipse
if ( min(abs(b/a),abs(b/c)) > orientation_tolerance )

    orientation_rad = 1/2 * atan( b/(c-a) );
    cos_phi = cos( orientation_rad );
    sin_phi = sin( orientation_rad );
    [a,b,c,d,e] = deal(...
        a*cos_phi^2 - b*cos_phi*sin_phi + c*sin_phi^2,...
        0,...
        a*sin_phi^2 + b*cos_phi*sin_phi + c*cos_phi^2,...
        d*cos_phi - e*sin_phi,...
        d*sin_phi + e*cos_phi );
    [mean_x,mean_y] = deal( ...
        cos_phi*mean_x - sin_phi*mean_y,...
        sin_phi*mean_x + cos_phi*mean_y );
else
```

```
    orientation_rad = 0;
    cos_phi = cos( orientation_rad );
    sin_phi = sin( orientation_rad );
end

% check if conic equation represents an ellipse
test = a*c;
switch (1)
case (test>0),  status = '';
case (test==0), status = 'Parabola found';  warning(
'fit_ellipse: Did not locate an ellipse' );
case (test<0),  status = 'Hyperbola found'; warning(
'fit_ellipse: Did not locate an ellipse' );
end

% if we found an ellipse return it's data
if (test>0)

% make sure coefficients are positive as required
if (a<0), [a,c,d,e] = deal( -a,-c,-d,-e ); end

% final ellipse parameters
    X0          = mean_x - d/2/a;
    Y0          = mean_y - e/2/c;
    F           = 1 + (d^2)/(4*a) + (e^2)/(4*c);
    [a,b]       = deal( sqrt( F/a ),sqrt( F/c ) );
    long_axis   = 2*max(a,b);
    short_axis  = 2*min(a,b);

% rotate the axes backwards to find the center point of the
original TILTED ellipse
    R           = [ cos_phi sin_phi; -sin_phi cos_phi ];
    P_in        = R * [X0;Y0];
    X0_in       = P_in(1);
    Y0_in       = P_in(2);

% pack ellipse into a structure
    ellipse_t = struct( ...
'a',a,...
'b',b,...
'phi',orientation_rad,...
'X0',X0,...
'Y0',Y0,...
'X0_in',X0_in,...
'Y0_in',Y0_in,...
'long_axis',long_axis,...
'short_axis',short_axis,...
'status','' );
else
% report an empty structure
```

```
    ellipse_t = struct( ...
'a',[],...
'b',[],...
'phi',[],...
'X0',[],...
'Y0',[],...
'X0_in',[],...
'Y0_in',[],...
'long_axis',[],...
'short_axis',[],...
'status',status );
end



% rotation matrix to rotate the axes with respect to an angle
phi
R = [ cos_phi sin_phi; -sin_phi cos_phi ];

% the axes
ver_line        = [ [X0 X0]; Y0+b*[-1 1] ];
horz_line       = [ X0+a*[-1 1]; [Y0 Y0] ];
new_ver_line    = R*ver_line;
new_horz_line   = R*horz_line;

% the ellipse
theta_r         = linspace(0,2*pi);
ellipse_x_r     = X0 + a*cos( theta_r );
ellipse_y_r     = Y0 + b*sin( theta_r );
rotated_ellipse = R * [ellipse_x_r;ellipse_y_r];

ellipse_plot = struct( ...
'xr',rotated_ellipse(1,:),...
'yr',rotated_ellipse(2,:),...
'rotated_ellipse',rotated_ellipse,...
'new_ver_line',new_ver_line,...
'new_horz_line',new_horz_line);

% check if we need to plot an ellipse with it's axes.
if (nargin>2) & ~isempty( axis_handle ) & (test>0)
% draw
    hold_state = get( axis_handle,'NextPlot' );
    set( axis_handle,'NextPlot','add' );
    plot( new_ver_line(1,:),new_ver_line(2,:),'r' );
    plot( new_horz_line(1,:),new_horz_line(2,:),'r' );
    plot( rotated_ellipse(1,:),rotated_ellipse(2,:),'r' );
    set( axis_handle,'NextPlot',hold_state );
end

end
```

```
function B = medfilt3(A,siz,padopt,CHUNKFACTOR)

%MEDFILT3 1-D, 2-D and 3-D median filtering.
%   B = MEDFILT3(A,[M N P]) performs median filtering of the
3-D array A.
%   Each output pixel contains the median value in the M-by-N-
by-P
%   neighborhood around the corresponding pixel in the input
array.
%
%   B = MEDFILT3(A,[M N]) performs median filtering of the
matrix A. Each
%   output pixel contains the median value in the M-by-N
neighborhood
%   around the corresponding pixel.
%

%% Note:
% If you work with large 3D arrays, an "Out of memory" error
may appear.
% The chunk factor thus must be increased to reduce the size
of the chunks.
if nargin~=4
    CHUNKFACTOR = 1;
end
if CHUNKFACTOR<1, CHUNKFACTOR = 1; end

%% Checking input arguments
if isscalar(A), B = A; return, end

if ndims(A)>3
    error('A must be a 1-D, 2-D or 3-D array.')
end

if all(isnan(A(:))), B = A; return, end

sizA = size(A);
if nargin==1
% default kernel size is 3 or 3x3 or 3x3x3
if isvector(A)
        siz = 3;
else
        siz = 3*ones(1,numel(sizA));
end
    padopt = 'replicate';
elseif nargin==2
% default padding option is "replicate"
    padopt = 'replicate';
end
```

```
%% Make SIZ a 3-element array
if numel(siz)==2
    siz = [siz 1];
elseif isscalar(siz)
if sizA(1)==1
        siz = [1 siz 1];
else
        siz = [siz 1 1];
end
end

%% Chunks: the numerical process is split up in order to avoid
large arrays
N = numel(A);
siz = ceil((siz-1)/2);
n = prod(siz*2+1);
if n==1, B = A; return, end
nchunk = (1:ceil(N/n/CHUNKFACTOR):N);
if nchunk(end)~=N, nchunk = [nchunk N]; end

%% Change to double if needed
class0 = class(A);
if ~isa(A,'float')
    A = double(A);
end

%% Padding along specified direction
% If PADARRAY exists (Image Processing Toolbox), this function
is used.
% Otherwise the array is padded with scalars.
B = A;
sizB = sizA;
try
    A = padarray(A,siz,padopt);
catch
if ~isscalar(padopt)
        padopt = 0;

warning('MATLAB:medfilt3:InexistentPadarrayFunction',...
            ['PADARRAY function does not exist: '...
'only scalar padding option is available.\n'...
'If not specified, the scalar 0 is used as default.']);
end
    A = ones(sizB+siz(1:ndims(B))*2)*padopt;
    A(siz(1)+1:end-siz(1),siz(2)+1:end-siz(2),siz(3)+1:end-
siz(3)) = B;
end
sizA = size(A);
```

```
if numel(sizB)==2
    sizA = [sizA 1];
    sizB = [sizB 1];
end

%% Creating the index arrays (INT32)
inc = zeros([3 2*siz+1],'int32');
siz = int32(siz);
[inc(1,:,:,:) inc(2,:,:,:) inc(3,:,:,:)] = ndgrid(...
    [0:-1:-siz(1) 1:siz(1)],...
    [0:-1:-siz(2) 1:siz(2)],...
    [0:-1:-siz(3) 1:siz(3)]);
inc = reshape(inc,[1 3 prod(2*single(siz)+1)]);

I = zeros([sizB 3],'int32');
sizB = int32(sizB);
[I(:,:,:,1) I(:,:,:,2) I(:,:,:,3)] = ndgrid(...
    (1:sizB(1))+siz(1),...
    (1:sizB(2))+siz(2),...
    (1:sizB(3))+siz(3));
I = reshape(I,[prod(single(sizB)) 3]);

%% Check if NANMEDIAN exists
existNaNmedian = exist('nanmedian','file');

%% Filtering
for i = 1:length(nchunk)-1
    ii=i;
    Im = repmat(I(nchunk(ii):nchunk(ii+1),:),[1 1 n]);
    Im = Im + repmat(inc,[nchunk(ii+1)-nchunk(ii)+1,1,1]);

    I0 = Im(:,1,:) +...
        (Im(:,2,:)-1)*sizA(1) +...
        (Im(:,3,:)-1)*sizA(1)*sizA(2);
    I0 = squeeze(I0);

if existNaNmedian
        B(nchunk(ii):nchunk(ii+1)) = nanmedian(A(I0),2);
else
        B(nchunk(ii):nchunk(ii+1)) = median(A(I0),2);
end
end
B = cast(B,class0);

end
```

9.4 Derivation of the second order probe response model

K_La was calculated based on the response of DO concentration to a step change in sparge gas (Equation 9-1). Equation 9-2 is the first order model that assumes that the DO probe has no response lag, equating C to C_p.

$$\frac{dC_p}{dt} = K_La(C^* - C) \quad \text{Equation 9-9-1}$$

$$\frac{dC_p}{dt} = K_La(C^* - C_p) \quad \text{Equation 9-2}$$

The response lag of the DO probe can be modelled according to the first order relationship described (Equation H.3) (Aiba and Huang, 1969).

$$\frac{dC_p}{dt} = K_p(C - C_p) \quad \text{Equation 9-3}$$

Incorporation of equation 9-3 into equation A2-2 yields the second order model. Dimensionless quantities (equations 9-4 and 5) are introduced (Keil and Fuchs, 1971).

$$Y_p = \frac{C_p^* - C_p}{C_p^* - C_{po}} \quad \text{Equation 9-4}$$

$$Y = \frac{C^* - C}{C^* - C_0} \quad \text{Equation 9-5}$$

Substituting equations 9-4 and 9-5 into equations 9-2 and 9-3 respectively produces the following equations;

$$\frac{dY}{dt} = -K_La.Y \quad \text{Equation 9-6}$$

$$\frac{dY_p}{dt} = K_p(Y - Y_p) \quad \text{Equation 9-7}$$

Variables in equations A2-6 and 7 are then separated to yield equation A2-8 and A2-9:

$$\frac{dY}{Y} = -K_La.dt \quad \text{Equation A2-8}$$

$$\frac{dY_p}{dt} = K_p.Y \quad - K_p.Y_p \qquad \text{Equation A2-9}$$

Integrating equation A2-8 yields equation A2-10. I is defined as the integration constant.

$$\ln(Y\ ) = I. - K_L a.t$$

$$Y \quad = I.e^{-K_L a.t} \qquad \text{Equation A2-10}$$

By substituting equation A2-10 back into equation A2-9, equation A2-11 is produced;

$$\frac{dY_p}{dt} = K_p.I.e^{-K_L a.t} - K_p.Y_p \qquad \text{Equation A2-11}$$

Solving equation A2-11 using non-homogeneous differential equations and the separation of variables;

$$\frac{dY_p}{Y_p} = K_p.dt \qquad \text{Equation A2-12}$$

When equation A2-12 is integrated, equation A2-13 is yielded, where J is an integration constant.

$$\ln(\cancel{Y_{po}}^{0} - Y_p) = J.K_p.t$$

$$Y_p = J.e^{-K_p.t} \qquad \text{Equation A2-13}$$

Equation A2-13 is the function form. It can further be represented in the associated complimentary form (equation A2-14):

$$Y_c = A'e^{-B't} \qquad \text{Equation A2-14}$$

The complimentary form of equation A2-11 is therefore deduced to be equation A2-15;

$$dY_c + K_p.Y_c = K_p.A'e^{-B't} - A'B'e^{-B't} \qquad \text{Equation A2-15}$$

However, from:

$$dY_c + K_pY_c = K_p.I.e^{-K_La.t} \qquad \text{Equation A2-16}$$

Equations A2-15 and A2-16 can be equated and simplified to yield A2-17;

$$(K_p.A' - A'B' = K_p.I) \qquad \text{Equation A2-17}$$

Since B_o=K_La, equation A2-17 can be rearranged to give A2-18;

$$A' = \frac{K_pL}{K_p - K_La} \qquad \text{Equation A2 -18}$$

Setting Y' as the complimentary form of equation A2-11 and including the probe response lag, equation A2-19 is obtained;

$$Y' = Y_p + Y_c \qquad \text{Equation A2-19}$$

Substituting equations A2-13 and A2-15 into equation A2-19 yields equation A2-20;

$$Y' = J.e^{-K_p.t} + A'e^{-B't} \qquad \text{Equation A2-20}$$

Incorporating equation A2-18 into equation A2-20 yields equation A2-21.

$$Y'(K_p - K_La) = (K_p - K_La).J.e^{-K_p.t} + K_p.I.e^{-K_La.t}$$

$$Y' = \frac{1}{(K_p - K_La)}.((K_p - K_La).J.e^{-K_p.t} + K_p.I.e^{-K_La.t}) \qquad \text{Equation A2-21}$$

Substituting $J = \frac{-K_L a}{(K_p - K_L a)}$ into equation A2-21 yields equation A2-22, and setting I = 1

$$Y' = \frac{1}{(K_p - K_L a)} - K_L a . e^{-K_p . t} + K_p . e^{-K_L a . t} \qquad \text{Equation A2-22}$$

Since Y' is defined as the DO with and incorporated probe response lag, it holds that

$$Y' = \frac{C_p^* - C_p}{C_p^* - C_p}$$

Substituting this into equation A2-22, and setting the initial concentration, C_{po} to zero, the second order model incorporating a probe response lag is given in equation A2-23.

$$\frac{C_p}{C_p^*} = 1 - \frac{1}{(K_p - K_L a)} \left(K_p . e^{-K_L a . t} - K_L a . e^{-K_p . t} \right) \qquad \text{Equation A2-23}$$

9.5 Camera specifications

Table 9-10: mvBlueFox 124G Compact Industrial CCD and CMOS Camera Specifications

USB interface (up to 480 Mbit/s with USB 2.0) All versions are USB 1.1 compatible	
8 Megapixels memory	Hardware LUT 10 bits lossless image transfer and bus bandwidth via USB bulk transfer method
Connectors: **- USB type B** **- Binder 4-pin with lock USB** **- D-Sub 9-pin male** **Digital I/O opto-isolated:**	 USB USB **digital I/O**
- 2 inputs (trigger) **- 2 outputs (strobe)**	**logic / PLC level** **30 V / 100 mA**
Features:	C-mount. CS-mount or optional S-mount CCD sensor with full frame shutter CMOS sensor with rolling shutter Back-focus-adjustment automatic gain control (AGC) Automatic exposure control (AEC) All parameters adjustable via bus interface ADC resolution: up to 12 bits (transfer 10/8 bits) Horizontal and vertical mirroring Expose and image transfer possible at the same time Hardware Real-Time Controller (HRTC) for time critical I/O and acquisition control by defining a sequence of operating steps Bus powered < 2.5W
Permissible ambient temperature: **- operation: - storage:**	0 to 45 ^{o}C / 30 to 80 %RH -20 to 60 ^{o}C / 20 to 90 %RH
Weight without lens:	**approx. 120g**
Size without lens (w x h x l):	**38.8 x 38.8 x 35 mm**
Protection class:	**IP40**
Conformity:	**Immunity: EN 61000-6-2:2005;**
Emission: **FCC class B; RoHs; CE**	**EN 61000-6-3:2007,**

9.6 Dissolved oxygen probe.

All the experiments were done using the Mettler Toledo InPro 6800 polarographic DO probe.

9.6.1 The operating principle of the probe

The amperometric polarographic DO probe's operating principle was based on a Clarkprobe. The Clarkprobe measures oxygen reduction on a platinum catalyst, basing on Equations 9-1 and 9-2.

$$O_2 + 4e^- + 2H_2O \rightarrow 4OH^- \qquad \text{Equation 9-1}$$

$$4Ag + 4Cl \rightarrow 4AgCl + 4e^- \qquad \text{Equation 9-2}$$

An oxygen permeable Teflon membrane was used to separate the electrodes from the sample medium. The voltage (constant polarizing) needed to reduce oxygen at the cathode was supplied by a transmitter. The oxygen molecules permeated the membrane and were then reduced at the cathode. At the anode, the anode metal was oxidised and released as silver ions into the electrolyte, which completed the electric circuit between the cathode and the anode. The two reactions (Equations 9-1 and 9-2) produced a current which was then measured by the transmitter and was proportional to the partial pressure of oxygen (PO2) in the sample medium. A reference electrode was also used to provide stability to the anode (Toledo, 2013).

9.6.2 The dissolved oxygen probe diagram.

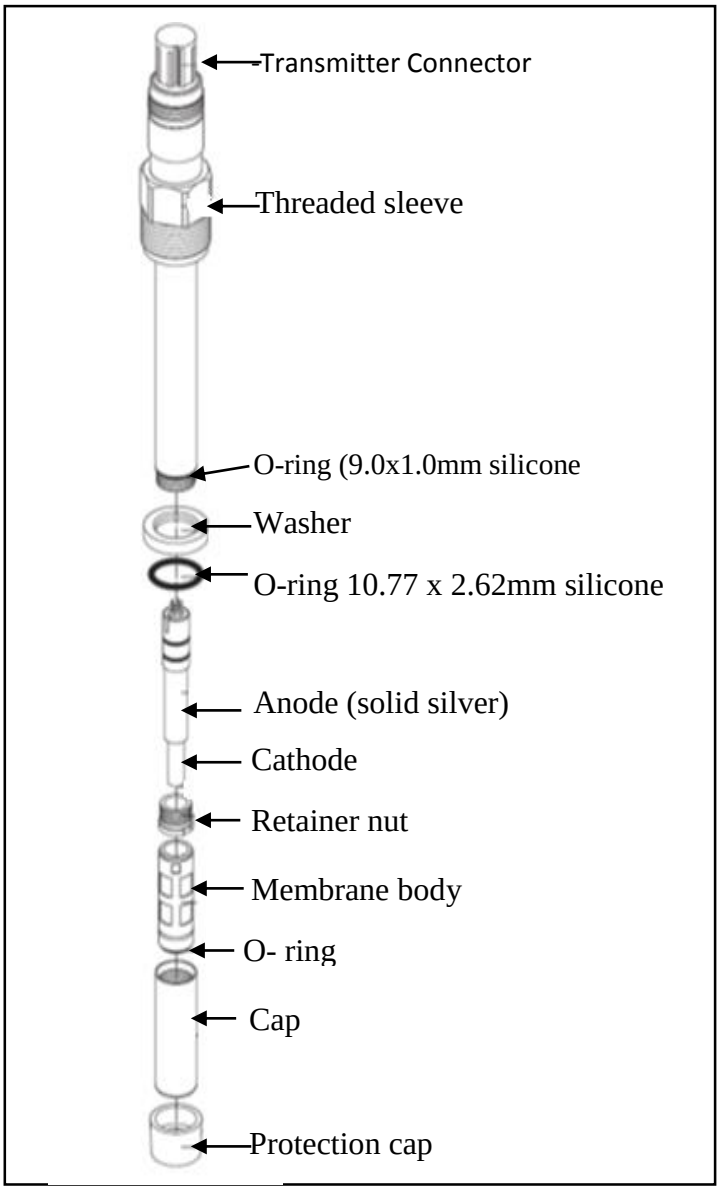

Figure 9-37: 12mm Mettler Toledo® Inpro® 6800 Dissolved Oxygen Probe Exploded View (Toledo, 2013).

9.6.3 Polarising the dissolved oxygen probe

When the DO was connected to the transmitter, the electrolyte had to be re-polarised. To perform the polarisation process, the DO probe was connected to the transmitter and immersed in tap water for over six hours. The voltage was set at –675mV, which is the recommended polarisation voltage for general purpose applications. Table 9-1 presents the time required to perform repolarisation of the probe after depolarisation. Depolarisation occurs during electrolyte changing, membrane changing or when the cable is disconnected or when no transmitter is connected to the probe. The duration for which a polarisation voltage is supplied to the sensor is defined as the polarisation time.

Table 9-11: Depolarisation and repolarisation time

Depolarisation time (t_{depol}) (mins)	Minimum required polarisation time (mins)
$t_{depol} > 30$	360
$30 > t_{depol} > 15$	6 X t_{depol}
$15 > t_{depol} > 5$	4 X t_{depol}
$t_{depol} < 5$	5 X t_{depol}

9.6.4 Dissolved oxygen probe specifications

Table 9-12: 12mm Mettler Toledo® Inpro® 6800 Dissolved Oxygen Probe Specifications.

Adapted from (Toledo, 2013)

Measurement principle	Amperometric, Polarographic
Working conditions	
Pressure resistance measurement	0.2 - 6 bar absolute
Mechanical pressure resistance	max. 12 bar absolute
Measuring temperature range	0-80 °C
Temperature range	-5-140 °C (sterilizable, autoclavable)
Construction	
Temperature compensation	Automatic with built-in RTD
Cable connection	VarioPin (IP68) straight or angled, K8S straight (digitalISM sensors)
O-ring material	Silicone FDA and USP VI approved
Membrane material	PTFE/Silicone/PTFE (reinforced with steel mesh)
Wetted metal parts	Stainless steel, Special material on request
Quick disconnect interior body	Standard
Cathode	Pt
Anode	Ag
Guard ring	No
Dimensions	
Sensor diameter	12 or 25 mm
Immersion length for 12mm sensor	70, 120, 220, 320, 420 mm
Immersion length for 25mm sensor	80,160, 260, 360 mm
Performance	
Detection limit	6 ppb
Accuracy	±1 % + 6 ppb of reading in liquids
Response time at 25°C	(air/N2) 98 % of final value <90 s
Sensor signal in ambient air	(25 °C) 50-110 nA
Residual signal in oxygen-free Medium	<0.1% of the signal in ambient air
Maximum flow error	0.05
Certification	
EHEDG, 3A	Yes
3.1 B (EN 10204.3/1.B)	Yes
ATEX certificate	Yes
FM Approval	Yes
FDA/USP VI	Yes
Quality control	Yes

9.7 Dissolved oxygen transmitter specifications.

Table 9-13: Dissolved Oxygen Transmitter M300 Specifications, Adapted from (Toledo, 2013).

M300 DO Transmitter	
Measuring current range	0 to 900 nA
Concentration range	0.00 to 50.00 ppm (mg/l)
Temperature input	NTC 22 kW
Temperature measuring range	-10 to 80 °C
Sensor maximum distance Analogue:	20 m
DO resolution	Auto / 0.001 / 0.01 / 0.1 / 1 (can be selected)
DO accuracy	±0.5% of full scale reading
Temperature resolution	Auto / 0.001 / 0.01 / 0.1 / 1 °C
Temperature accuracy	±0.25 °C
Polarization voltage	-675 mV (for analogue sensors)
Dimensions (housing - H x W x D)	96 x 96 x 140 mm
Front bezel - (H x W)	102 x 102 mm
Max. depth	125 mm (excludes plug-in connectors)
Weight	0.6 kg
Material	ABS/polycarbonate
Ingress rating	IP 65 (front)/IP 20 (housing)

9.8 Flowmeter calibration

The flowrate of the air entering the column was measured using a Cole Parmer high flow 150 mm rotameter. The rotameter was equipped with a needle valve for air flow adjustment. A uniformly tapered tube, a scale and a float were assembled for flow indication. The balance between the acceleration of free fall and the fluid forces under the float was correlated to the float height to give the fluid flow rate. Flow rate measurement was influenced by a combination of factors such as the float density, the relative diameters of the tapered tube and the float, as well as the operating conditions of temperature and pressure. To cater for gas compressibility with variation in pressure, an assumption of the standard conditions was made (air temperature of 70 ^{o}C and 1 atmosphere pressure) for calibration and thus there was no temperature correction done (Cole Parmer, 2006).

Q corrected = $Q_G^o \sqrt{\frac{P}{760}} . \frac{530}{T}$ $\qquad\qquad$ $Q_G^o = Q_A^o \sqrt{(\frac{0.00120}{\rho_G^o})}$

Where;

Q_A^o ; Standard air flow reading from meter

ρ_G^o; Density of gas in gm/ml at standard conditions

Q_G^o; Standard gas flow in same units

P; Absolute pressure of the gas inlet in mm of mercury

T; Absolute temperature in $R = {}^{o}F + 460$

When the valve is at the inlet, the working pressure is considered to be at the outlet of the tube, hence for pressure correction, a pressure gauge between the rotameter and air inlet for the column was used to measure the pressure. The operating conditions could then be referenced to those obtained at rotameter calibration.

Table 9.14 gives the Cole Parmer calibration data for specific tube and float types at the standard conditions. Pressure correction was done on the correlation between the scale readings and the flow rates. From the corrected flow rates, relationships between the scale readings and the superficial velocity within the specific system were then determined (Figure 9.38).

Table 9-14: Cole Parmer rotameter data.

Maximum flow	Minimum flow	Flow units	Metering fluid	Date
45227	2182	std. ml/min	air	30-Nov-1999

Tube number	044-40-ST	Metering Pressure	14.70 psia
Float material	316 stainless steel	Metering Density	0.001200 g/mL
Float density	8.04 g/ml	Metering viscosity	0.01812 cp
Standard conditions	1 atm & 70 ^{o}F	Density @ STD Cond	0.001200 g/mL
Room temperature	70 ^{o}F	Accuracy	Standard
Metering temperature	70 ^{o}F	Barometric Pressure	14.70 psia

Scale Reading at Center of Float	
Scale Reading (mm)	Flow rate (mL/min)
10	2182
20	4668
30	7256
40	10040
50	12988
60	16007
70	19057
80	22199
90	25161
100	28245
110	31655
120	35172
130	38315
140	41968
150	45227

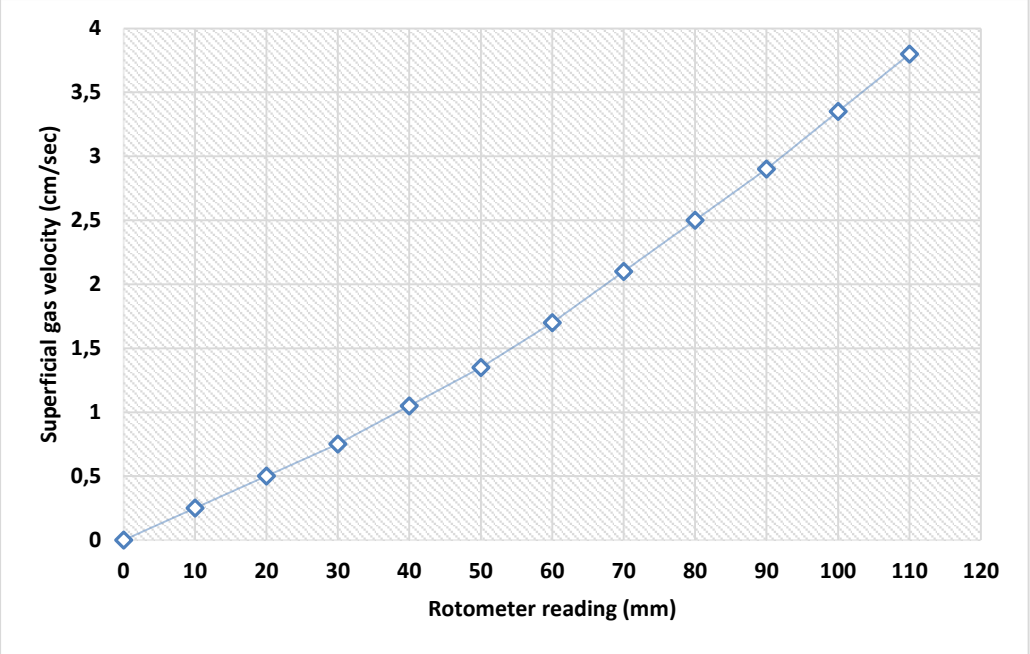

Figure 9-38: Relationships between the scale readings and the superficial velocity.